

AD744094

PULSE PAIR ESTIMATION OF  
DOPPLER SPECTRUM PARAMETERS

By

Fredrick C. Benham  
Herbert L. Groginsky  
Aaron S. Soltes  
George Works

RAYTHEON COMPANY  
Equipment Development Laboratories  
Wayland, Massachusetts 01778

Contract No. F19628-71-C-0126

Project No. 6672

Task No. 667204

Work Unit No. 66720401

DDC  
RECEIVED  
JUN 30 1972  
C

FINAL REPORT

Period Covered: 1 February 1971 through 31 January 1972

30 March 1972

Approved for public release; distribution unlimited

Contract Monitor: Graham M. Armstrong, Meteorology Laboratory

Prepared for

AIR FORCE CAMBRIDGE RESEARCH LABORATORIES  
AIR FORCE SYSTEMS COMMAND  
UNITED STATES AIR FORCE  
BEDFORD, MASSACHUSETTS 01730

Reproduced by  
NATIONAL TECHNICAL  
INFORMATION SERVICE  
U.S. Department of Commerce  
Springfield, VA 22151

Unclassified

Security Classification

DOCUMENT CONTROL DATA - R & D

(Security classification of title, body of abstract and indexing annotation must be entered when the overall report is classified)

1. ORIGINATING ACTIVITY (Corporate author) Raytheon Company Equipment Development Laboratory Wayland, Massachusetts 01778		2a. REPORT SECURITY CLASSIFICATION Unclassified
		2b. GROUP N/A
3. REPORT TITLE PULSE PAIR ESTIMATION OF DOPPLER SPECTRUM PARAMETERS		
4. DESCRIPTIVE NOTES (Type of report and inclusive dates) Scientific Final 1 February - 31 January 1972 Approved 24 May 1972		
5. AUTHOR(S) (First name, middle initial, last name) Herbert L. Groginsky George A. Works Aaron S. Soltes Frederick C. Benham		
6. REPORT DATE 30 March 1972	7a. TOTAL NO. OF PAGES 148	7b. NO. OF REFS 7
6a. CONTRACT OR GRANT NO F19628-71-C-0126	9a. ORIGINATOR'S REPORT NUMBER(S) None	
b. Project, Task, Work Unit Nos. 6672-04-01		
c. DoD Element 62101F	9b. OTHER REPORT NO(S) (Any other numbers that may be assigned this report) AFCRL-72-0222	
d. DoD Subelement 686672		
10. DISTRIBUTION STATEMENT A-Approved for public release; distribution unlimited.		
11. SUPPLEMENTARY NOTES Tech, other	12. SPONSORING MILITARY ACTIVITY Air Force Cambridge Research Laboratories (LY) L. G. Hanscom Field Bedford, Massachusetts 01730	
13. ABSTRACT The results of an expanded study and investigation of the Pulse Pair technique for estimating the first and second moments (mean and variance) of doppler spectra for radar backscatter from atmospheric phenomena are presented. The theory is extended to include the effects of non-ideal conditions, such as noise, and experimentally verified by extensive performance tests using simulated weather signals with controllable parameters. A proposed experimental model of a real-time digital pulse pair processor is defined and compared with alternate processing techniques. Based on the encouraging results of the study, recommendations are made to carry the theory into practice; these include the construction of a real-time digital pulse pair processor with flexible characteristics to gather and reduce data for evaluation while operating with real radars, and the development of additional related theory needed to guide the experimental effort.		

Unclassified

Security Classification

14. KEY WORDS	LINK A		LINK B		LINK C	
	ROLE	WT	ROLE	WT	ROLE	WT
"Pulse Pair" Estimation Theory "Pulse Pair" Processors Spectral Analysis Simulating Weather Radar Return Pulse Doppler Radar Weather Radar						

Unclassified

Security Classification

PULSE PAIR ESTIMATION OF  
DOPPLER SPECTRUM PARAMETERS

By

Fredrick C. Benham  
Herbert L. Groginsky  
Aaron S. Soltes  
George Works

RAYTHEON COMPANY  
Equipment Development Laboratories  
Wayland, Massachusetts 01778

Contract No. F19628-71-C-0126

Project No. 6672  
Task No. 667204  
Work Unit No. 66720401

FINAL REPORT

Period Covered: 1 February 1971 through 31 January 1972

30 March 1972

Approved for public release; distribution unlimited

Contract Monitor: Graham M. Armstrong, Meteorology Laboratory

Prepared for

AIR FORCE CAMBRIDGE RESEARCH LABORATORIES  
AIR FORCE SYSTEMS COMMAND  
UNITED STATES AIR FORCE  
BEDFORD, MASSACHUSETTS 01730

## ABSTRACT

The results of an expanded study and investigation of the Pulse Pair technique for estimating the first and second moments (mean and variance) of doppler spectra for radar backscatter from atmospheric phenomena are presented. The theory is extended to include the effects of non-ideal conditions, such as noise, and experimentally verified by extensive performance tests using simulated weather signals with controllable parameters. A proposed experimental model of a real-time digital pulse pair processor is defined and compared with alternate processing techniques. Based on the encouraging results of the study, recommendations are made to carry the theory into practice; these include the construction of a real-time digital pulse pair processor with flexible characteristics to gather and reduce data for evaluation while operating with real radars, and the development of additional related theory needed to guide the experimental effort.

## TABLE OF CONTENTS

<u>Section No.</u>		<u>Page</u>
1.0	INTRODUCTION	1-1
1.1	Scope	1-1
1.2	Summary	1-1
1.3	Technical Background	1-4
2.0	THEORY OF PULSE PAIR ESTIMATION	2-1
2.1	The Pulse Pair Estimators	2-1
2.2	Estimation Accuracy	2-3
2.3	Hardware Implications	2-8
2.4	Waveform Flexibility	2-8
2.5	Summary	2-14
3.0	EXPERIMENTAL EVALUATION	3-1
3.1	Porcupine Radar Weather Return	3-1
3.1.1	Estimation of Mean and Spread by Conventional Spectral Analysis	3-1
3.1.2	Estimates of Mean and Spread by Pulse Pair Processing	3-4
3.1.3	Comparison of the Estimators	3-4
3.2	Simulated Radar Return	3-8
3.2.1	Purpose, Capabilities and Advantages	3-8
3.2.2	Generating Sequences of Simulated Doppler Radar Target Return with Controllable Parameters	3-10
3.2.3	Performance of Pulse Pair Estimators	3-18
3.2.4	Performance of Spectral Analysis Estimator	3-28
3.2.5	Comparison of the Width Estimators	3-34
4.0	HARDWARE REALIZATION	4-1
4.1	General Description of the Pulse-Pair Processor	4-1
4.2	Technical Description of the Pulse-Pair Processor	4-2
4.3	System Design	4-3
4.3.1	IF Amplifier - Phase Detector	4-3
4.3.2	Digitizer	4-7
4.3.3	Correlator	4-7
4.3.4	Digital Integrators	4-13
4.3.5	Function Generators	4-13
4.4	Performance	4-14
4.4.1	Comparison with the CMF	4-14
4.4.2	Comparison with Analog Spectrum Analyzers	4-16
4.4.3	FFT Processing	4-16
4.5	Conclusions	4-17
5.0	CONCLUSIONS AND RECOMMENDATIONS	5-1
References		

TABLE OF CONTENTS (Cont'd.)

<u>APPENDIX</u>	<u>TITLE</u>
A	Analysis of Accuracy of Spectral Parameter Estimates by Pulse Pair Estimation
B	Mathematical Derivations Relating to the Generation of Simulated Doppler Return
C	Fortran Main Programs
C-1	DOPGEN
C-2	PPSTAT
C-3	SPEC
D	Fortran Subroutines
D-1	FORT
D-2	PAIR
D-3	UNPK
D-4	CDCC
D-5	BESI
D-6	STAR
D-7	GNRN
E	Spectral Analysis Plots of Typical Sequences of Simulated Doppler Radar Target Return

LIST OF ILLUSTRATIONS

<u>Figure No.</u>	<u>Title</u>	<u>Page</u>
1	Spectral Density Parameters	2-1a
1a	Standard Deviation of Pulse Pairs Center Frequency Estimate ( $\hat{f}_0$ ) vs Spectral Width ( $wT$ ) with per Pulse S/N a Parameter, for Uniform Pulse Spacing	2-4
2	Standard Deviation of Pulse Pairs Width Estimate ( $\hat{wT}$ ) vs True Spectral Width ( $wT$ ) with Per Pulse S/N a Parameter, for Uniform Pulse Spacing	2-5
3	Accuracy of Pulse Pairs Estimate of Mean Velocity vs Spectral Width, for Independent Pairs (from Rummler, Ref. (4))	2-6
4	Fractional Accuracy of Pulse Pairs Estimate of Spectral Width vs True Spectral Width for Independent Pairs (from Rummler, Ref. (4))	2-7
5	Pulse Pair Waveforms	2-9
6	Tradeoff Characteristic of Pulse Pair Mean Frequency Measurement for Fixed Radar Energy $\mathcal{E}$	2-11
7	Tradeoff Characteristic of Pulse Pair Width Measurement for Fixed Radar Energy $\mathcal{E}$	2-12
8	Typical Data Spectrum for $N = 1024$	3-2
9	Overall Block Diagram of the Software Simulation System for Investigating and Comparing the Performance of the Pulse Pair and Spectrum Analyzer Estimators of Spectral Parameters	3-9
10	Block Diagram of Simulated Doppler Return Generator	3-13
11	Flowchart of DOPGEN	3-15
12	FFT Processed Simulated Doppler Spectrum of Weather Data	3-17

LIST OF ILLUSTRATIONS (Cont.)

<u>Figure No.</u>	<u>Title</u>	<u>Page</u>
13	Flowchart of PPSTAT	3-19
14	Theoretical Accuracy of Pulse Pair Estimators of Mean Frequency ( $\hat{f}_0$ ) vs Number of Pulse Pairs Compared with Simulation Results	3-21
15	Theoretical Accuracy of Pulse Pair Estimates of Mean Frequency ( $\hat{f}_0$ ) vs Spectral Width ( $w$ ) compared with Simulation Results	3-22
16	Theoretical Accuracy of Pulse Pair Estimates of Spectral Width ( $\hat{w}$ ) vs Number of Samples Compared with Simulation Results	3-23
17	Theoretical Accuracy of Pulse Pair Estimates of Spectral Width ( $\hat{w}$ ) vs Actual Spectral Width ( $w$ ) Compared with Simulation Results	3-24
18	Theoretical Accuracy of Pulse Pair Estimates of Spectral Width ( $\hat{w}$ ) vs S/N Compared with Simulation Results (for $f_0 = 300$ Hz; $w = 78$ Hz)	3-25
19	Theoretical Accuracy of Pulse Pair Estimates of Spectral Width ( $\hat{w}$ ) vs S/N Compared with Simulation Results (for $f_0 = 600$ Hz; $w = 156$ Hz)	3-26
20	Theoretical Accuracy of Pulse Pair Estimates of Spectral Width ( $\hat{w}$ ) vs S/N Compared with Simulation Results (for $f_0 = 900$ Hz; $w = 234$ Hz)	3-27
21	Flowchart of SPEC	3-29
22	Spectral Analysis Width Estimates ( $\hat{w}$ ) vs. Threshold Level for Simulation Input Data ( $f_0 = 300$ Hz; $w = 78$ Hz)	3-31
23	Spectral Analysis Width Estimates ( $\hat{w}$ ) vs. Threshold Level for Simulation Input Data ( $f_0 = 600$ Hz; $w = 165$ Hz)	3-32

LIST OF ILLUSTRATIONS (Cont.)

<u>Figure No.</u>	<u>Title</u>	<u>Page</u>
24	Spectral Analysis Width Estimates ( $\hat{w}$ ) vs. Threshold Level for Simulation Input Data ( $f_o = 900$ Hz; $w = 234$ Hz)	3-33
25	Pulse Pair Processor Signal Flow Diagram	4-4
26	PPP Block Diagram	4-5
27	Porcupine IF Amplifier	4-7
28	FFT Complex Multiplier	4-9

## LIST OF TABLES

<u>Table No.</u>	<u>Title</u>	<u>Page</u>
1	Comparison of Pulse-Pair $\hat{f}_0$ with Spectral Analysis $\hat{f}_0$ for T = 20:2:30	3-5
2	Comparison of Pulse-Pair $\hat{w}$ with Spectral Analysis $\hat{w}$ for T = 20:2:30	3-6
3	List of Recorded Sequences of Simulated Doppler Return Generated, with Parameters as shown. (PRF = 3300 pps in all cases)	3-16
4	Comparison of Pulse Pair and Spectrum Analysis; Estimates of Spectral Width	3-35
5	Peak Signal-to-Noise Improvement of Spectrum Analyzer	3-36
6	Comparison of Pulse Pair and Spectrum Analyzer Derived Width Estimates (Spectrum Analyzer Threshold Set 5 dB above Average Background Noise)	3-37
7	Proposed Design Goals for Pulse Pair Processor	4-15

## 1.0 INTRODUCTION

### 1.1 Scope

This is the Final Report on Contract F19628-71-C-0126, which is devoted to the study and investigation of the pulse pair measurement technique for determination of the first and second moments of Doppler spectra of radar backscatter from atmospheric phenomena. This technique promises to greatly simplify and thereby reduce the costs of deriving quantitative data from a pulse Doppler weather radar. Initial efforts in the application of the pulse pair technique to weather radar signals were conducted under a portion of a prior contract with the Weather Radar Branch of the AFCRL Meteorology Laboratory (F19628-68-C-0345). The emphasis on the present contract has been to extend the theory and to experimentally verify the performance of the pulse pair estimating technique to include the effects of non-ideal conditions, such as noise, that are encountered in an operational environment with real equipment; and to prepare a design specification for a real time pulse pair signal processor that could be utilized in weather radar research.

In the interests of overall continuity and perspective, and to facilitate understanding, this report provides a unified, self-sufficient presentation of the theory and experimental work to date, including some of the early results from the previous contract.

### 1.2 Summary

Major steps forward that were taken during the present contract include (1) establishing a theoretical foundation for quantitatively predicting the performance capabilities of the pulse pair estimators under various combinations of conditions, and optimizing the design parameters of the radar-processor system; and (2) experimentally verifying the theory by hundreds of quantitatively controlled performance tests conducted with the aid of the simulation system developed for this purpose.

These studies have demonstrated analytically, the feasibility of implementing a real time signal processor, using the pulse pair computing algorithm as its central core, to obtain quantitative estimates of mean velocity and velocity spread under a wide variety of conditions and for a wide variety of radars. This report describes the initial concepts and features of a processor enabling experimental confirmation of its predicted performance, in a form

suitable for performing meteorological research with Doppler radars as well. With the instrument proposed here it will be possible to collect and reduce data under a wide variety of conditions economically. This will make it possible to establish a broad data base from which the operational utility of a Doppler weather radar may be inferred. The proposed signal processor will then provide a benchmark for sizing and designing a signal processor for operational use.

The key features available in a pulse pair signal processor are

1. quantitative (digital) estimates of spectral mean, spectral width and target reflectivity in real time
2. large numbers of contiguous range gates may be processed simultaneously (up to 1024 cells in the proposed implementation)
3. selectable dwell time may be used to adjust the block length of the signal processor to the radar scanning requirement and to the meteorological conditions (integration of up to 1024 samples per range cell to be provided in proposed signal processor)
4. range resolution may be obtained (resolution equivalent to 100 ft (.5 $\mu$ s) in the proposed implementation)
5. predictable performance based on self contained data (confidence bounds on all estimates are computable based on signal processor derived S/N data)
6. sliding window operation is feasible (estimates based on the most recent N seconds of data)
7. the storage required consists essentially of three complex words per range cell (last sample, summary crosscorrelation data, summary power data) while the computing power required is to be able to calculate 2 complex multiplies and adds at the input data rate
8. additional waveform flexibility (non uniform p. r. f. and pulse widths-- limited frequency agility)
9. sensitivity comparable to spectrum analyzers
10. independent AGC for each range bin to improve overall dynamic range

as well as the features common to all digital signal processors, namely

11. non critical adjustments
12. long term, drift free, stable performance without calibration
13. flexibility in interfacing with a variety of radars.

The digital outputs of the processor can be displayed, recorded, or remoted for further display or processing.

To fully utilize the processor capabilities it must operate in conjunction with a coherent radar receiver that has a wide dynamic range and is able to accept AGC control voltages from the processor at a range cell-to-range cell rate. To insure compatibility, it is proposed to incorporate in the processor a self-contained receiver with the required characteristics that will accept I.F. and reference signals from the radar, gain control voltages from the processor, and deliver the required in-phase and quadrature complex video signals to the processor. Since the processor measures signal amplitudes to form the AGC control voltage for each range cell, this information is available as a digital output. Together with the large useful receiver dynamic range, as an added benefit the processor amplitude output in conjunction with range information can also be utilized for other purposes, such as the calculation of target reflectivity.

It should be noted that although there are other methods of estimating spectral mean, the pulse pair technique provides quantitative estimates of this parameter in digital form, and is the only known method for estimating spectral width in real time.

The balance of this report is devoted primarily to the technical aspects of the pulse pair program. The technical background is presented in the succeeding portion of this Introduction; the theory of Pulse Pair Estimation, including original analyses performed on the present contract, appears in Section 2; Section 3 deals with the methods and results of Experimental Evaluations of the pulse pair technique, including that performed with real radar data on the prior contract and that utilizing simulated radar return on the present contract; Section 4 describes the proposed Hardware Realization of a Pulse Pair Processor capable of operating on real radar data in real time; and Section 5 presents the conclusions that have been drawn and the Recommendations that have been formulated as a result of the Study and Investigation.

Detailed Analyses, Computer Programs, and Spectral Plots are included in the Appendices in support of the main text of this report.

### 1.3 Technical Background

A commonly occurring problem in radar measurements is to estimate the spectral mean and variance of a unimodal Gaussian signal imbedded in white Gaussian noise. The classical technique used is to form spectral estimates from the time sequence, and then form estimates of the spectral mean and variance by standard formulae. It is not difficult to show that these techniques are not optimum and result in signal processor dependent bias errors which affect the system sensitivity.

When both mean and variance are unknown, the optimum spectral parameter estimates can only be obtained implicitly from the solution of a transcendental equation in which the form of the underlying spectrum is known. To overcome these defects, various investigators have resorted to threshold tests to reject the noisy frequencies, in order to apply classical mean and variance estimators to the residue after thresholding.

This report describes a new technique, known as pulse pair analysis, which bypasses the stage of spectrum analysis, and directly estimates spectral mean and variance. Not only does this technique result in a less complex set of calculations to be made by the processor, but it has a form which is based on an optimum estimation theory and as such is relatively free of arbitrary choices. Furthermore, the technique is robust with respect to underlying spectral shape, and permits more flexibility in the choice of radar waveform.

Its major disadvantage with respect to classical spectral parameter estimation is the fact that the technique does not indicate the presence of multi-peaked spectra. When the full spectral analysis is available clutter regions may be identified and possibly rejected, and separated non-standard spectral shapes may be detected. Pulse pair analysis, being a spectral shape independent estimation technique, requires a clutter rejection device preceding it (where necessary), and yields only indirect evidence of peculiar spectrum conditions (abnormally broad widths) for indicating the presence of multiple lobed spectra.

As for sensitivity, simulation evidence, to be presented in a later section, indicates that the sensitivity of the pulse pair estimation is comparable to that of the shape independent spectrum processing techniques.

## 2.0 THEORY OF PULSE PAIR ESTIMATION

### 2.1 The Pulse Pair Estimators

It may be shown<sup>(1)</sup> that the optimum estimate of the spectral mean and variance of a sequence of pairs of measurements which are uncorrelated is given by

$$\text{Arg} \left[ \frac{1}{\hat{W}} \int S \left( \frac{f-\hat{f}}{\hat{W}} \right) e^{-j2\pi fT} df \right] = \arg X \quad (2-1)$$

$$\left| \frac{1}{\hat{W}} \int S \left( \frac{f-\hat{f}}{\hat{W}} \right) e^{-j2\pi fT} df \right| = \frac{|X|}{Y - \sigma_N} \quad (2-2)$$

where

$$X = \frac{1}{N} \sum_{k=1}^N r_{1k} r_{2k}^* \quad (2-3)$$

$$Y = \frac{1}{2N} \sum_{k=1}^N \left[ |r_{1k}|^2 + |r_{2k}|^2 \right] \quad (2-4)$$

$r_{ik}$  is the observed signal,  $S(f)$  is the underlying spectral density function, and  $\sigma_N$  is the mean equivalent noise cross-section (see Figure 1).

It is possible to rewrite these equations in a more illuminating form by defining

$$R(t) = \int S(f) e^{j2\pi ft} dt \quad (2-5)$$

We get

$$\arg \left\{ e^{j\pi \hat{f} T} R(\hat{W}T) \right\} = \arg X \quad (2-6)$$

$$|R(\hat{W}T)| = \frac{|X|}{Y - \sigma_N} \quad (2-7)$$

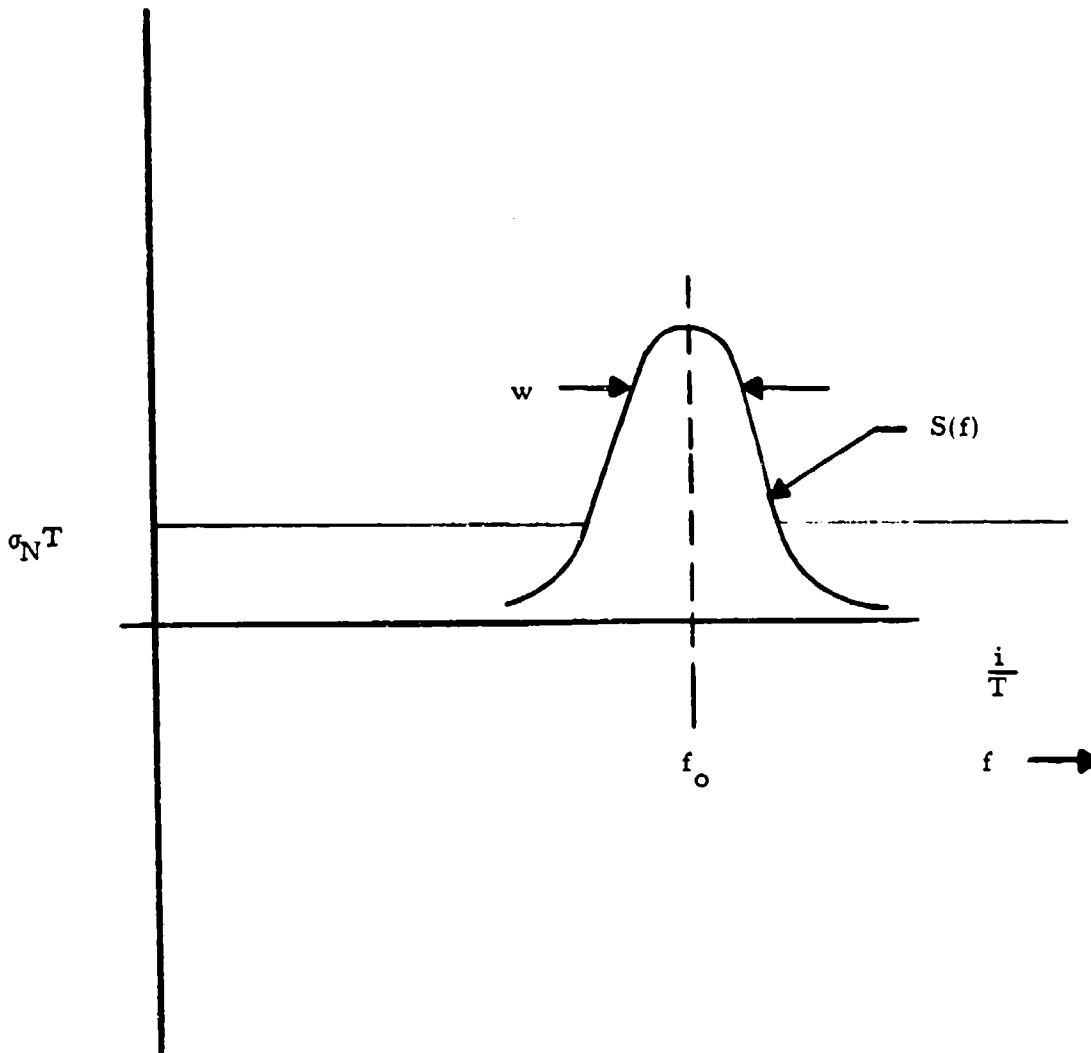


Figure 1. Spectral Density Parameters

Thus the latter equation alone determines  $\hat{\omega}$ , and furthermore, if  $R(T)$  is real, the first equation is independent of  $\hat{\omega}$ .

Essentially this result says that if the underlying spectral density function of the signal is characterized by a spectrum whose shape is invariant to frequency shift and broadening in the specified manner, then these two parameters may be estimated from the pair wise measurement directly by estimating the complex correlation function of the data.

It is important to note that for small  $T$

$$R(\hat{\omega}T) \cong R(0) - 1/2 \hat{\omega}^2 R''(0) (2\pi T)^2 \quad (2-8)$$

(No first order term is present because  $S(f)$  by definition has mean zero.) Also by definition  $R(0)$  and  $R''(0)$  are both unity (the first to have unit energy, the second to define the parameter  $\hat{\omega}$ , i. e., unit variance for the underlying signal shape). As a result, in this case, the estimator of spectral width parameter is given by

$$\hat{\omega}^2 = \frac{2}{(2\pi T)^2} \left[ 1 - \frac{|X|}{Y - \sigma_N} \right] \quad (2-9)$$

and the estimator of the spectral mean is given by

$$\hat{f} = \frac{1}{2\pi T} \arg X. \quad (2-10)$$

These are the pulse pair spectral parameter estimators suggested by Rummler. (2)(3)(4)

The approximations made in arriving at these results indicate that no difficulty in utilizing these estimators should arise beyond that expected from sampling considerations. Thus frequencies in excess of  $\frac{1}{T}$  will be ambiguously folded by the mean estimator, and the variance estimator will be degraded when the underlying spectral width begins to approach the sampling frequency.

It is also important to note that the explicit estimators do not depend directly on any particular spectral shape. This is not true of estimators of these same parameters based on spectral measurements.

## 2.2 Estimation Accuracy

Since (2-9) and (2-10) are explicit functions of the data, it is straightforward to analyze the expected performance of the estimators. The analysis is complicated by the nonlinearity of the estimator functions.

Appendix A gives an approximate analysis of the performance of both the mean and the width estimators. It is shown there that the estimator is unbiased and that when the per pulse signal to noise ratio is useful, the variance of these estimators is given by

$$2M \text{Var} (2\pi \hat{f}_0 T) = e^{(2\pi w T)^2} \left[ \frac{N}{S} \left( \frac{N}{S} + 2 \left( 1 - e^{-2(2\pi w T)^2} \right) \right) + 2\pi w T \sqrt{\pi} \right] \quad (2-11)$$

and

$$2M (2\pi w T)^2 \text{Var} (2\pi \hat{w} T) = \frac{N}{S} \left[ \frac{N}{S} \left( 1 + 2e^{-(2\pi w T)^2} \right) + 2 \left( 1 - e^{-(2\pi w T)^2} \right) \right] \quad (2-12)$$

$$+ \frac{3}{8} (2\pi w T)^3 \sqrt{\pi}$$

where

M = number of pairs in the estimate ( $\approx$  number of data points in the sample)

N/S = per pulse noise to signal ratio

These formulae were derived for Gaussian random variables with Gaussian shaped spectra. More general formulae are available in Appendix A.

The general formulae were derived for a uniform train of samples and account for all correlations in the data.

Figures 1a and 2 show plots of these functions. Comparable figures<sup>(4)</sup> derived for the case of independent pulse pair measurements, (i.e., from a nonuniform pulse train, with successive pairs spaced so far apart that the echoes are completely decorrelated) are shown in Figures 3 and 4. Comparison of these figures, which show negligible differences at useful signal to noise ratios, are indication again of the robustness of the technique.

Figure 1a. Standard Deviation of Pulse Pairs  
Center Frequency Estimate ( $\hat{f}_0$ ) vs Spectral  
Width ( $wT$ ) with per pulse S/N a Parameter,  
for Uniform Pulse Spacing

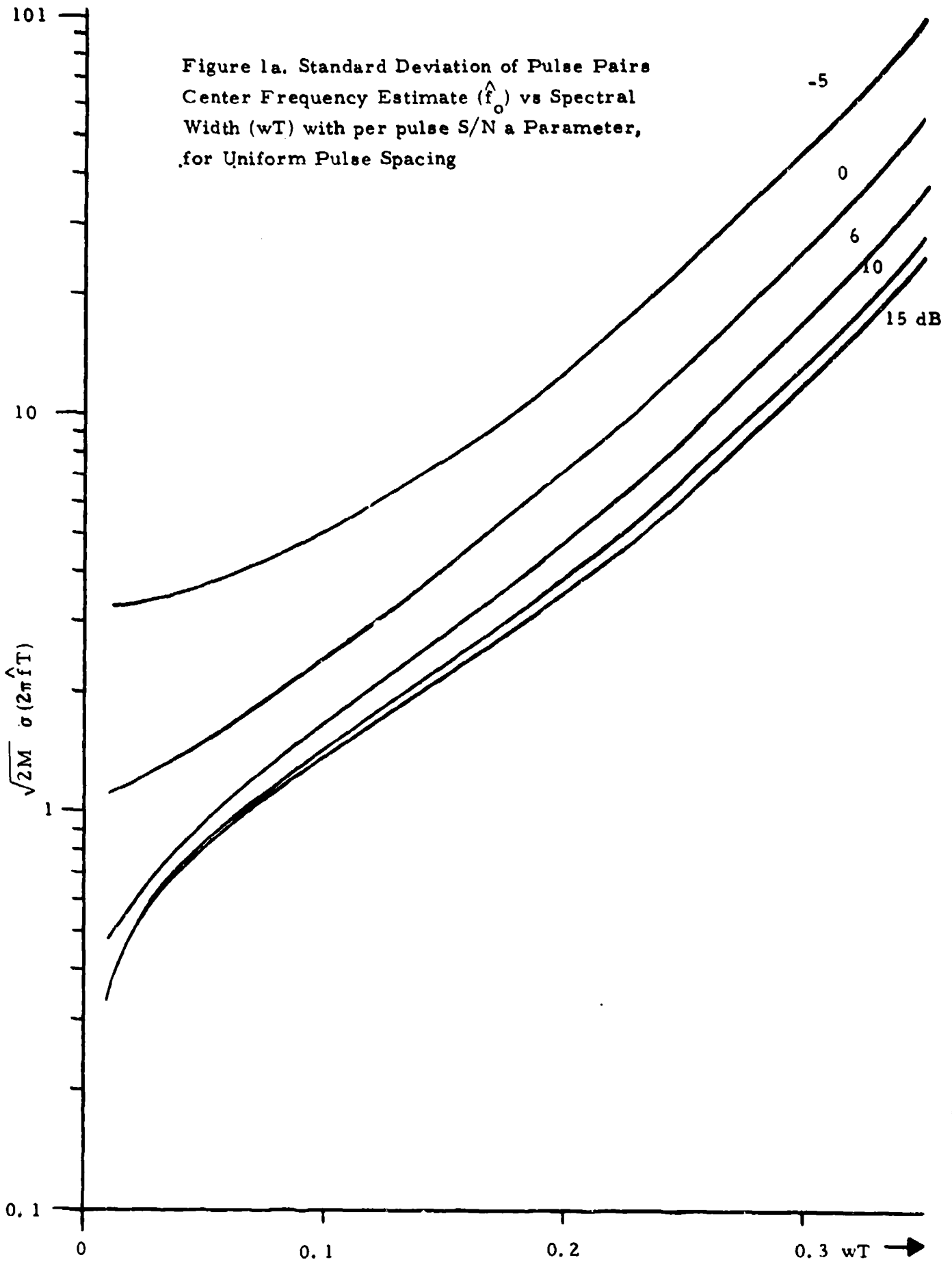
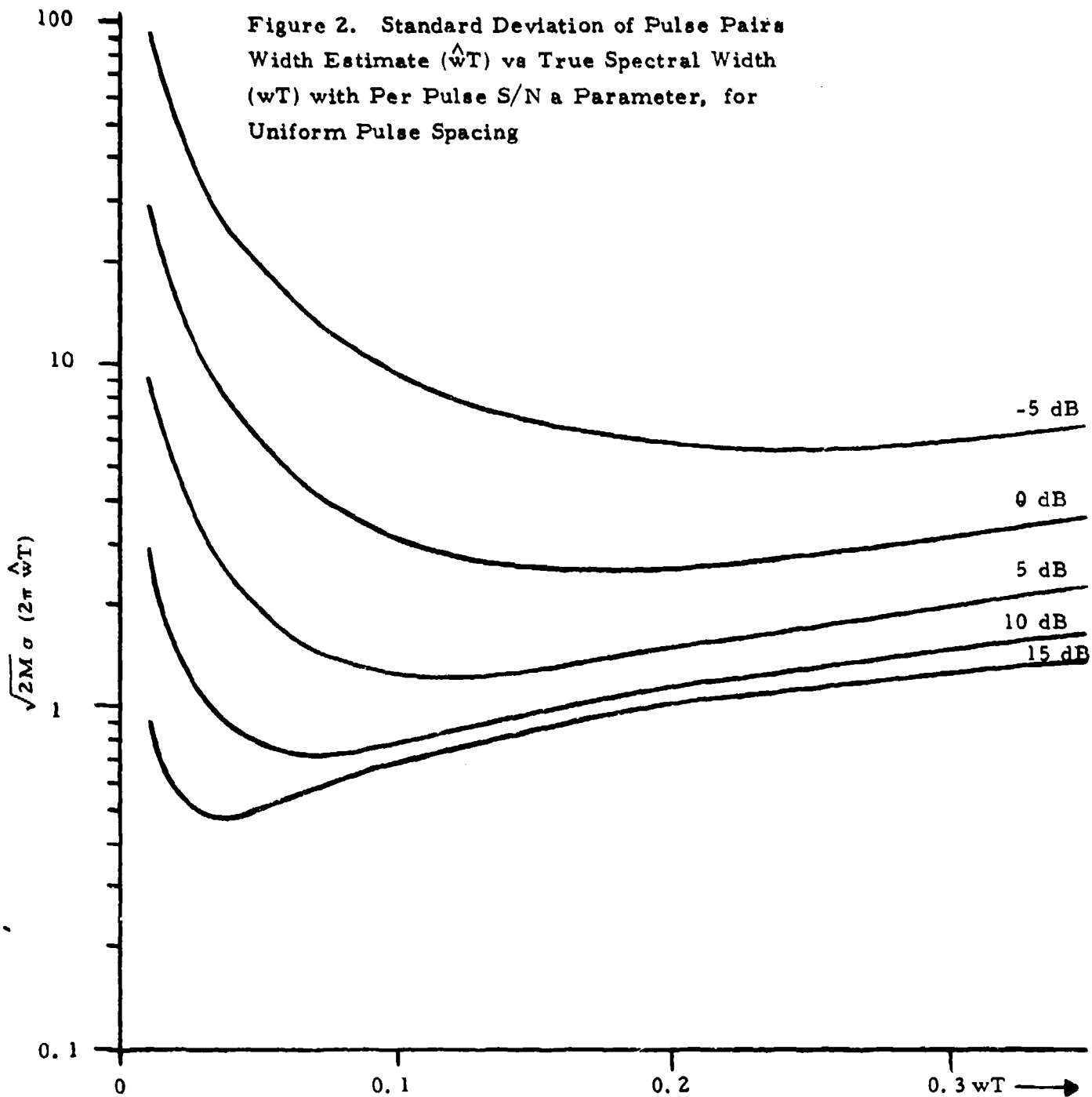


Figure 2. Standard Deviation of Pulse Pairs Width Estimate ( $\hat{wT}$ ) vs True Spectral Width ( $wT$ ) with Per Pulse S/N a Parameter, for Uniform Pulse Spacing



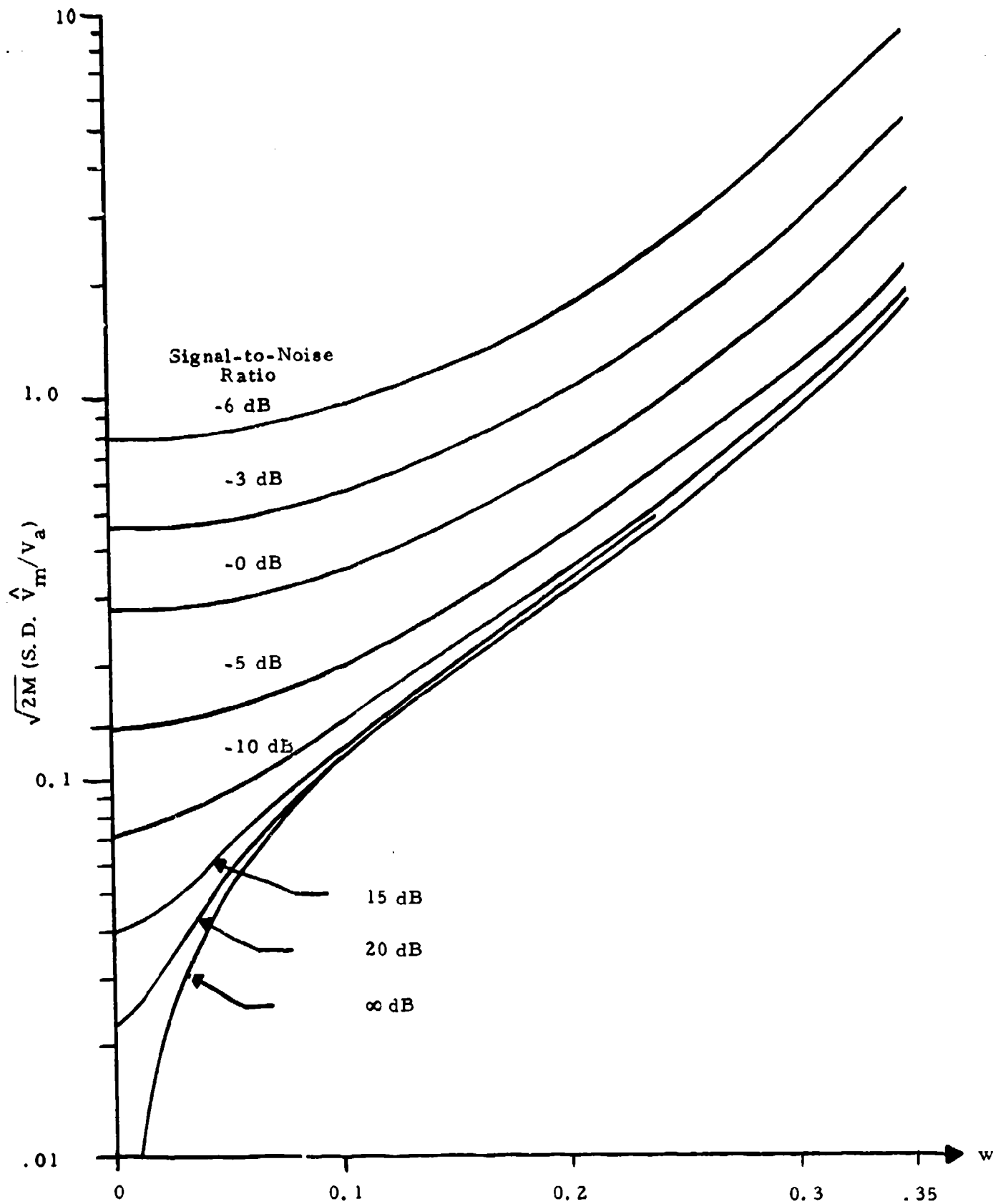


Figure 3. Accuracy of Pulse Pairs Estimate of Mean Velocity vs. Spectral Width, for Independent Pairs (from Rummler, Ref. (4))

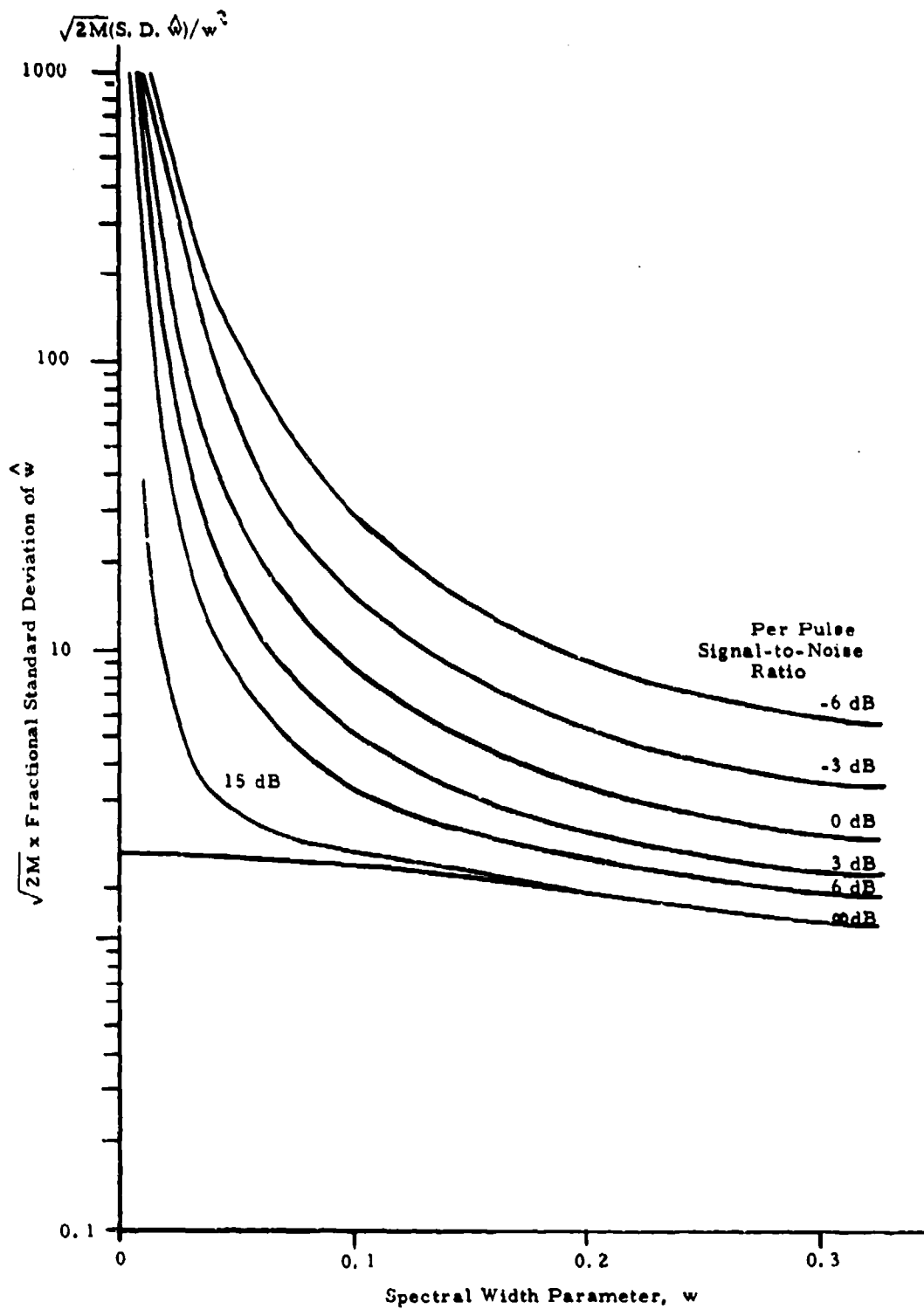


Figure 4. Fractional Accuracy of Pulse Pairs Estimate of Spectral Width vs. True Spectral Width for Independent Pairs (from Rummler, Ref. (4))

### 2.3 Hardware Implications

The pulse pair technique calculation in essence requires 2 complex pair multiplies and adds for each new data point in order to form X and Y as indicated in (2-3) and (2-4). The conversion of these to mean and variance estimates is an operation which need not be carried out at the input data rate. To bring this into sharp focus, a digital spectrum analyzer capable of processing up to 1024 complex samples at a single range, would require 5 times the number of comparable arithmetic operations and up to 500 times the data storage of a comparable pulse pair processor.

This efficiency in signal processing makes it possible to consider implementing a real time signal processor which can obtain spectral mean and variance estimates in real time with selectable dwell time per gate of up to a 1000 complex samples per dwell, with as many as 1000 range cells processed simultaneously. Available technology currently permits these calculations to be made at a 2 MHz data rate, thereby permitting range resolution 0.5 $\mu$ s (i. e., 250 ft.) and even higher thruput rate processors are being developed now.

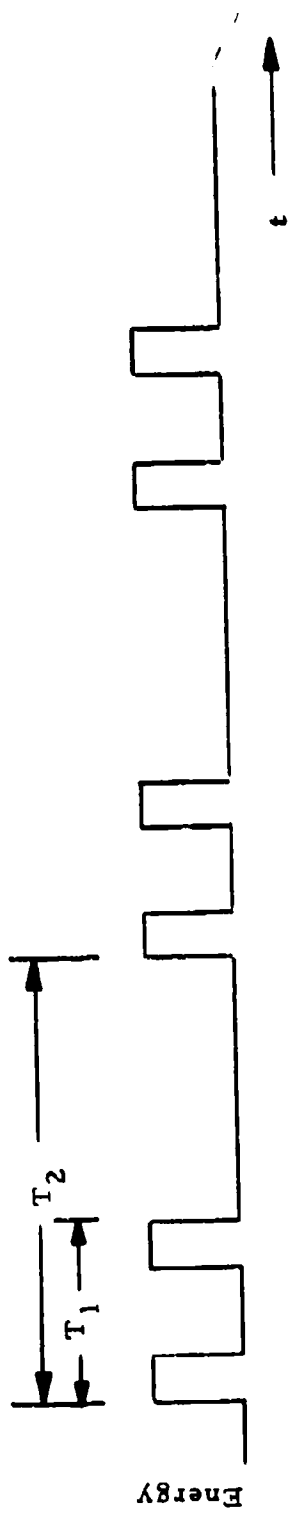
In a later section we describe a candidate signal processor implementing this technique to the above performance specifications. That section details the flexibility and performance which may be expected of a relatively modest signal processor.

### 2.4 Waveform Flexibility

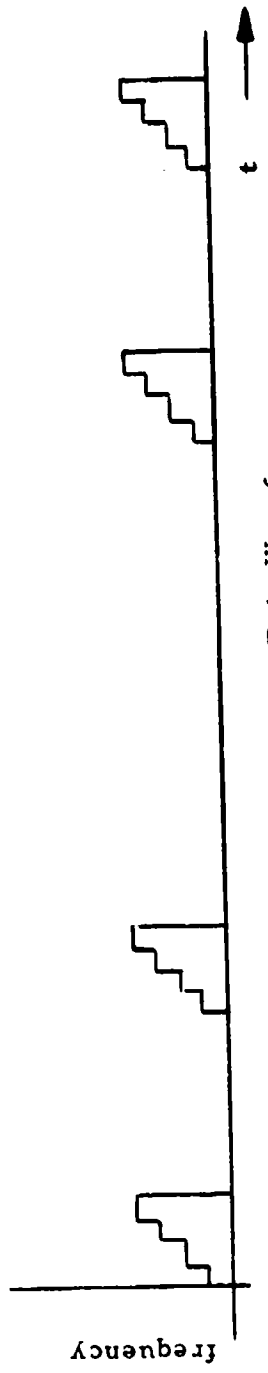
The restriction of the processor to consecutive pairs makes possible a great deal of waveform flexibility which can be used to advantage to overcome certain inherent radar limitations. Prime among these are the range-Doppler coupling which makes the unambiguous Doppler interval of the radar vary inversely with its unambiguous range interval. For weather radars, this amounts to a reduction of the Doppler analysis band of the radar as its range is extended.

The pulse pair technique makes it possible to use the waveform shown in Figure 5a to change the range-Doppler coupling relationship to

$$f_d \approx \frac{1}{T_2} \quad (2-13)$$



a) Simple Pair Spaced Waveform:



b) Frequency Modulated Pulse Pair Waveform

Figure 5. Pulse Pair Waveforms

This makes it possible to increase the Doppler coverage band on relatively small cells located at greater distances from the radar. Selection of  $T_1$  and  $T_2$  permits the radar to operate with an unambiguous Doppler spread reciprocally related to the dimension of an isolated cell. In weather radars such a technique might permit the unambiguous Doppler measurement of such conditions as severe convective cells and possibly local CAT conditions at low angles and long ranges.

The second waveform possibility, shown in Figure 5b, is available with both equally and unequally spaced pairs. The accuracy equations, (2-11) and (2-12), reveal that a key performance parameter is the per pulse signal to noise ratio. The equations indicate that there is an optimum S/N per pulse which minimizes the measurement errors for a fixed radar energy. That is, if S/N and M are related by the equation

$$\mathcal{E} = M \cdot (S/N) \quad (2-14)$$

(which indicates that a fixed energy is available to the measurement that may be distributed in any way between the number of pairs processed and the S/N used per pulse) then either equation (2-11) or (2-12) has a minimum at a definite value of M.

In particular, it may be shown that for the measurement of mean velocity, the optimum per pulse S/N is given by

$$(S/N)_{\text{opt}} = (2\pi wT \sqrt{\pi})^{-1/2} \quad (2-15)$$

and at that point the measurement variance is given by

$$\text{Var } (2\pi \hat{f}_o T)_{\text{opt}} = \frac{e}{\mathcal{E}} \frac{(2\pi wT)^2}{\left[ 1 - e^{-2(2\pi wT)^2} + \left( 2\pi wT \sqrt{\pi} \right)^{1/2} \right]} \quad (2-16)$$

Figures 6 and 7 indicate the sensitivity of this condition to nonoptimum conditions for mean Doppler and width measurements respectively. It is important to note that minimum error for both measurements does not occur at the same value of signal to noise ratio. Indeed, the curves show that substantially more per pulse S/N is required to minimize width errors.

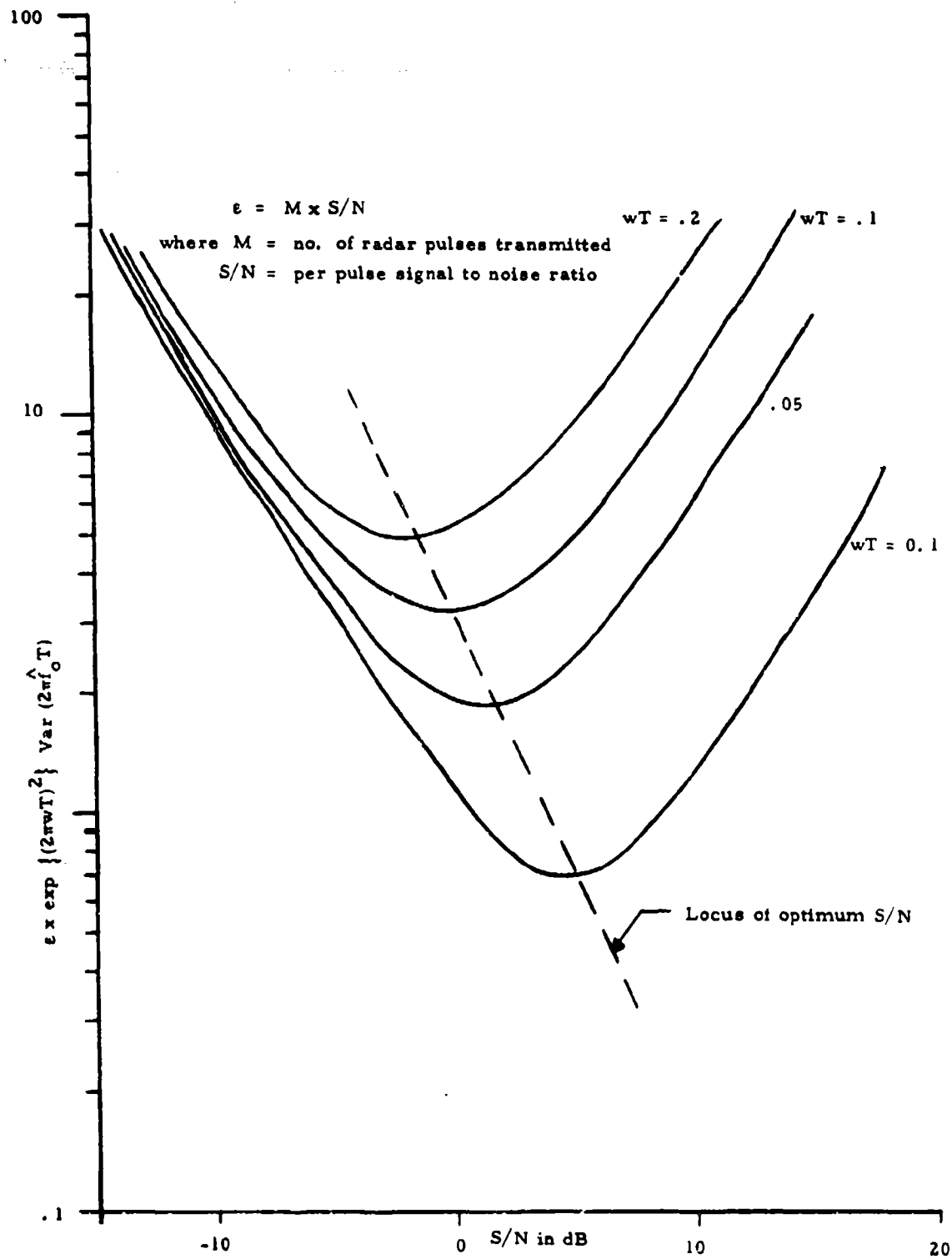


Figure 6. Tradeoff Characteristic of Pulse Pair Mean Frequency Measurement for Fixed Radar Energy  $\epsilon$

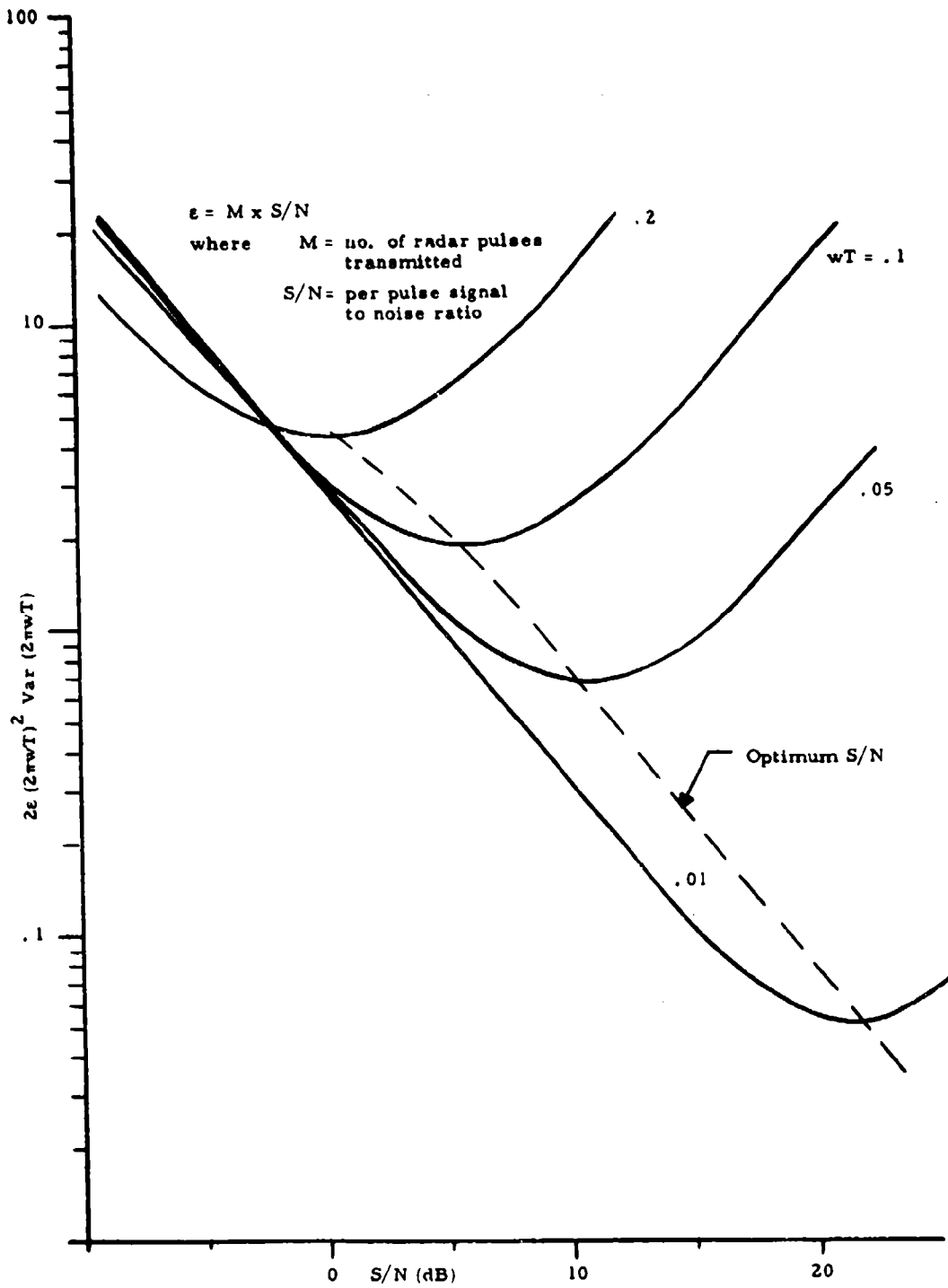


Figure 7. Tradeoff Characteristic of Pulse Pair Width Measurement for Fixed Radar Energy  $\epsilon$

The tradeoff characteristics may be used to establish the benefits to be obtained by the frequency modulation waveform of Figure 5b as follows. Suppose that the radar and meteorological parameters are such that only normalized widths of 0.05 or greater are of interest. Then Figure 7 indicates that the data should be collected at the signal to noise ratio of 7.5 dB per pulse. Suppose then that it were required to make that measurement to an accuracy of 10%. Then

$$\frac{\sigma_{\hat{w}}^2}{w^2} = \frac{\sigma_{2\pi \hat{w}T}^2}{(2\pi wT)^2} = 0.01 \quad (2-17)$$

For  $wT = 0.05$ , Figure 7 indicates that

$$2\epsilon (2\pi wT)^2 \sigma_{2\pi \hat{w}T}^2 = 0.8 \quad (2-18)$$

so that

$$\begin{aligned} \epsilon &= \frac{0.4}{(2\pi wT)^4 \frac{\sigma_{\hat{w}}^2}{w^2}} \\ &= 36 \text{ dB} \end{aligned} \quad (2-19)$$

Thus, at least  $M = (36 - 7.5) \text{ dB}$   
 $= 930$  pulses must be processed to achieve the requisite accuracy.

If the peak power in the pulse were such that 13.5 dB per pulse were available for the measurement, this theory suggests that transmission of four frequency coded subpulses each with 7.5 dB per pulse signal to noise ratio for a total transmission of 250 groups of four might result in better overall accuracy than would the same length of uncoded transmission. The improvement in performance would be negligible at  $wT = .05$  for the conditions given, but at  $wT = 0.1$  the frequency modulation would improve the accuracy by 40% =  $(\sqrt{2}-1)$ .

There is an important caveat which must be considered in this regard; namely, that additional receivers may be required to implement the frequency modulation system for extended targets.

## 2.5 Summary

The pulse pair technology offers new potential for Doppler weather radar systems. It permits the economic implementation of a real time signal processor which can produce prodigious data reduction, reducing the enormous amount of data produced by such a radar to more manageable dimensions. It does so without a sacrifice in sensitivity in cases of interest.

It makes it possible to consider new radar modulation techniques permitting the radar to collect the data more efficiently. Thus a frequency and pulse pair spacing agile radar, which has merit in both increasing the data rate (number of pulse pairs available) and suppressing some of the range-Doppler ambiguities, can be processed without penalty in a pulse pair analyzer.

The pulse pair technique produces estimates which have predictable accuracy and are free of arbitrary parameter selection (such as the threshold level in the spectrum analyzer technique). In a digital processor, the block length of the analysis interval may be varied on command so that the processor can easily be properly matched to the radar operating conditions (p. r. f. and scan rate).

If data rates were not a consideration, it is clear from the structure of the processor, that it could be implemented as a sliding window processor, so that running averages of the most recent  $N_1$  pulse pair data could be used to obtain continuously updated mean and variance estimates.

In short, it appears that the pulse pair processing technique offers an efficient means of automating pulse Doppler weather radar processing with a technique which is accurate, sensitive and flexible. The equipment used in conjunction with clutter cancelling techniques should permit operation in a significant background of ground clutter.

Its ability to signal the presence of unusual spectral shape is perhaps its ultimate limitation.

### 3.0 EXPERIMENTAL EVALUATION

This section describes several efforts to date to experimentally verify the theoretically predicted accuracy capabilities of the pulse pair estimators of spectral mean and spread and to compare their performance with other methods of estimation using identical input data. The initial experiment, which was conducted on the previous contract, compared the results of pulse pair and conventional spectral analysis processing of real Porcupine Radar weather return<sup>(5, 6)</sup>. The limitations encountered with this approach to evaluation motivated the more extensive and precise experimental evaluations accomplished on the present contract using simulated radar return. Although all of the experiments to date have involved non-real time pulse pair processing of the tape recorded radar output data, real time processing is both feasible and advantageous; a proposed real time hardware processor is described in Section 4.

#### 3.1 Porcupine Radar Weather Return

A sequence of 10240 consecutive raw complex video samples (both in-phase and quadrature) were tape recorded from the output of the Porcupine weather radar during a light rain. The PRF was 3300 pps, the antenna elevation angle was 40°, and the data was obtained from the range cell with the maximum S/N. The analog data was then quantized for subsequent processing on a digital computer by the "pulse pair" method, with conventional spectral analysis as a control. The latter was required since the true spectral parameters of the radar doppler return from the rain were unknown.

##### 3.1.1 Estimates of Mean and Spread by Conventional Spectral Analysis

The recorded data was processed by conventional spectral analysis in three different block lengths: one block of 8192 complex samples; two blocks of 4096 samples; and ten blocks of 1024 samples. A typical plot of the amplitude of the spectral components of one of the ten blocks of 1024 samples (representing approximately 1 second of weather data) as analyzed by a digital computer programmed to execute a Fast Fourier Transform is shown in Figure 8, "Typical Data Spectrum for a Sequence of 1024 Samples." The ragged appearance of the spectrum is due partly to noise and partly to the distributed nature of the weather target.

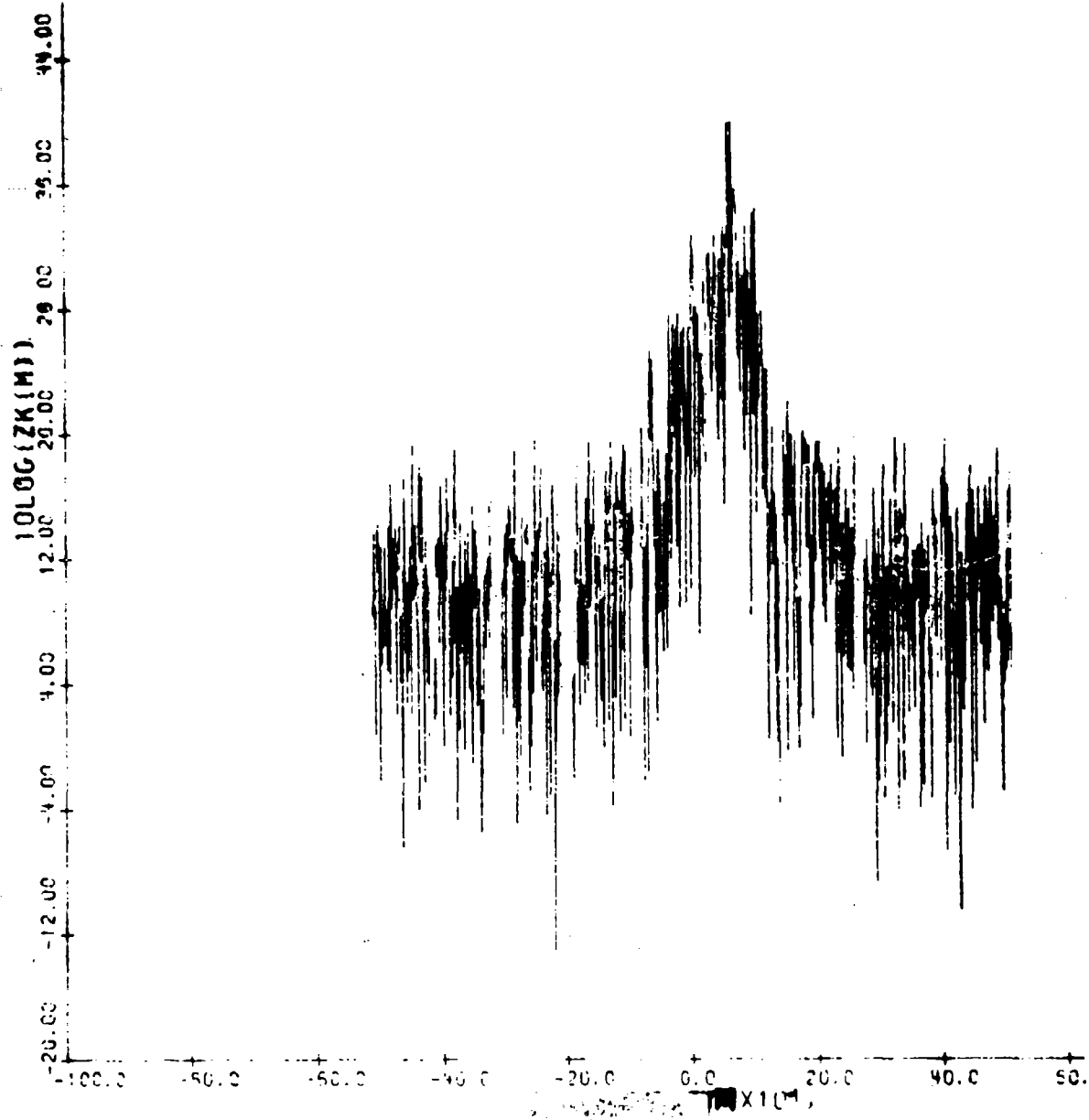


Figure 8. Typical Data Spectrum for N = 1024

The computer was programmed as follows to estimate the first moment ( $\hat{f}_0$ ) of the doppler spectrum and the second moment ( $\hat{w}^2$ ) about  $\hat{f}_0$ .

Letting  $z(n) = x(n) + jy(n)$  denote the  $n^{\text{th}}$  sample in a block of length  $N$ , the spectral amplitudes

$$P(k) = \left| \frac{1}{N} \sum_{n=0}^{N-1} a(n) z(n) e^{-\frac{j2\pi kn}{N}} \right|^2, \quad k = 0, \dots, N-1 \quad (3-1)$$

are computed, where the  $a(n)$  are 60 dB Dolph Chebyshev weight coefficients for a block of length  $N$ .

The unambiguous frequency interval is then shifted from  $0 \leq k \leq N-1$  to  $-\frac{N}{2} + 1 \leq m \leq \frac{N}{2} - 1$  by the transformation

$$Z(m) = \begin{cases} P(m-1), & 1 \leq m \leq N/2 \\ P(m+N), & -\frac{N}{2} + 1 \leq m \leq 0. \end{cases} \quad (3-2)$$

as shown in Figure (4).

The spectral mean and width could be calculated in accordance with

$$\hat{f}_0 = \frac{\text{PRF}}{N} \bar{m}, \quad \text{where } \bar{m} = \frac{\sum m Z(m)}{\sum Z(m)} \quad (3-3)$$

and

$$\hat{w} = \frac{\text{PRF}}{N} \left( \frac{\sum (m - \bar{m})^2 Z(m)}{\sum Z(m)} \right)^{1/2} \quad (3-4)$$

However, these classical algorithms for the mean and width of the distribution make no provision for the effects of noise, although it is evident from Figure 8 that portions of the spectral plots are predominantly noise, which would tend to obscure and degrade the estimates of the spectral parameters. Neither is there a developed theory for the effects of noise on their accuracy for spectra derived data. Nevertheless, despite the lack of guidance from theory, it is necessary to employ some additional (though not necessarily optimum) technique together with the spectral analysis estimators to improve their accuracy so that they may serve as standards of comparison for the pulse pair estimators. A common

method is to select a threshold level referenced to the noise level or to the peak of the spectrum, and to use only those spectral components whose amplitudes exceed the threshold in the computation of spectral mean and width as a special set, which falls within the general class of spectral analysis estimators. Such a preliminary computational step, prior to the above calculation of the mean and width, has been introduced into the spectral analysis estimator computer program.

Rather than restrict the results of the spectral analysis estimates to a single, possibly poor choice of threshold, the estimates for  $\hat{f}_0$  and  $\hat{w}$  were computed for each block of data over a range of assumed noise thresholds from 20 dB to 30 dB below the spectral peak, and are shown in Tables 1 and 2 respectively. It will be noted that the estimates of  $\hat{f}_0$  vary with threshold level within each block over a range of from 5.5% to 12.9% of the nominal value, depending upon the specific block.

The spectral analysis estimates of  $\hat{w}$  are even more sensitive to the value of threshold. They vary with threshold level within each block over a much larger range of from 51% to 68% depending upon the specific block. The potential problem of using such measurements as a standard of comparison for evaluating the performance of the pulse pair estimator is noted here in passing, and will be discussed further later on.

### 3.1.2 Estimates of Mean and Spread by Pulse Pair Processing

The identical Porcupine radar data processed by spectral analysis were also processed by the pulse pair technique. The ten blocks of digitized sequences of 1024 samples were inputted to a computer programmed to implement the pulse pair estimators of equations (2.9) and (2.10). These results are also shown in Table 1 and 2 respectively. The estimate of  $\hat{w}$  includes a correction for noise, the level of which was deduced from the experimental data by assuming that the peaked portion of the spectrum was composed of signal plus noise, while the flat skirts were noise alone.

### 3.1.3 Comparison of the Estimators

Numerical comparisons of the pulse pair and spectral analysis estimates of  $\hat{f}_0$  and  $\hat{w}$  obtained from the Porcupine weather return data may be made from the results in Tables 1 and 2.

Table 1. Comparison of Pulse-Pair  $\hat{f}_0$  with Spectral Analysis  $\hat{f}_0$  for T=20:2:30

Block Nos.	Block-length, N	Pulse-Pair $\hat{f}_0$	Spectral Analysis $\hat{f}_0$					
			T=20	T=22	T=24	T=26	T=28	T=30
1	1024	178.27	189.45	185.44	180.25	177.57	173.42	172.94
2	1024	182.95	181.68	180.12	175.40	166.78	159.57	155.96
3	1024	175.80	169.22	167.03	161.68	157.44	155.76	154.49
4	1024	184.06	166.70	167.21	159.46	154.13	153.01	151.73
5	1024	199.08	192.13	187.70	183.82	179.05	175.49	174.44
6	1024	208.83	220.03	215.70	210.29	201.63	198.43	196.65
7	1024	196.50	208.18	204.82	202.96	197.26	193.72	190.70
8	1024	203.98	220.10	219.21	215.03	211.20	211.50	208.87
9	1024	181.00	179.55	167.99	161.42	161.42	158.72	156.72
10	1024	186.10	177.47	179.18	178.66	175.63	170.07	167.96
1-4	4096	180.26	179.80	178.40	177.29	172.37	167.84	164.60
5-8	4096	201.90	201.88	199.02	192.94	189.17	184.55	182.22
1-8	8192	190.78	192.89	191.16	189.38	183.51	179.17	174.62

Table 2. Comparison of Pulse-Pair  $\hat{w}$ ' with Spectral Analysis  $\hat{w}$  for T=20:2:30

Block Nos.	Block-length, N	Pulse Pair $\hat{w}$	Spectral Analysis $\hat{w}$					
			T=20	T=22	T=24	T=26	T=28	T=30
1	1024	213.46	153.23	224.27	274.52	313.05	333.53	341.41
2	1024	206.24	100.78	128.19	191.50	251.93	288.23	310.62
3	1024	188.96	128.02	178.45	227.94	266.36	294.83	307.83
4	1024	208.71	163.90	225.26	279.31	308.01	326.38	337.02
5	1024	222.75	154.17	207.06	259.84	295.05	316.47	324.52
6	1024	224.16	150.87	209.01	271.00	322.57	348.36	359.21
7	1024	206.15	139.04	173.37	222.04	263.00	296.26	310.12
8	1024	199.50	109.49	116.40	166.44	220.44	260.65	284.81
9	1024	246.70	162.39	224.70	282.27	321.15	351.33	363.45
10	1024	227.75	114.42	169.82	220.21	263.83	297.03	316.04
1-4	4096	204.33	102.65	110.25	130.38	182.89	325.84	274.93
5-8	4096	213.29	125.67	153.12	212.89	265.84	303.07	322.57
1-8	8192	209.19	110.65	120.26	151.47	203.84	255.55	294.68

These tables show the values of  $\hat{f}_0$  and  $\hat{w}_0$  as estimated block by block by pulse pairs and for each threshold level for the spectral analysis method. The blocks of 1024 samples have been numbered sequentially to identify the data from which the estimates were derived. The different estimates for a given block of data appear on a horizontal line alongside that block.

As was noted above, the spectral analysis estimate of  $\hat{f}_0$  varies with the threshold, T. It agrees best with the pulse pair estimate of  $\hat{f}_0$  when T = 20 dB, for which case the agreement is within better than 1% when the block length, N, is 4096 or greater. Since the spectral analysis estimates of  $\hat{f}_0$ , which were used as the control, do not vary too widely, it was generally concluded that the pulse pair estimate of  $\hat{f}_0$  was definitely satisfactory under the conditions for which the data was taken.

On the other hand, the spectral analysis estimates of doppler spread,  $\hat{w}$ , are quite sensitive to the value of T. Varying as they do over a range of about 60%, they do not provide a satisfactory standard of comparison for evaluating the performance of the pulse pair estimates of  $\hat{w}$ . Without a knowledge of the true doppler spread of the weather radar return, it was impossible to draw any conclusions as to the effectiveness of the pulse pair method for estimating  $\hat{w}$  with this particular data.

It appeared clear from the above results, that real radar weather return of opportunity did not provide a promising source of data from which the behavior of the pulse pair estimators could be quantitatively explored. Not only is there no assurance of obtaining data with the range of spectral and S/N parameters required for a valid exploration, but the accuracy with which the true values of the parameters embedded in the data (which are needed as a basis for comparison) can be established is in itself a function of the parameters. Since we cannot reasonably evaluate one unknown against another unknown, the alternate approach of using simulated radar return with prescribed parameters was indicated.

## 3.2 Simulated Radar Return

### 3.2.1 Purpose, Capabilities and Advantages

In view of the limitations encountered in attempting to evaluate the pulse-pair estimators by means of real Porcupine Radar weather return data, (see 3.1 above) more extensive experimental verification of their theoretically predicted performance was undertaken on the present contract using simulated radar weather return.

The use of simulation techniques to generate the input data for evaluating the performance of the estimators provides many advantages which overcome the principal limitations of the use of real radar data for evaluation purposes. Primarily, it makes possible the generation of statistically significant numbers of simulated complex radar samples with prescribed spectral distributions (mean frequency and width) and S/N. This permits the generation of data tapes with controllable parameters made to order and in sufficient quantities per case to suit the evaluation needs. Since the true parameters are known in advance, a direct and precise determination of estimator performance accuracy can be made at all times. The ensemble of precise results can then be analyzed by the computer to determine the statistical behavior of the estimators against the synthetic distributed weather targets as a function of the controllable parameters, number of samples entering into the estimate, etc., and the results compared with the theory.

The particular cases chosen for the simulation tests were tailored to facilitate comparison with the theoretical performance predictions derived in Section 2. A PRF of 3300, the highest available for the Porcupine Radar was used for all cases. A spectral mean of 300 Hz and width of 78 Hz were selected for the initial cases. These values are equivalent to a weather target velocity mean and spread of approximately 8 meters per second and 2 meters per second respectively, as observed with the Porcupine Radar. To vary the S/N parameter, two extreme values of S/N were chosen, including 0 dB and  $\infty$  dB (no noise present) and two cases closer to the poor S/N condition. To conveniently vary the theoretically significant  $wT$  parameter, several multiples of the initial mean and spread were selected to yield target velocity distributions with 16 meters mean, 4 meters spread; and 24 meters mean, 6 meters spread. Each of these cases was varied over the range of four S/N values established initially.

An overall block diagram of the software simulation system utilized for investigating the pulse pair technique appears in Figure 9. The system is capable of generating sequences of simulated radar doppler return signals with controllable parameters; estimating the mean and width of the spectral distributions by both pulse pair and spectral analysis techniques; performing statistical analyses of estimator accuracy; and plotting and/or printing out the results.

The simulation system is programmed in FORTRAN and was run on the CDC 6600 Computer at AFCRL. To conveniently suit the capacity and capabilities of the computer, the simulation system was divided into separable steps, which could be run at different times. To facilitate such division into steps, the sequences of simulated radar doppler return which were to be used as input data to

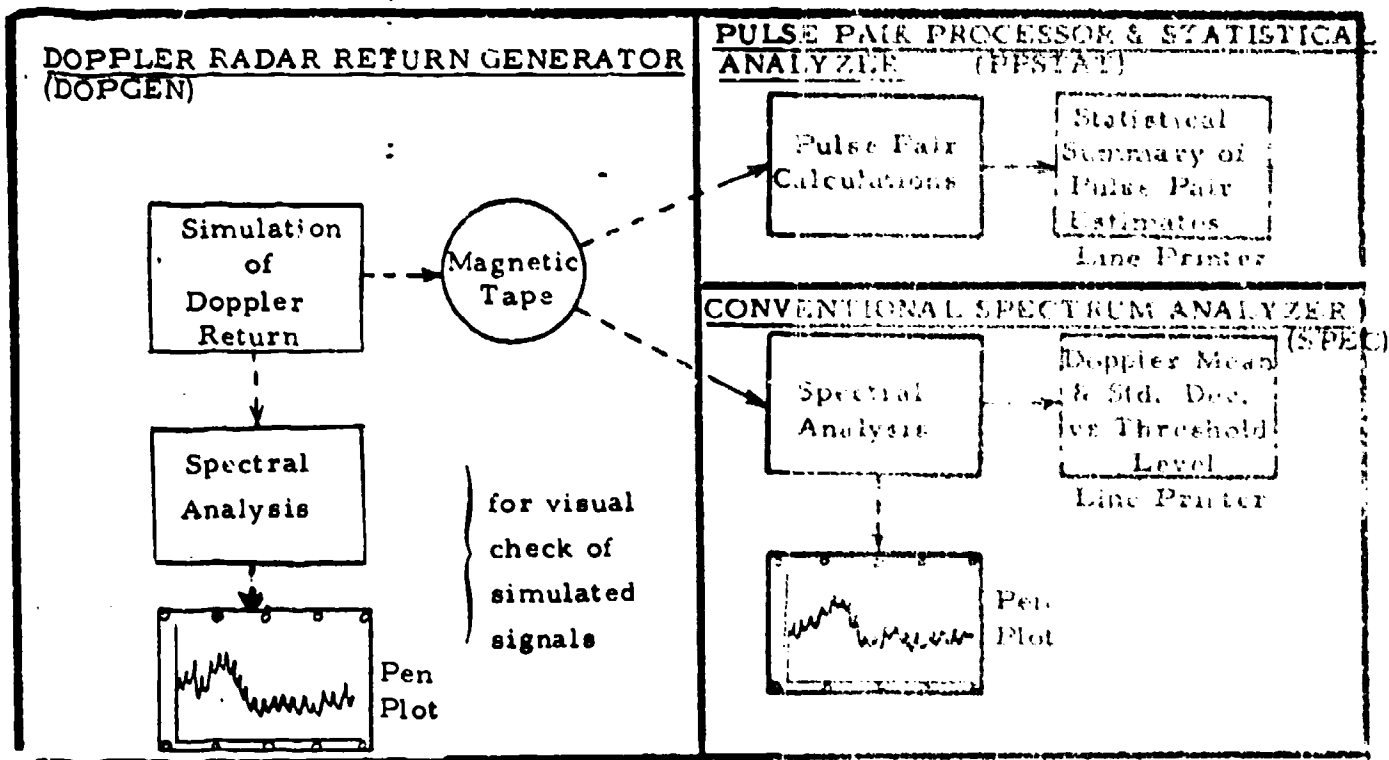


Figure 9. Overall Block Diagram of the Software Simulation System for Investigating and Comparing the Performance of the Pulse Pair and Spectrum Analyzer Estimators of Spectral Parameters

the signal processors under investigation were recorded on magnetic tape for later processing and reference. A library of such input data tapes was generated to provide desired numbers of statistically independent sequences of simulated return, with desired combinations of spectral parameters and S/N. The signal processing schemes, and modifications thereto, could thereby be statistically evaluated and compared on the basis of identical input data. Provision was also made to visually verify the validity of the simulated data; designated sequences of returns from among those generated could be selected for spectral analysis by conventional FFT and automatically plotted for visual check.

The forthcoming sub-sections deal in greater detail with the generation of the simulated doppler returns; the comparative performance of the pulse pair and spectrum analysis estimators against the simulated input data; and a comparison of pulse pair estimator performance as experimentally determined by simulation with that predicted from theory. Excellent correlation between theory and experiment are shown.

### 3.2.2 Generating Sequences of Simulated Doppler Radar Target Return with Controllable Parameters

In the real Porcupine Radar case, a uniform PRF was used to generate sequences of uniformly spaced coherent echoes reflected from distributed meteorological targets as observed in a fixed range gate. The uniformly spaced echoes, in the form of digitized complex numbers derived from the phase detected coherent video output, were then processed two at a time to yield the pulse pair estimates of the target spectral parameters.

The object of the simulation program is to generate similar sequences of uniformly spaced complex numbers equivalent to radar echoes reflected from a distributed target with a given radial velocity distribution, as sampled at a given uniform PRF and with a given output S/N. The problem is mathematically equivalent to that of numerically generating a sequence of sampled values of a stationary Gaussian process having a specified correlation function or power spectrum. The method employed is adapted from Levin<sup>(7)</sup>.

## A. Theory

The following parameters of the desired sequence must be controllable:

<u>Term</u>	<u>Symbol</u>	<u>Units</u>
MEAN DOPPLER	$f_0$	Hz
SECOND MOMENT	$m_2 = w^2$	Hz <sup>2</sup>
SAMPLING RATE	PRF	Hz
S/N RATIO (per pulse)	B	dB

1. Spectral Distribution - An approximation to the desired spectral distribution of the radar video data is achieved by playing Gaussian noise of zero mean and unity variance through a filter consisting of two cascaded, low-pass networks. The transfer function of the filter is given by:

$$H(s) = \frac{a^2}{(s + a)^2} \quad \text{where } a = 2\pi w \text{ and } s = \text{complex frequency (rad/sec)} \quad (3-5)$$

From this expression it is possible to derive the second moment and half power point of the filter. The second moment is given by:

$$m_2 = \frac{\left(\frac{1}{2\pi}\right)^2 \int_{-j\infty}^{+j\infty} H(s) H(-s) (-s^2) ds}{\int_{-j\infty}^{+j\infty} H(s) H(-s) ds} = w^2 \quad (3-6)$$

The half power point (-3dB) occurs at

$$\omega_3 = a [\sqrt{2-1}]^{1/2} \quad (3-7)$$

By Z-transform theory, the recursion relation for the equivalent digital filter is given by the impulse invariant transformation; namely, if

$$H(s) = \frac{a^2}{(s+a)^2}$$

then,

$$H(Z) = \frac{Z^{-1} a^2 T e^{-aT}}{(1 - e^{-wT} Z^{-1})^2}; \text{ where } T = \frac{1}{\text{PRF}} \quad (3-8)$$

The resulting recursion relation is then

$$y_n = x_{n-1} a^2 T e^{-aT} + 2 e^{-aT} y_{n-1} - e^{-2aT} y_{n-2} \quad (3-9)$$

Simulation of radar quadrature data is achieved as illustrated in

Figure 10. The sequences  $\{x_1, x_2\}$  are two independent Gaussian sequences which are then played through the same filter,  $H(Z)$ , specified by (3-8) and (3-9).

Complex multiplication of the output sequences  $\{y_1, y_2\}$  by  $e^{j2\pi f_0 nT}$  shifts the mean frequency from zero to  $f_0$ .

Transient effects of the filter are minimized by discarding a number of initial terms. This number has been set at three times the fractional bandwidth of the filter (with respect to the PRF) and it is given by:

$$\text{No. of discarded initial terms} = \frac{3 \cdot (\text{PRF}) \pi}{w} \quad (3-10)$$

2. Signal to Noise Ratio - When Gaussian noise is added to sequences  $\{y_1^i, y_2^i\}$  (See Figure 10), the per-pulse signal to noise ratio (S/N) is specified by:

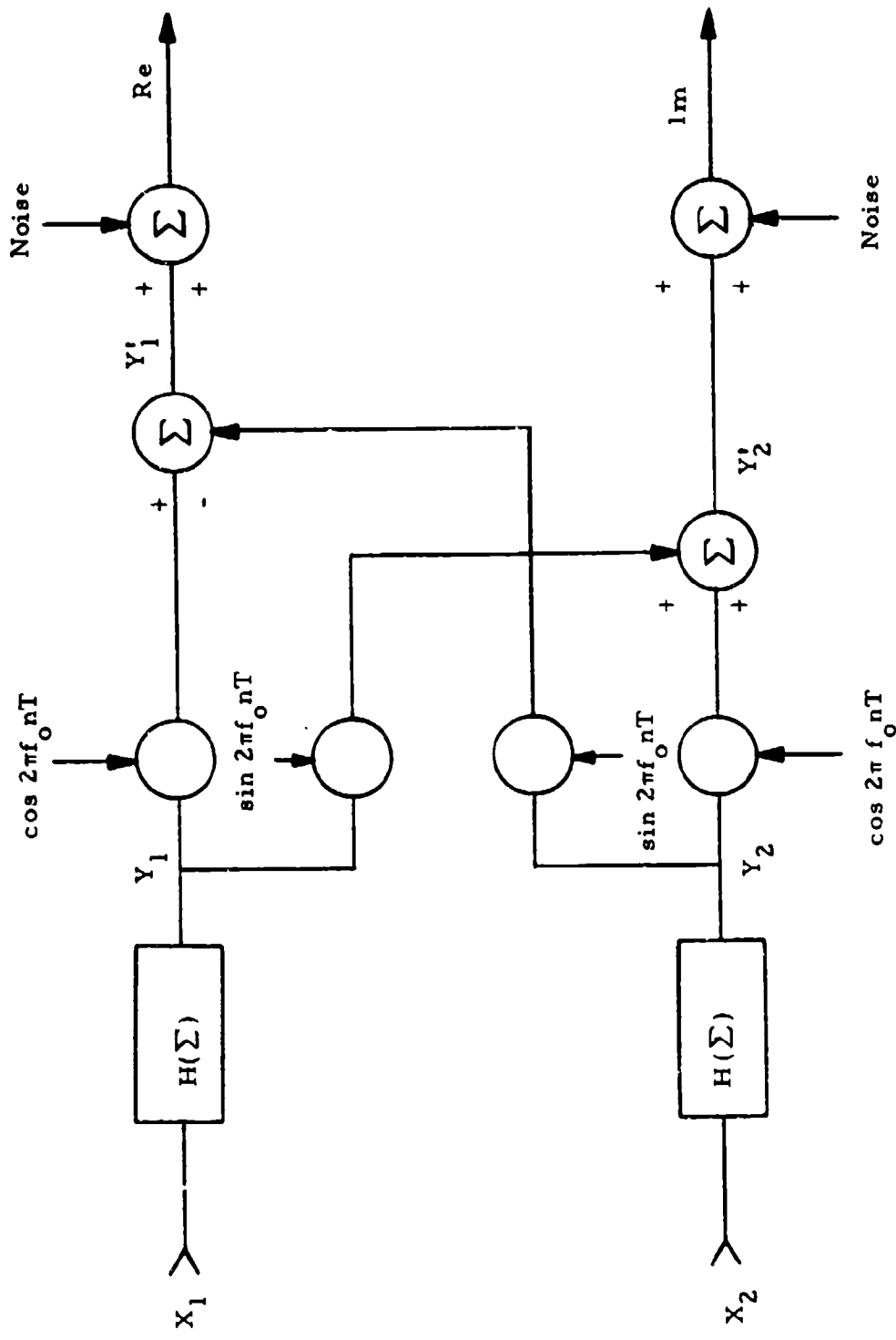


Figure 10. Block Diagram of Simulated Doppler Return Generator

$$S/N = \frac{a^4 T^2 (3e^{-aT} + e^{aT})}{\sigma_N^2 (e^{aT} - e^{-aT})^2} = B \text{ [dB]} \quad (3-11)$$

where  $\sigma_N^2$  is the variance of the added, zero mean, Gaussian noise. A given S/N ratio is then achieved by specifying  $\sigma_N^2$  as

$$\sigma_N^2 = \frac{a^4 T^2 (3e^{-aT} + e^{aT}) 10^{-B/10}}{(e^{aT} - e^{-aT})^2} \quad (3-12)$$

where B is the desired S/N ratio in dB.

Mathematical derivations relating to the above processes appear in Appendix B.

#### B. Description of Computer Program

The program developed for generating the simulated doppler target return on the AFCRL CDC 6600 is called DOPGEN. The flowchart for DOPGEN is shown in Figure 11, and the program statements coded in FORTRAN appear in Appendix C1.

Input to the program is in the form of data cards on which are specified:

- (1) mean Doppler frequency;
- (2) standard deviation of Doppler frequency;
- (3) per-pulse signal-to-noise ratio;
- (4) FFT plot control; and,
- (5) number of blocks (N) of 1024 complex samples.

Upon reading the first data card, the program generates 1024 complex samples which simulate Doppler return (a PRF of 3300 is used throughout). The data block is then written on magnetic tape along with twelve ancillary words containing information about the data. This procedure continues until N independent data blocks are written with the specified Doppler mean and standard deviation.\* A second data card can be used to change the mean and the width of the Doppler spectrum or to change the S/N ratio. If no more data blocks

\* Since each data block occupies about 3.5 ft. of magnetic tape, 685 data blocks will fit on a standard 2400 ft. long tape.

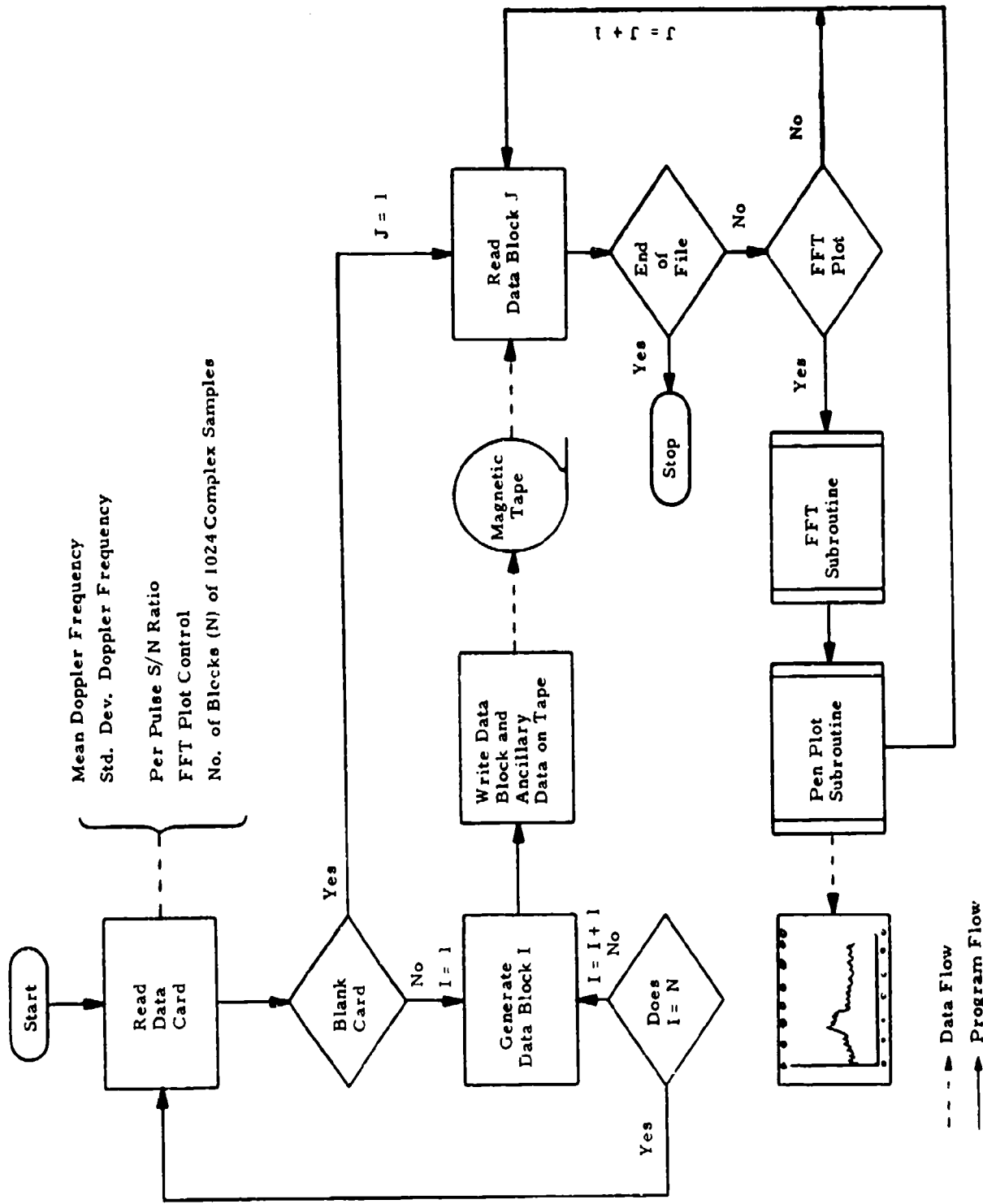


Figure 11. Flowchart of DOPGEN

are to be generated, as indicated by a blank data card, the program rewinds the tape and reads each block to verify the readability of the tape. In addition, for those data blocks on which the FFT plot control parameter (one of the ancillary words) is set to one, the program performs an FFT on the data and plots the transformed data on a Calcomp Plotter (available at AFCRL). This is used as a check to verify the validity of the simulated data - a sample plot is shown in Figure 12.

A library of 390 separate sequences of 1024 complex samples was generated by the DOPGEN simulation program and recorded on magnetic tape for use as input data. Each sequence of 1024 samples constitutes a data block. Three pairs of mean doppler and doppler standard deviation were run, each at four conditions of S/N; a PRF of 3300 pps, representative of the Porcupine Radar, was used in all cases. Thirty independent data blocks with specific parameters as shown in Table 3 were generated for each combination of parameters. A sample spectral analysis plot for each of the twelve combinations is presented in Appendix E.

Block No.	$f_o$ Mean Doppler (Hz)	w Std. Dev. Doppler (Hz)	S/N (dB)	Tape
41-70	300	78	5	RPK07
101-130	600	156	$\infty$	RPK08
131-160	600	156	0	RPK08
161-190	600	156	5	RPK08
191-220	600	156	15	RPK08
221-250	900	234	$\infty$	RPK08
251-280	900	234	0	RPK08
251-280	900	234	5	RPK08
311-340	900	234	15	RPK08
341-370	300	78	$\infty$	RPK09
371-400	300	78	0	RPK09
401-430	300	78	5	RPK09
431-460	300	78	15	RPK09

Table 3. List of Recorded Sequences of Simulated Doppler Return Generated, with Parameters as shown.  
(PRF = 3300 pps in all cases)

PRF 3300 pps  
 Number of Samples 1024  
 Cycles per Sample Point 3.22  
 Doppler Mean Frequency 300 Hz  
 Doppler Standard Deviation 78 Hz  
 S/N 5 db

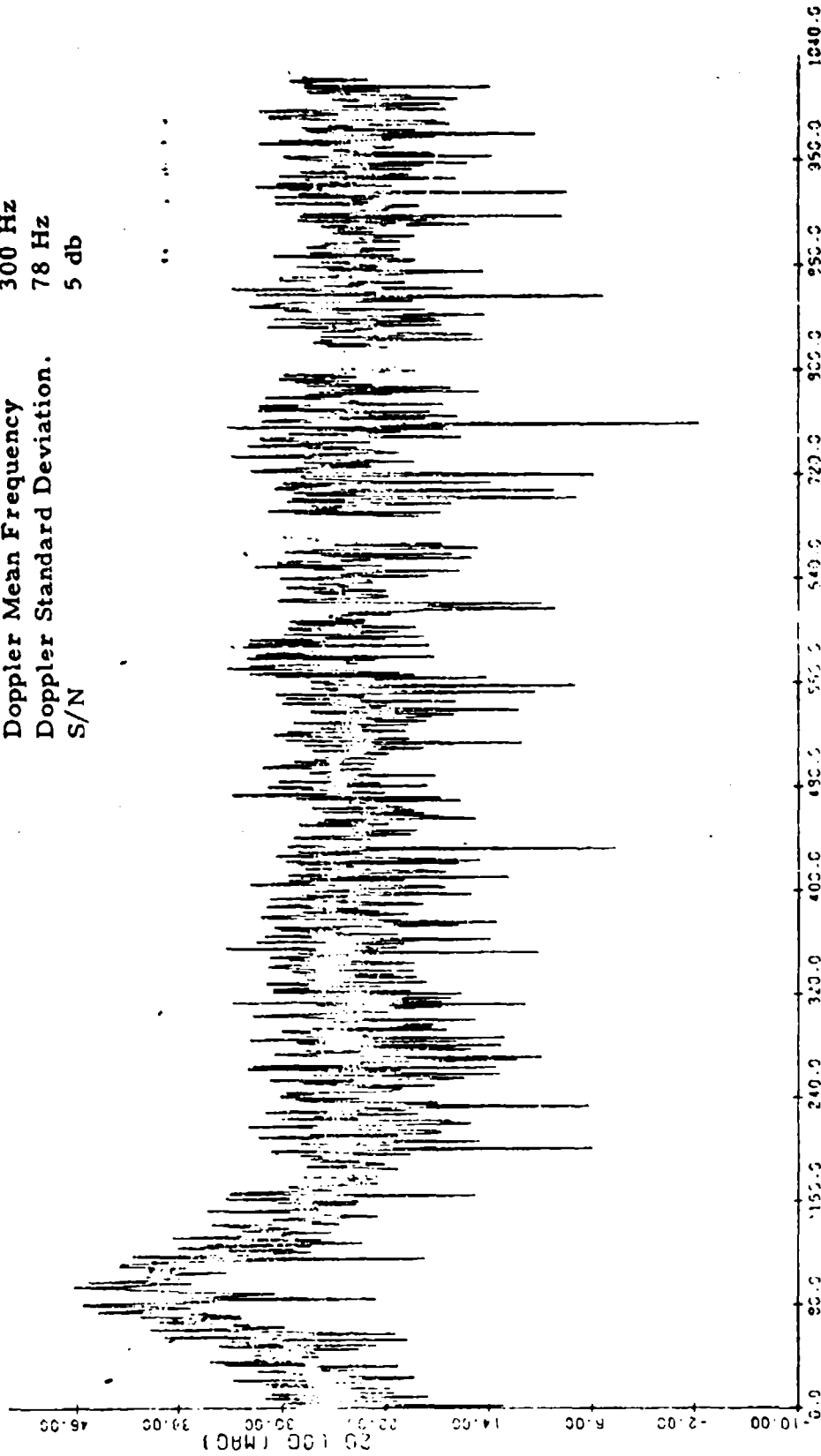


Figure 12. FFT Processed Simulated Doppler Spectrum of Weather Data

### 3.2.3 Performance of Pulse Pair Estimators

#### A. Computer Program

As shown in Figure 9 of the overall simulation system, the tape recorded sequences of simulated doppler return are processed by the pulse pair algorithms to yield estimates of spectral mean and width as a function of the number of pulse pairs entering into the estimate. The resulting estimates are then compared with the known given spectral parameters of the input data and the performance of the pulse pair estimators is statistically analyzed and summarized to produce printouts of estimator accuracy versus number of pulse pair samples for each simulated test condition.

The program for pulse pair processing and statistical evaluation is called PPSTAT. A flowchart of PPSTAT appears in Figure 13, and the coded FORTRAN statements for this program may be found in Appendix C-2. As shown in the flowchart, before reading the magnetic tape generated by DOPGEN, PPSTAT reads from a data card two data block numbers (the numbers are assigned by DOPGEN and are contained in the ancillary data associated with each block). Pulse Pair estimates are then made on consecutive data blocks starting with the first block number and continuing to the data block with the second block number. The estimates are made on samples of size 16, 32, 64, 128, 256, 512, and 1024. After operating on the variable sample sizes from each data block, the program performs a statistical summary of all the Pulse Pair estimates to yield estimator accuracy versus sample size.

#### B. Results

The hundreds of pulse pair estimates of spectral mean and width produced, analyzed, and printed out by the simulation system are presented in a manner intended to facilitate comparison with theoretically predicted performance capabilities. The close correlation shown between theory and experiment in the Figures that follow confirms the validity of the theory under the practical conditions of noise background, correlation between pulse pairs, etc. Analytic predictions of pulse pair estimator performance for particular sets of conditions can, therefore, be made with confidence.

The following comparisons between pulse pair experimental data and theory have been calculated and plotted from the results of the simulation tests.

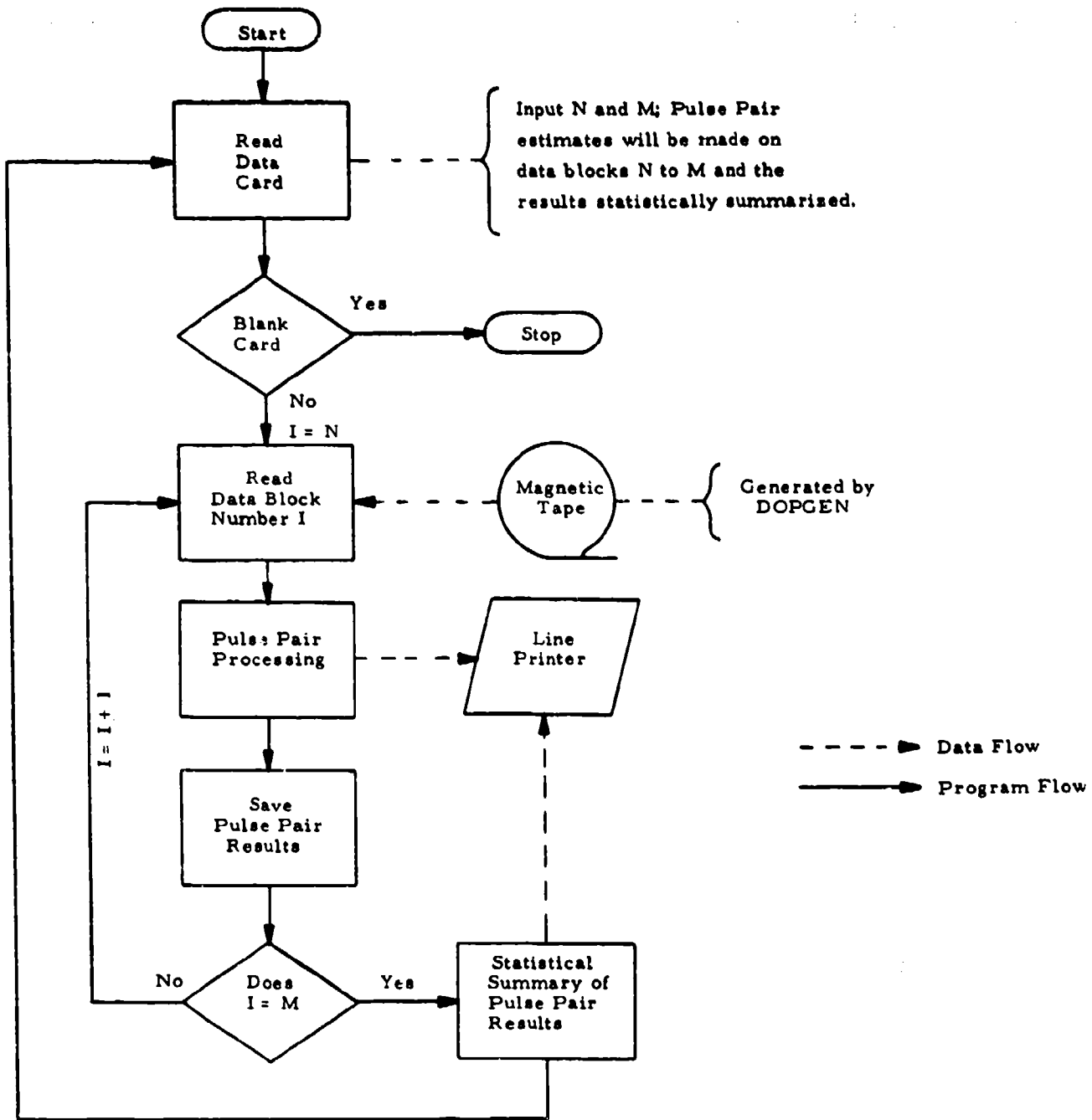


Figure 13. Flowchart of PPSTAT

Figure

Data Compared

- 14 Accuracy of Mean Frequency Estimates vs Number of Pulse Pairs
- 15 Accuracy of Mean Frequency Estimates vs Spectral Width
- 16 Accuracy of Spectral Width Estimates vs Number of Pulse Pairs
- 17 Accuracy of Spectral Width Estimates vs Actual Spectral Width
- 18 Accuracy of Spectral Width Estimates vs Signal-to-Noise Ratio  
(for  $f_0 = 300$  Hz;  $w = 78$  Hz)
- 19 Accuracy of Spectral Width Estimates vs Signal-to-Noise Ratio  
(for  $f_0 = 600$  Hz;  $w = 156$  Hz)
- 20 Accuracy of Spectral Width Estimates vs Signal-to-Noise Ratio  
(for  $f_0 = 900$  Hz;  $w = 234$  Hz)

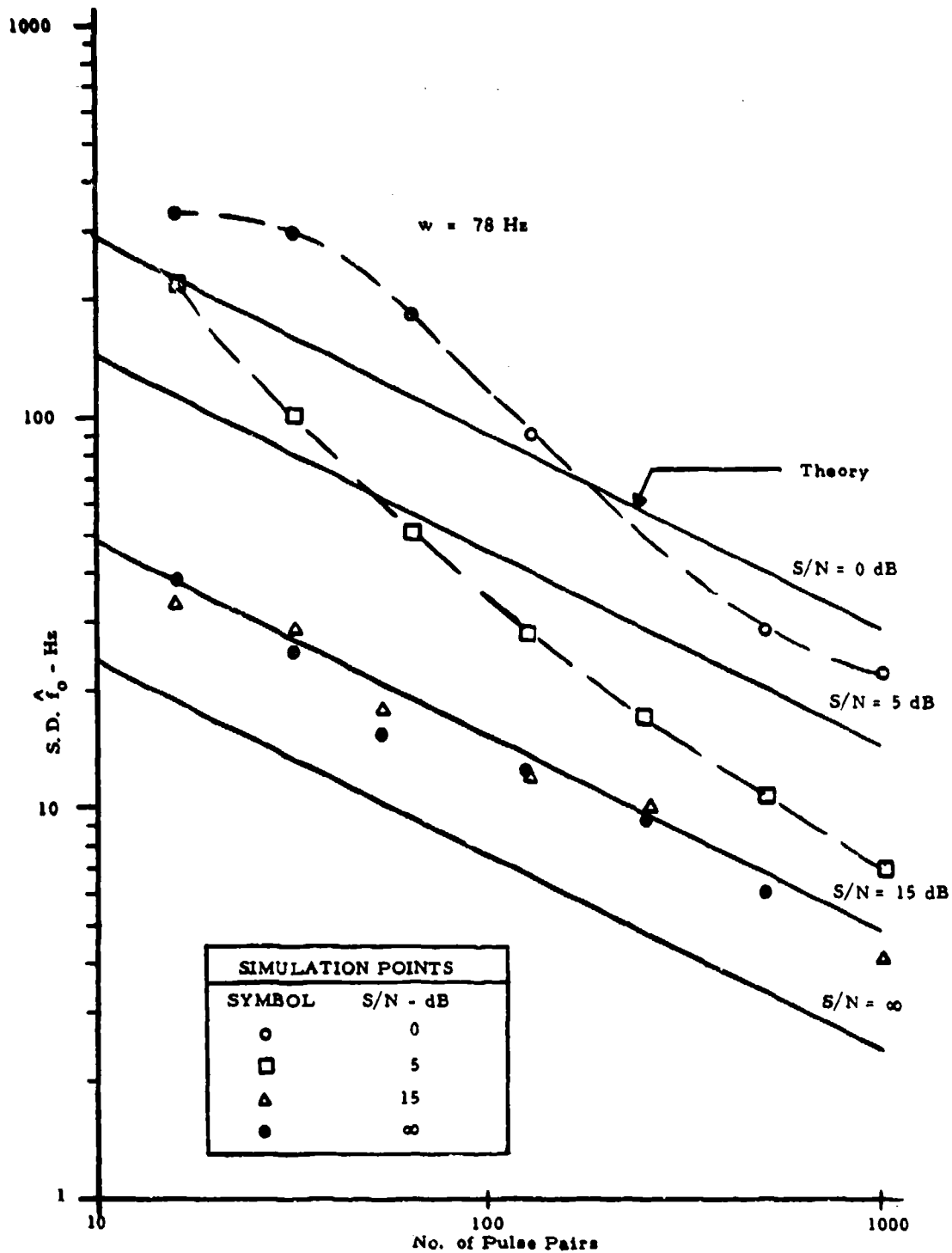


Figure 14. Theoretical Accuracy of Pulse Pair Estimates of Mean Frequency ( $\hat{f}_0$ ) vs Number of Pulse Pairs Compared with Simulation Results

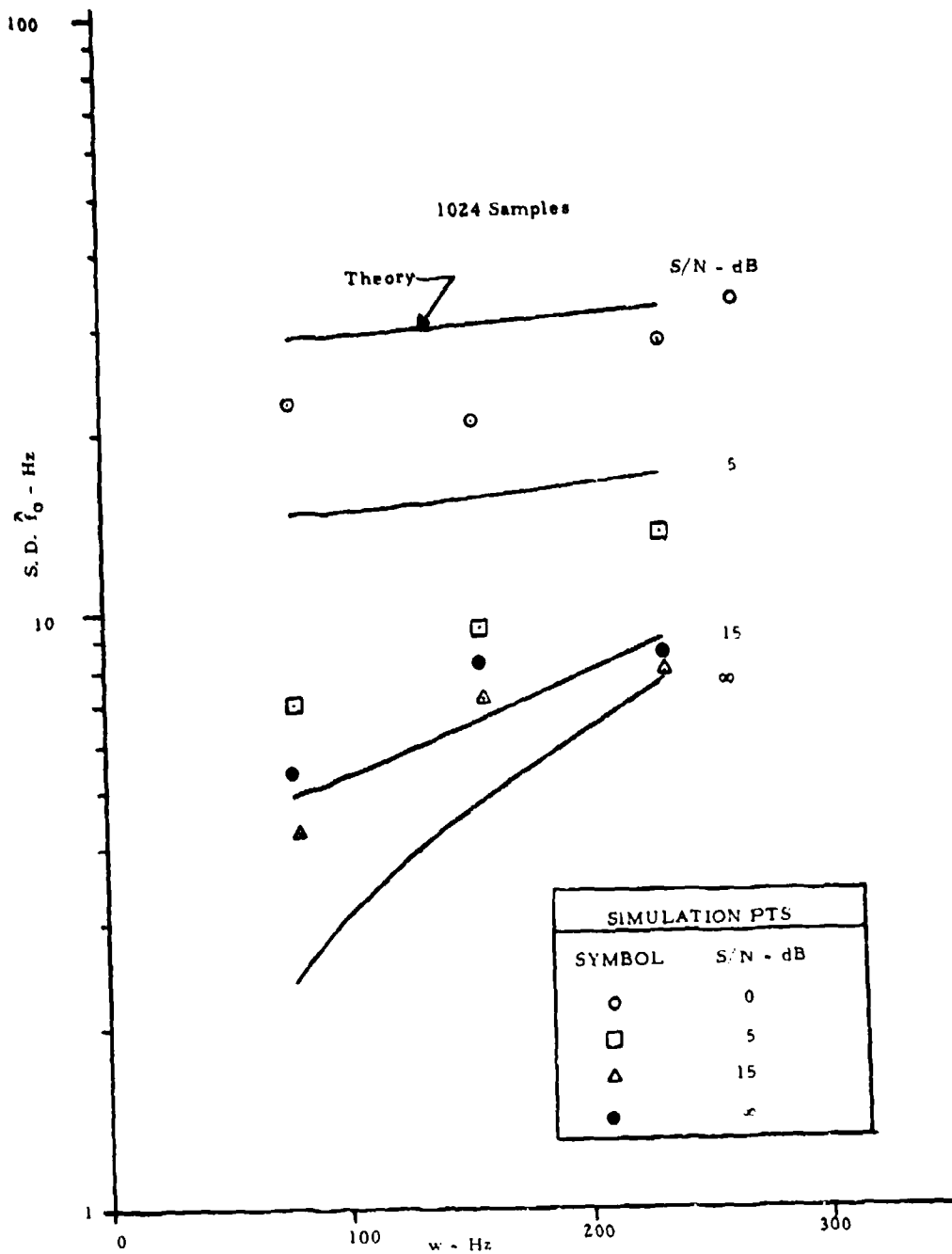


Figure 15. Theoretical Accuracy of Pulse Pair Estimates of Mean Frequency ( $\hat{f}_0$ ) vs Spectral Width ( $w$ ) with Simulation Results

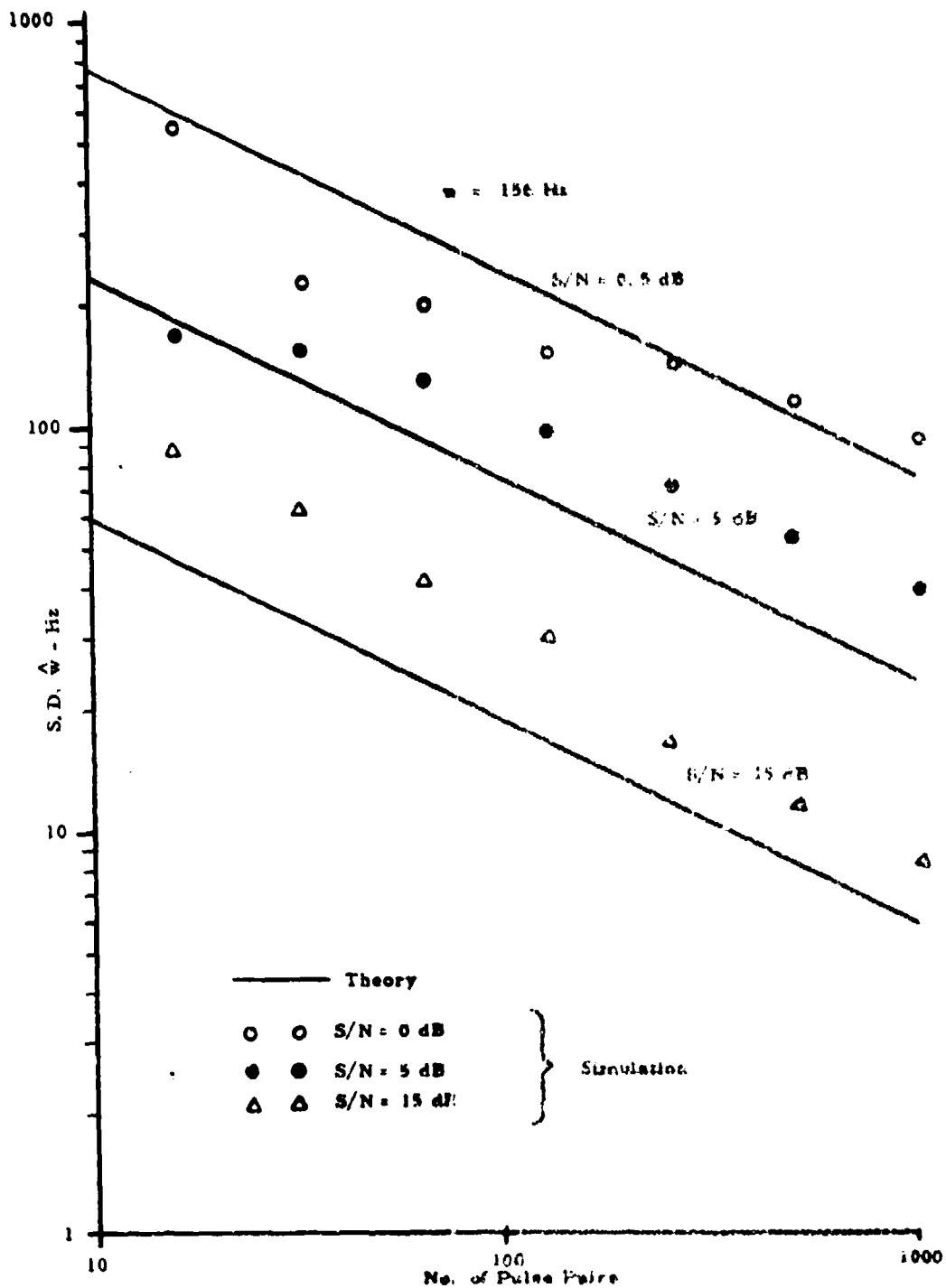


Figure 16. Theoretical Accuracy of Pulse Pair Estimates of Spectral Width ( $w$ ) vs Number of Samples Compared with Simulation Results

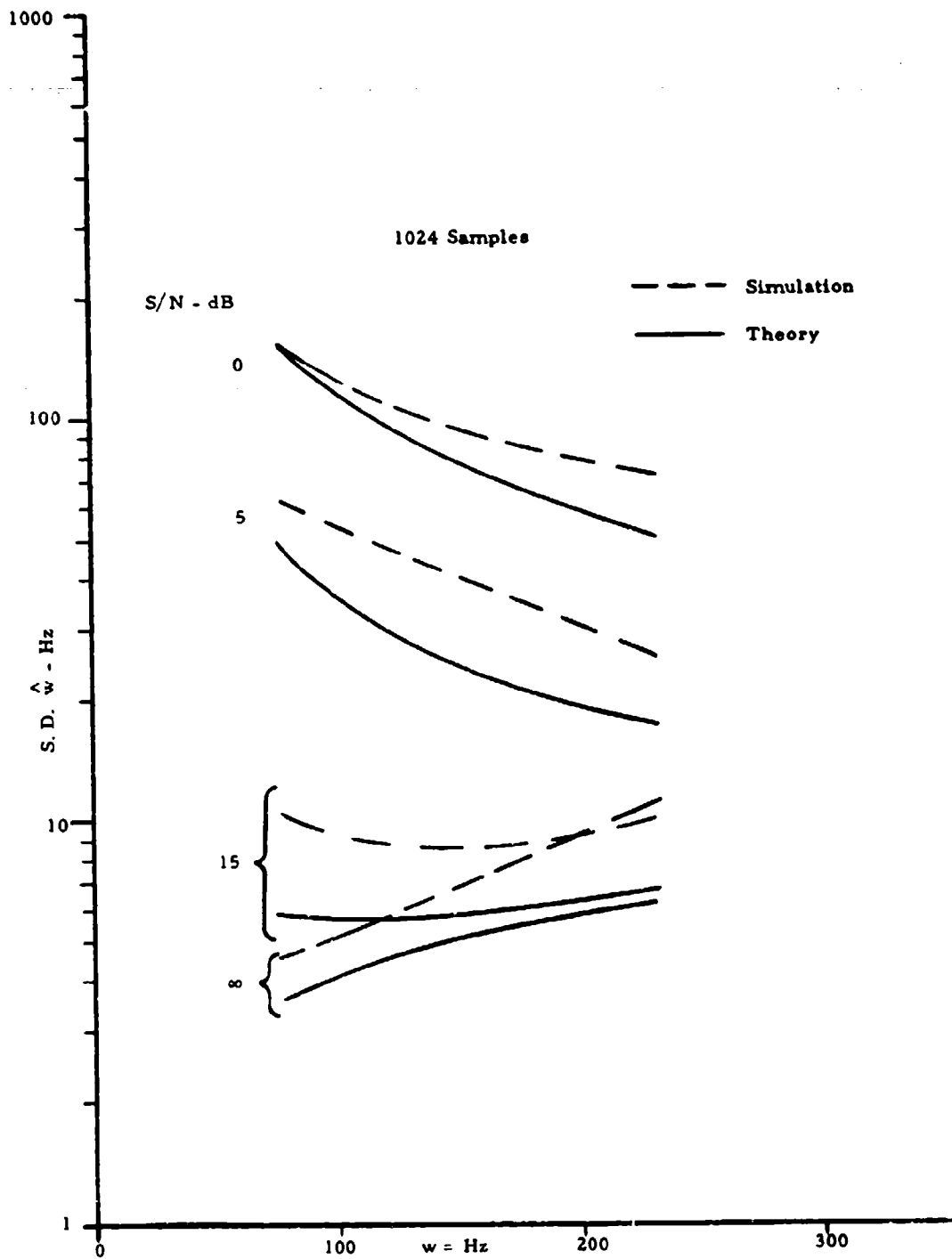


Figure 17. Theoretical Accuracy of Pulse Pair Estimates of Spectral Width ( $\hat{w}$ ) vs Actual Spectral Width ( $w$ ) Compared with Simulation Results

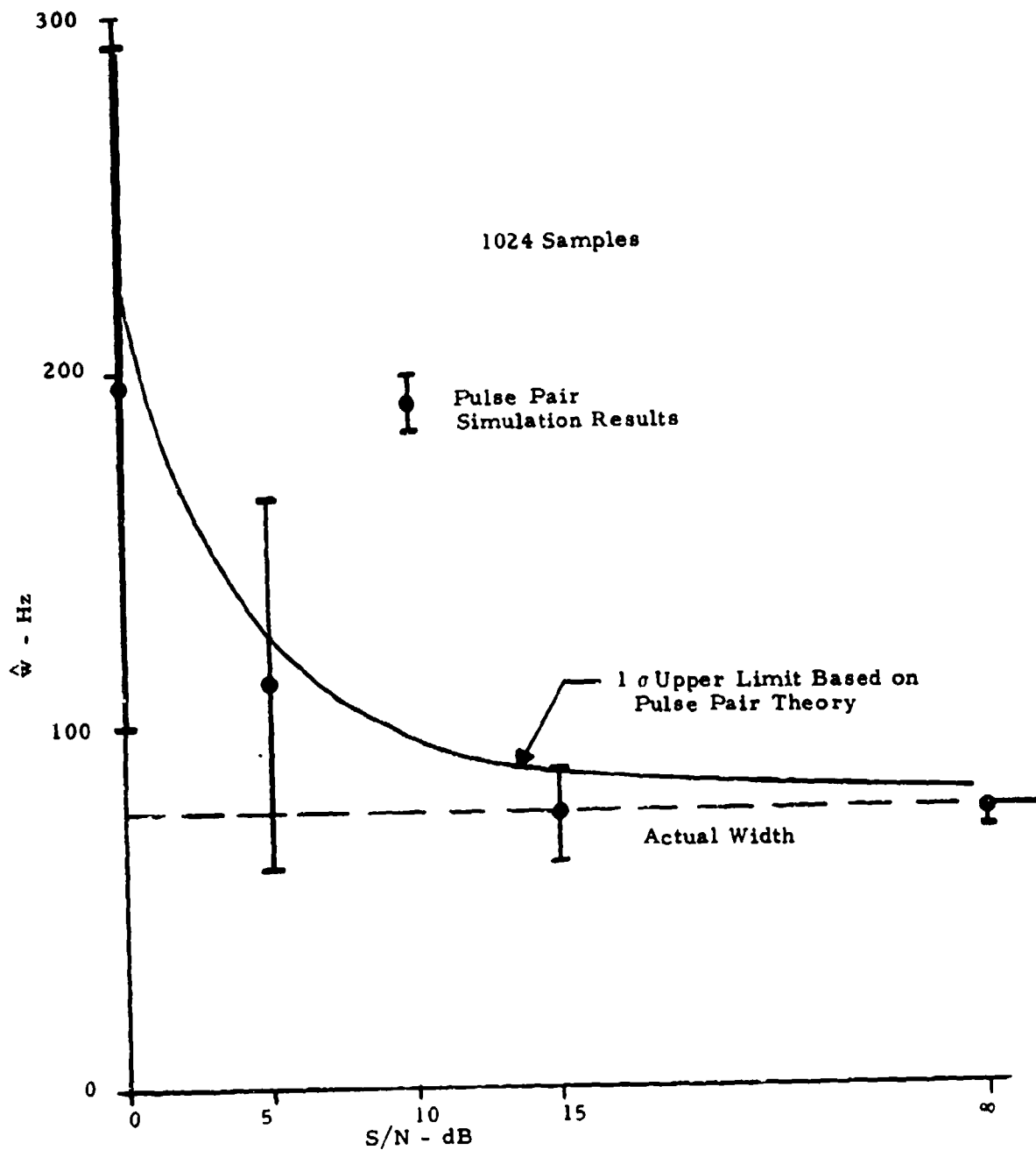


Figure 18. Theoretical Accuracy of Pulse Pair Estimates of Spectral Width ( $\hat{w}$ ) vs S/N Compared with Simulation Results (for  $f_0 = 300$  Hz;  $w = 78$  Hz)

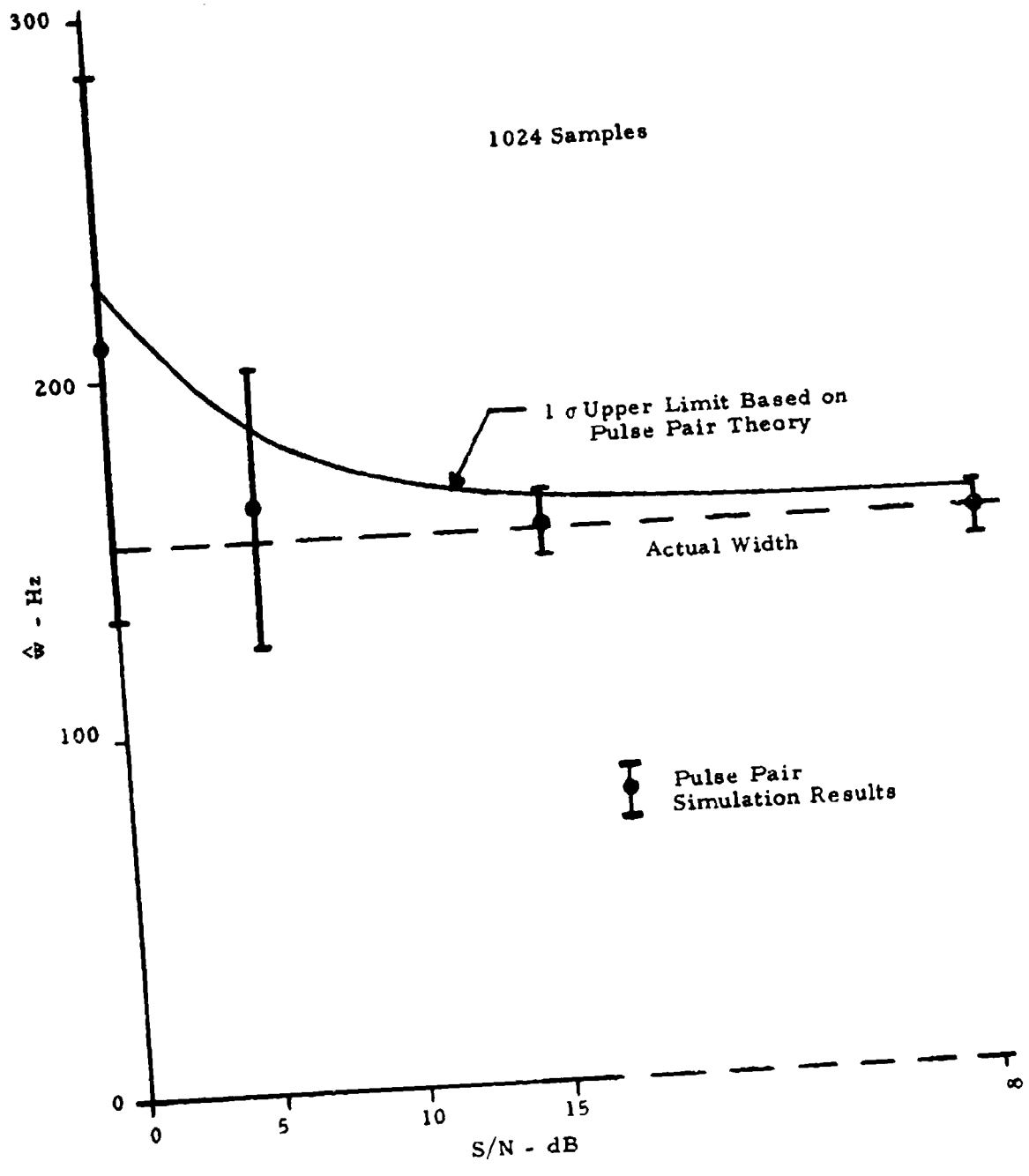


Figure 19. Theoretical Accuracy of Pulse Pair Estimates of Spectral Width ( $\hat{w}$ ) vs S/N Compared with Simulation Results (for  $f_o = 600$  Hz;  $w = 156$  Hz)

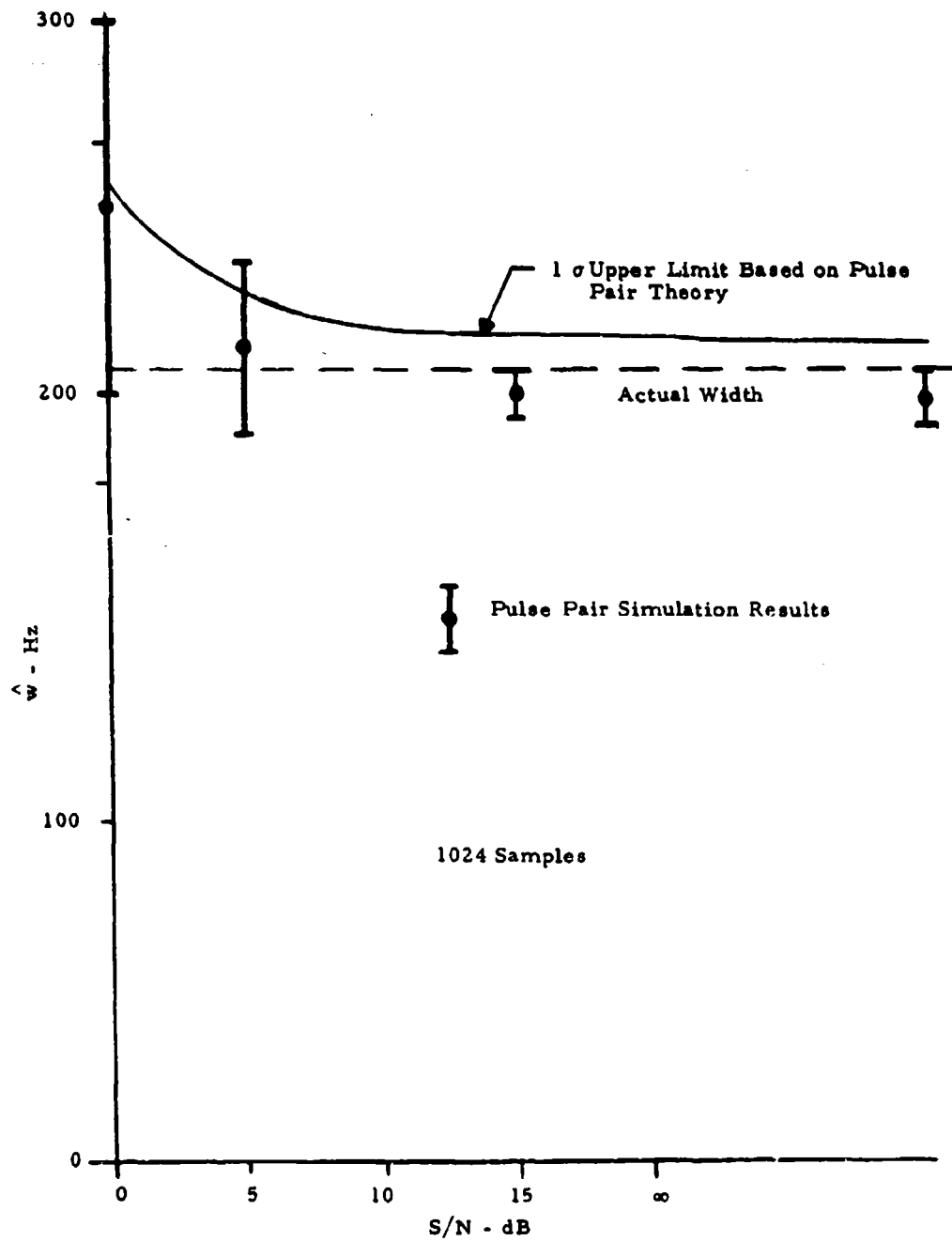


Figure 20. Theoretical Accuracy of Pulse Pair Estimates of Spectral Width ( $\hat{w}$ ) vs S/N Compared with Simulation Results (for  $f_0 = 900$  Hz;  $w = 234$  Hz)

### 3.2.4 Performance of Spectral Analysis Estimator

#### A. Computer Program

In order to provide a standard against which to compare the performance of the pulse pair estimators under varying conditions of signal to noise, the simulated doppler return generated by DOPGEN was also analyzed by the conventional spectral analysis method. As in the case of real Porcupine radar data (Section 3.1.1 above), the spectral parameter estimates were obtained in two steps. First, a spectral analysis is performed on an entire data block to yield its spectrum; then the mean and spectral width parameters are calculated from all spectral components above a given threshold level, for a range of threshold levels. The resulting estimates are printed out as functions of threshold level. This spectral analysis program is designated SPEC. As shown in the flowchart, Figure 21, the Spectral Analysis program searches the tape generated by DOPGEN and reads the data block whose number is specified on the input data card. The 1024 complex samples are then weighted using 60 dB Dolph-Chebyshev weighting coefficients and input into the FFT sub-routine. If desired, the FFT output will be plotted. Next, the mean and standard deviation are calculated based on all FFT output points above a specified threshold level. The threshold level is automatically incremented in steps of 2 dB starting at 2 dB below the maximum FFT output point and continuing to 40 dB below the maximum point. The mean and standard deviation values are printed on the line printer as a function of threshold level. The above procedure is repeated for each input data card until a blank card is encountered. SPEC coded in FORTRAN appears in Appendix C3.

#### B. Results

It was concluded in the discussion of results with Porcupine Radar input data (Section 3.1 above) that the spectral analysis estimator of  $\hat{f}_0$  was definitely satisfactory. Therefore, no further analysis and evaluation of the performance of this estimator was done with the results of the simulation tests.

On the other hand, there was interest in how well the thresholded spectral analysis estimator of spectral width ( $\hat{w}$ ) would show up against the simulated input data.

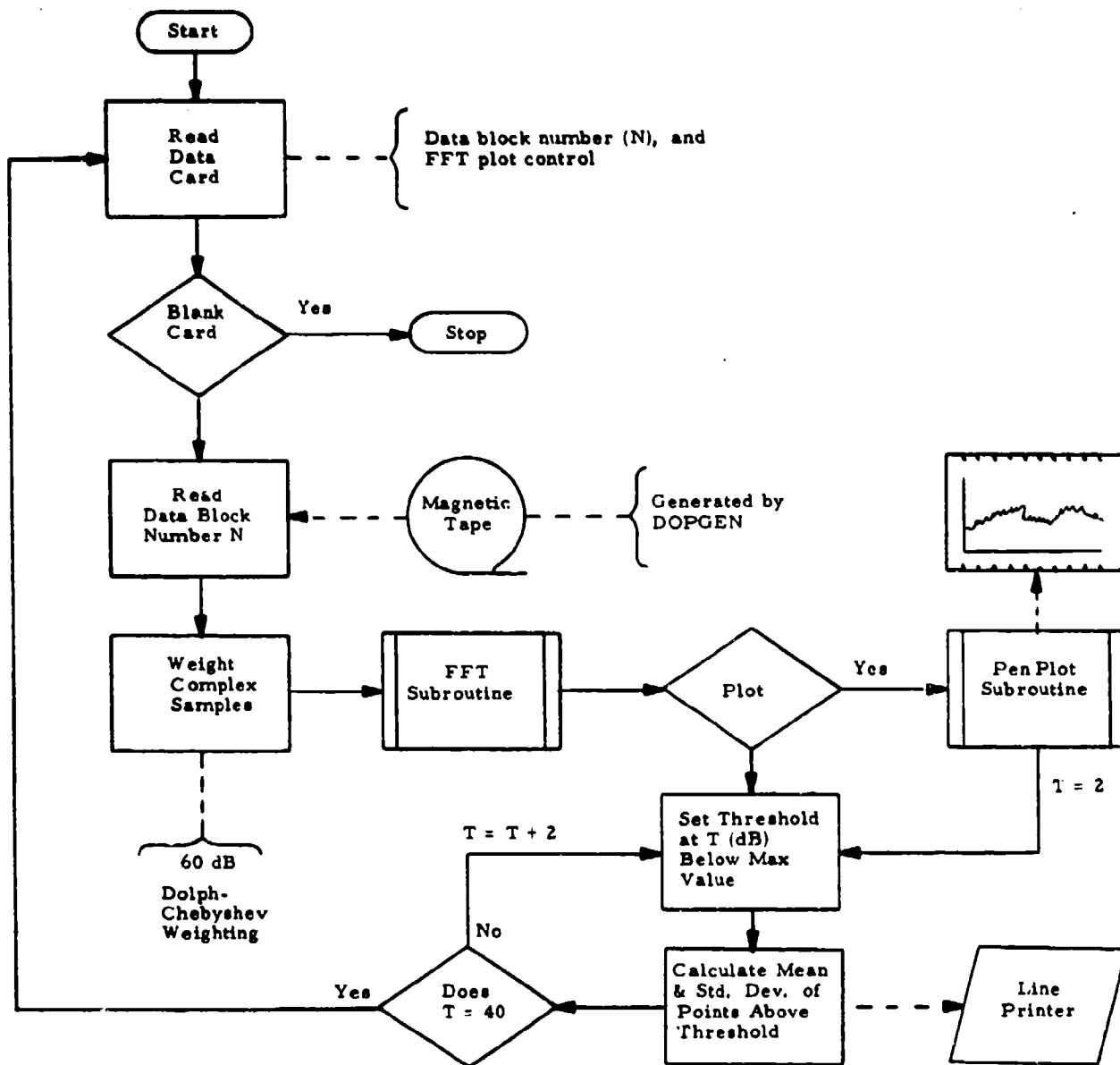


Figure 21. Flowchart of SPEC

Typical results are plotted in Figures 22, 23, and 24. Each figure depicts the width estimates produced by a single block of samples for different combinations of input data parameters,  $f_0$ ,  $w$  and  $S/N$ , as a function of threshold level. As was indicated earlier, no claim is made that the thresholded estimator of Eq.(3-4) is optimum. It is, however, straightforward and readily implementable by computer. To preclude possible bias effects from aliasing, the spectral width was calculated about the true mean,  $f_0$ . Despite these precautions, the width estimates again are shown to be very sensitive to the value of the threshold. Only in the cases of very high  $S/N$  do the estimates asymptotically approach the true width.

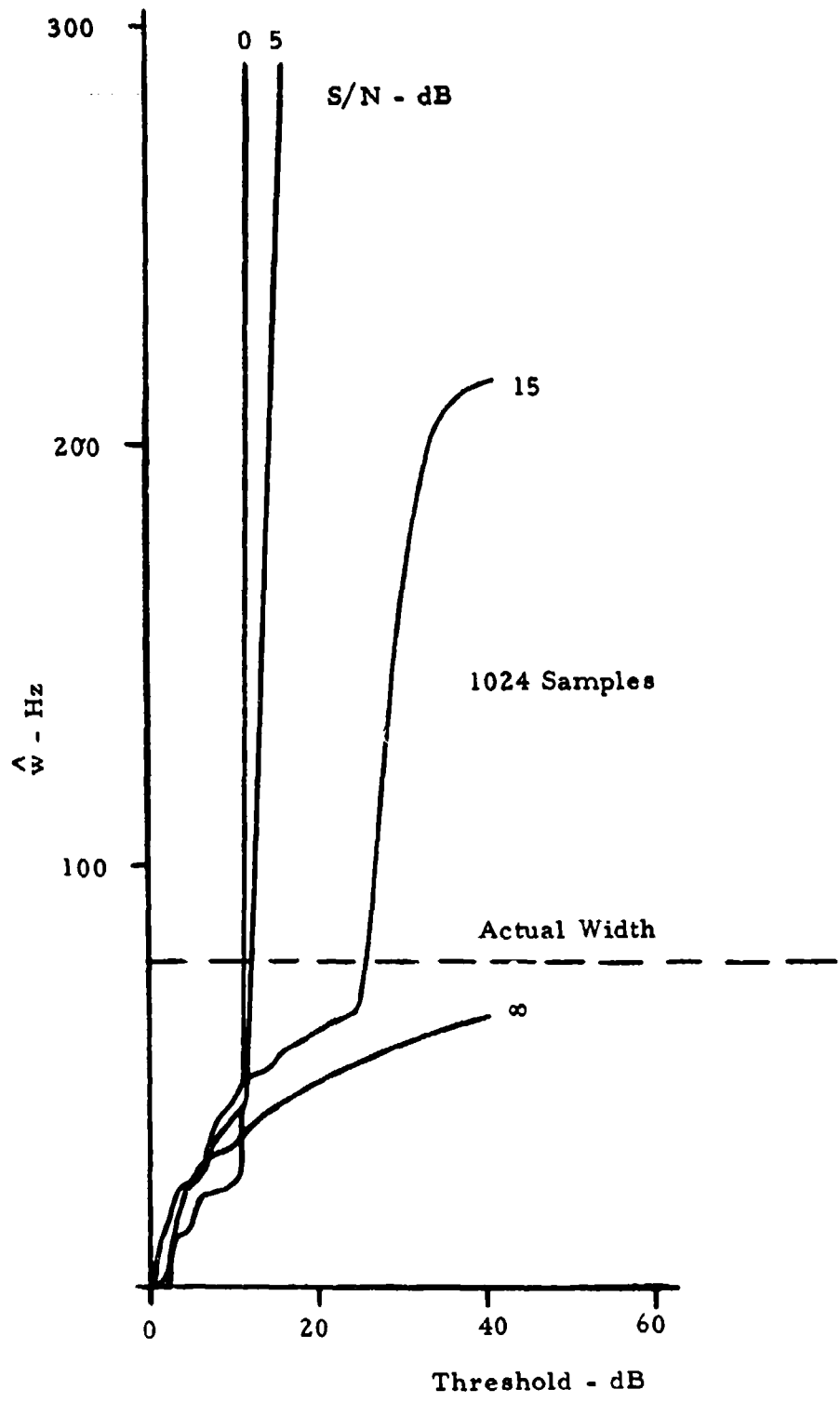


Figure 22. Spectral Analysis Width Estimates ( $\hat{w}$ ) vs Threshold Level for Simulated Input Data ( $f_0 = 300$  Hz;  $w = 78$  Hz)

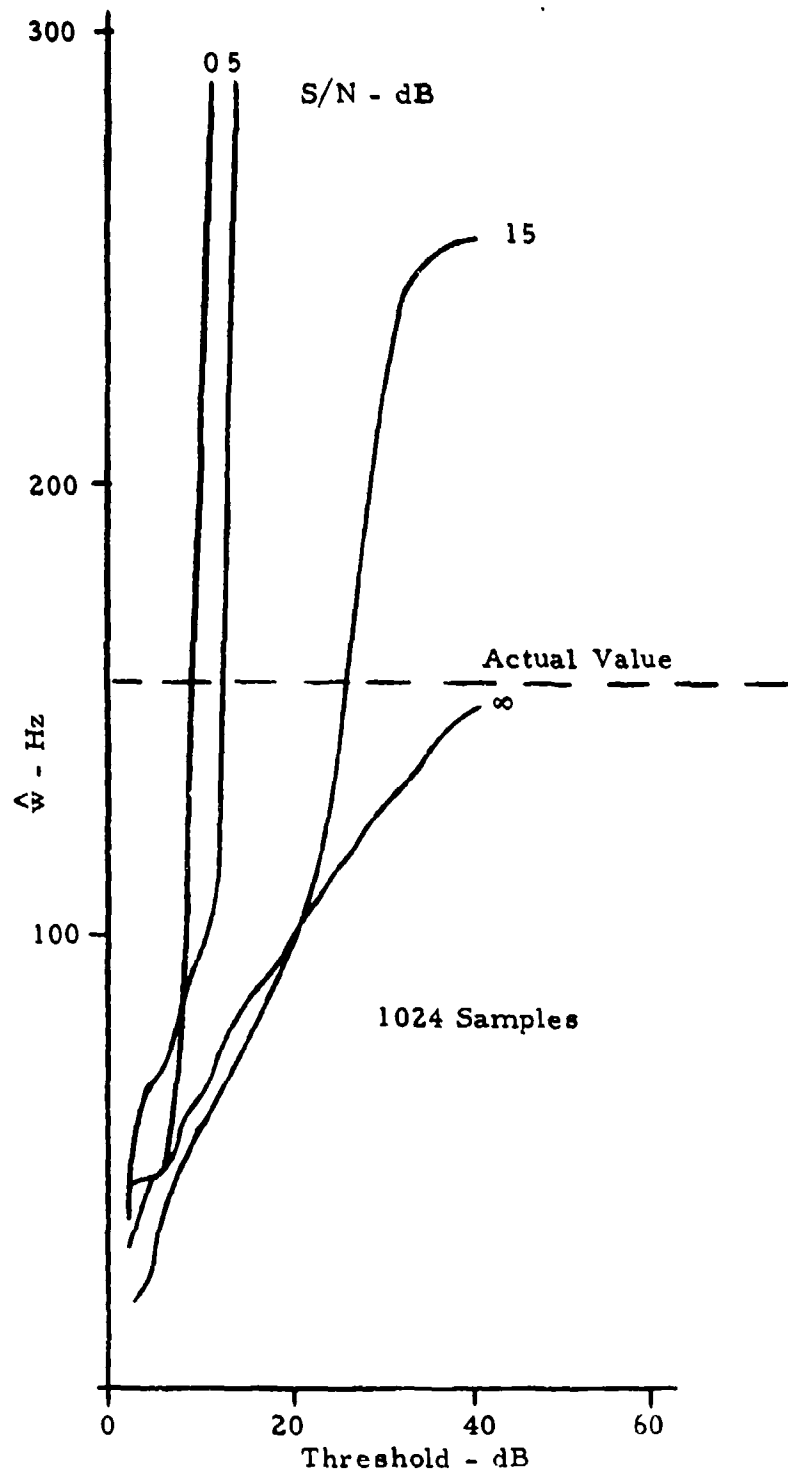


Figure 23. Spectral Analysis Width Estimates ( $\hat{w}$ ) vs Threshold Level for Simulated Input Data ( $f_o = 600$  Hz;  $w = 156$  Hz)

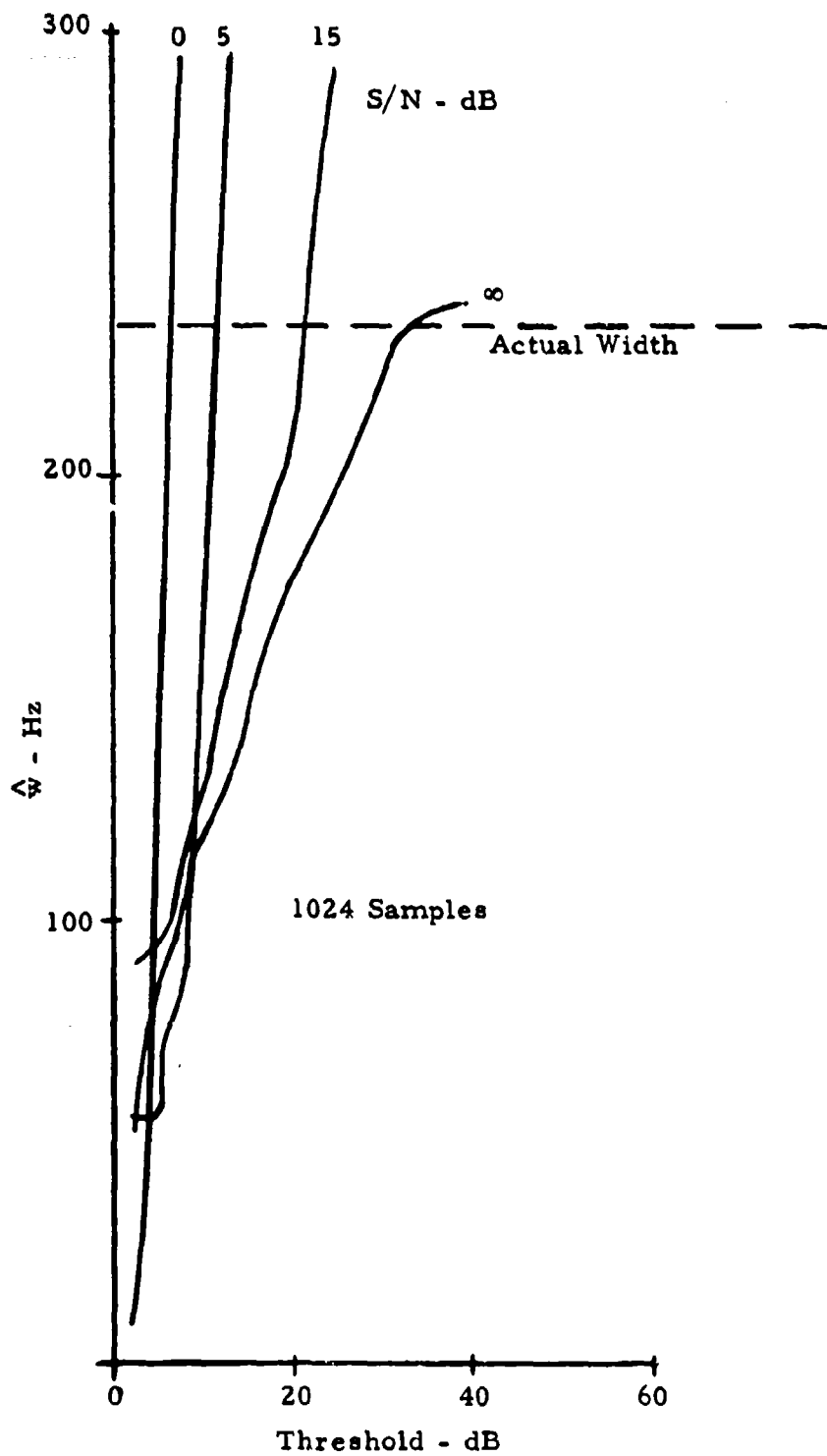


Figure 24. Spectral Analysis Width Estimates ( $\hat{w}$ ) vs. Threshold Level for Simulated Input Data ( $f_0 = 900$  Hz;  $w = 234$  Hz)

### 3.2.5 Comparison of the Width Estimators

The accuracy achieved by the pulse pair width estimator in the simulation tests is compared in Table 4 with the accuracy predicted from theory, and the estimates yielded by the spectral analysis estimator. The results are shown for all 12 cases of  $f_0$ ,  $w$  and  $S/N$ . (It should be noted that the pulse pair data is presented in the form of the standard deviation of the estimates from the true value, based on a statistical analysis of 20 estimates on as many independent blocks of simulated data for each case shown; whereas the spectrum analysis results are for a single block of samples for each case, as a function of threshold level.)

Table 4 and Figures 18-20 show that the pulse pair width estimates obtained with the 1024 samples and  $S/N$  in excess of 5 dB per pulse produces width errors of less than 3 dB for all cases tested. Translated into meteorological terms, for the Porcupine radar, actual widths of .2 m/sec were estimated at .3 m/sec with the equivalent at a 1/3 sec look (at 3300 pulses/sec) at a signal-to-noise ratio of 5 dB.

For a signal which is a Gaussian random variate with spectral density function

$$S(f) = \frac{\sigma_s^2}{\sqrt{2\pi} w} e^{-\frac{f^2}{2w^2}}$$

imbedded in white noise with spectral density coefficient  $N_0$ , the ratio of the peak spectral value to the rms noise background level in the frequency domain is given by

$$R_s = \frac{S(0)}{N_0} = \frac{\sigma_s^2}{\sqrt{2\pi} w N_0}$$

If this datum is sampled at the rate  $1/T$ , the per pulse signal-to-noise ratio is given by

$$\begin{aligned} S/N &= \frac{T}{N_0} \int c(f) df \\ &= \frac{T \sigma_s^2}{N_0} \end{aligned}$$

Table 4. Comparison Between Pulse Pair & Spectrum Analysis; Estimates of Spectral Width

Actual Parameters of Input Data		ESTIMATES										
		Pulse Pair Standard Deviation for 20 Blocks		$\hat{w}$ (Hz) by Spectrum Analysis (for 1 Block)								
		Theory	Simulation	Threshold Level -dB								
$f_o$ (Hz)	$w$ (Hz)	S/N (dB)	S.D. $\hat{w}$ (Hz)	S.D. $\hat{w}$ (Hz)	8	12	16	20	24	28	32	
1	300	78	0	110.	153.	23	263	634	722	748	752	752
2	300	78	5	46.	62.	37	79	369	559	617	628	630
3	300	78	15	8.7	10.4	38	51	57	62	66	131	193
4	300	78	$\infty$	3.05	4.6	33	39	45	49	54	56	59
5	600	156	0	70.	92.	86	399	608	686	699	702	702
6	600	156	5	29.	39.	88	133	380	506	545	555	556
7	600	156	15	6.7	8.6	51	66	82	98	123	195	239
8	600	156	$\infty$	4.5	7.0	61	75	88	102	113	124	133
9	900	234	0	51.	71.	422	655	752	767	772	772	773
10	900	234	5	21.	25.	93	264	464	562	586	591	592
11	900	234	15	8.5	10.0	118	151	184	216	292	327	336
12	900	234	$\infty$	7.1	11.3	107	129	155	177	193	215	233

1024 Samples Per Block

thus

$$D \hat{=} R_i/S/N = \frac{1}{\sqrt{2\pi} wT} .$$

Thus the spectral peak output of the simulated signals exceeds the input signal-to-noise ratio by approximately the values shown in Table 5.

Table 5

Peak Signal-to-Noise Improvement of Spectrum Analyzer

W (Hz)	D in dB
78	12.3
156	9.3
234	6.3

This calculation shows that the spectrum analyzer output reduction to mean and variance may be expected to perform extremely poorly when the threshold is set at approximately  $D + S/N$  (in dB) below the peak output. These points correspond approximately to the break points shown on Figures 22 to 24. Assuming that the spectrum analyzer threshold had been set 5 dB above the noise background level (high enough to assure that the noise peaks would not disturb the measurement), Figures 22 to 24 indicate that the measured widths would be as shown in Table 6.

It should again be noted that the data shown on Figures 22 - 24 represents only a single spectral sample and that the thresholds shown are measured with respect to the sample peak value. Table 6 attempts to incorporate this factor by using the breakpoints of the measurement, as the threshold level. These are at approximately the threshold shown in Table 6.

In summary, the spectrum analyzer measurements appear to consistently underestimate the width parameter while the pulse pair technique overestimates it. The simulation indicates that the accuracies available for basically the same data conditions are roughly comparable for the cases tested. Figures 22 - 24 indicate a marked sensitivity to threshold settings which is not directly evident in the pulse pair measurements. It is important to note that the pulse pair measurement of width uses an estimate of the noise background level also and thus has a

Table 6

Comparison of Pulse Pair and  
Spectrum Analyzer Derived Width Estimates

(Spectrum Analyzer Threshold Set 5 dB Above Average Background Noise)

Actual Width w	S/N Threshold Spectrum Analysis Estimate			Pulse Pair Estimate $\hat{w}$
	dB		$\hat{w}$	
78	0	7.3	22	180
	5	12.3	44	112
	15	22.3	64	75
156	0	4.3	47	209
	5	9.3	92	163
	15	10.3	95	157
234	0	1.3	37	283
	5	6.3	76	240
	15	16.3	204	226

corresponding parameter uncertainty in its process. In other words, both techniques require a measurement of the noise alone background to obtain useful final results.

The conclusion to be drawn from this comparison is that the pulse pair technique shows no evident lack of sensitivity as compared with the spectrum analyzer approach in situations characteristic of the meteorological applications.

## 4.0 HARDWARE REALIZATION

This section describes a real time digital processor design to reduce the pulse pair technique to practice. A brief theoretical review of the signal processing algorithms to be implemented, is followed by discussions and block diagrams of the processor and its key components. Design goals for the proposed pulse pair processor are defined, and its performance compared with CMF, Analog Spectrum Analyzer, and Fast Fourier Transform processors. Finally, the design tradeoffs to be considered during the design phase are discussed.

### 4.1 General Description of the Pulse-Pair Processor

This processor operates on the output of a radar, and is capable of producing real-time independent estimates of the spectral mean and width of a Doppler radar signal for each range cell viewed by the radar.

The processor accepts the radar IF signal and system trigger as inputs and computes the mean frequency (mean velocity) and spectral width (velocity distribution) in each of 256, 512, 768 or 1024 range cells, selectable by a front panel switch. Each range cell has a width of 0.5, 1 or 2 microseconds selectable by a front panel switch. The processor produces both analog outputs for viewing on real time displays, and digital outputs which may be remoted or recorded for future computer processing. An internal digital automatic gain control system independently measures the signal amplitude and adjusts the gain of the processor for each range cell processed to maintain a 90 dB dynamic range.

Although the pulse pair technique will work with either coherent or non-coherent radars, a coherent receiver output is necessary in order to provide complex samples of the target return to the processor. In addition, to achieve independent spectral estimates from range cell to range cell, the receiver gain must have a wide dynamic range and be range cell-to-cell controllable. Accordingly, the receiver requirements must be included as part of the processor considerations; how much of an existing radar receiver can be used as is and how much must be modified or incorporated as part of the processor depends upon the characteristics of the particular radar whose output is to be processed. The receiver for the Pulse Pair Processor described below is interfaced to match the Porcupine Radar.

## 4.2 Technical Description of the Pulse Pair Processor

The PPP performs spectral mean and width estimations according to equations (4-1) and (4-3) respectively, which are equivalent to earlier equations (2-9) and (2-10). They are rewritten here in more convenient form for the discussion of hardware.

$$\hat{f}_0 = \frac{\text{PRF}}{2\pi} \phi(\overline{z_{k+1} z_k^*}) \quad (4-1)$$

$$\hat{w} = \frac{\text{PRF}}{\pi\sqrt{2}} \sqrt{1 - \frac{|\overline{z_{k+1} z_k^*}|}{|\overline{z_k}|^2 - N_0^2}} \quad (4-2)$$

where the  $z$ 's are complex samples of signal plus noise, and  $N_0^2$  is the receiver noise power in the absence of signal.  $z^*$  denotes the complex conjugate of  $z$ . Equation (4-1) estimates mean frequency by determining the phase differences in pairs of complex samples ( $z_{k+1}$ ,  $z_k$ ), averaging these differences to find the mean phase difference, and scaling this mean phase difference by the PRF to form a mean frequency estimate. The phase differences averaged are weighted according to sample amplitude so that phase differences from strong returns count more than differences from weak returns. The results in Section 3 showed that as the number of samples processed increases, the accuracy of  $f_0$  improves asymptotically.

Equation (4-2) estimates spectral width  $\hat{w}$  in terms of signal coherence, including a correction for noise,  $N_0$ .

$$a = \frac{|\overline{z_{k+1} z_k^*}|}{|\overline{z_k}|^2 - N_0^2} \quad (4-3)$$

which may be measured. The parameter  $a$  is well-defined for all sampled signals including those with multimodal spectra. It may be seen from equation (4-3) that in the absence of noise  $a = 1$  for sinusoidal signals, and that  $a$  does not depend on mean signal frequency, which may exceed the complex sampling frequency (PRF). As is usual in sampled data systems, the signal bandwidth must not exceed the PRF.

Figure 25 shows the signal flow of the PPP algorithm applied to the sampled Doppler signal from one range cell. A delay and multiplier are used to form the products  $z_{k+1} z_k^*$ , which are then averaged. The sample energies  $|z_k|^2$  are also averaged, and function generators are used to compute  $\hat{f}_0$  and  $\hat{w}$ .

There are a number of alternate ways of deriving the noise correction term ( $\bar{N}_0^2$ ) required for the calculation of the width estimate. One such method is depicted in Figure 25. A measurement of receiver noise ( $n_0^2$ ) (which may be made, for example, at the output of the receiver at a range in excess of that in which any signal return may be expected) is corrected for the receiver gain applicable to the particular range cell, and introduced as the noise correction ( $\bar{N}_0^2$ ) in the width estimate ( $\hat{w}$ ). The correction factor is obtained by calibrating the receiver. The mean power output ( $\hat{p}$ ), which is made up of averaged measurements of signals plus noise, is delivered for use as the range cell's control signal to set the receiver AGC at its range.

Detailed design of the noise correction scheme has been deferred pending a hardware tradeoff study of alternate schemes, to be performed as part of a future hardware fabrication effort. The description of the system design which follows does not include the noise correction feature.

#### 4.3 System Design

The PPP system, shown in Figure 26, comprises a fast AGC IF amplifier, a two-point correlator, three (or four) digital integrators, a timing generator and several function generators. The PPP accepts 30 MHz IF input and produces digital and analog  $\hat{f}_0$ ,  $\hat{w}$ , range and integrated video outputs. The major subsystems of the PPP are described below.

##### 4.3.1 IF Amplifier Phase Detector

Achievement of the processor 90 dB dynamic range requires independent gain control in each range cell processed, which implies that the AGC voltage must be a time varying signal with a bandwidth comparable to the IF bandwidth. Such a system requires an IF amplifier of unusual design and closely integrated IF amplifier and AGC loop designs. For this reason, the IF amplifier and phase detectors are included in the PPP.

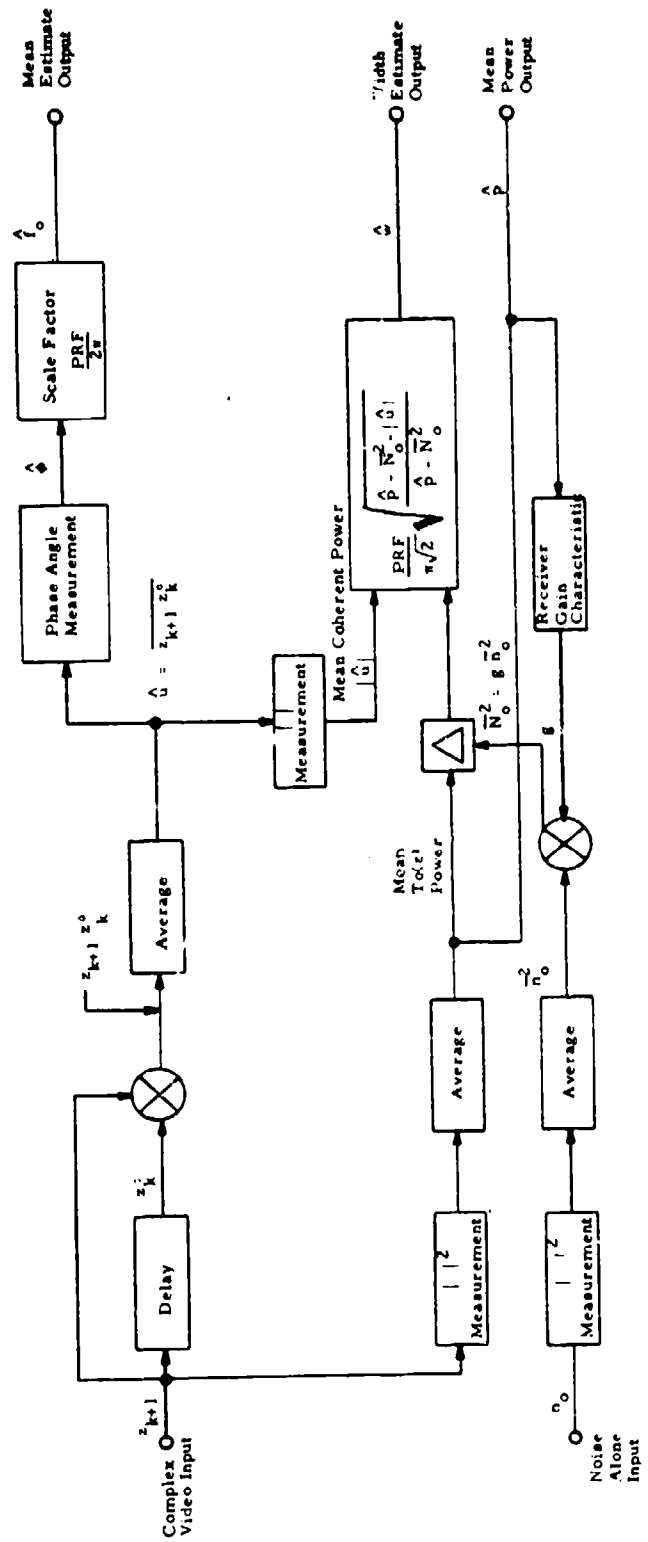


Figure 25. Pulse Pair Processor Signal Flow Diagram



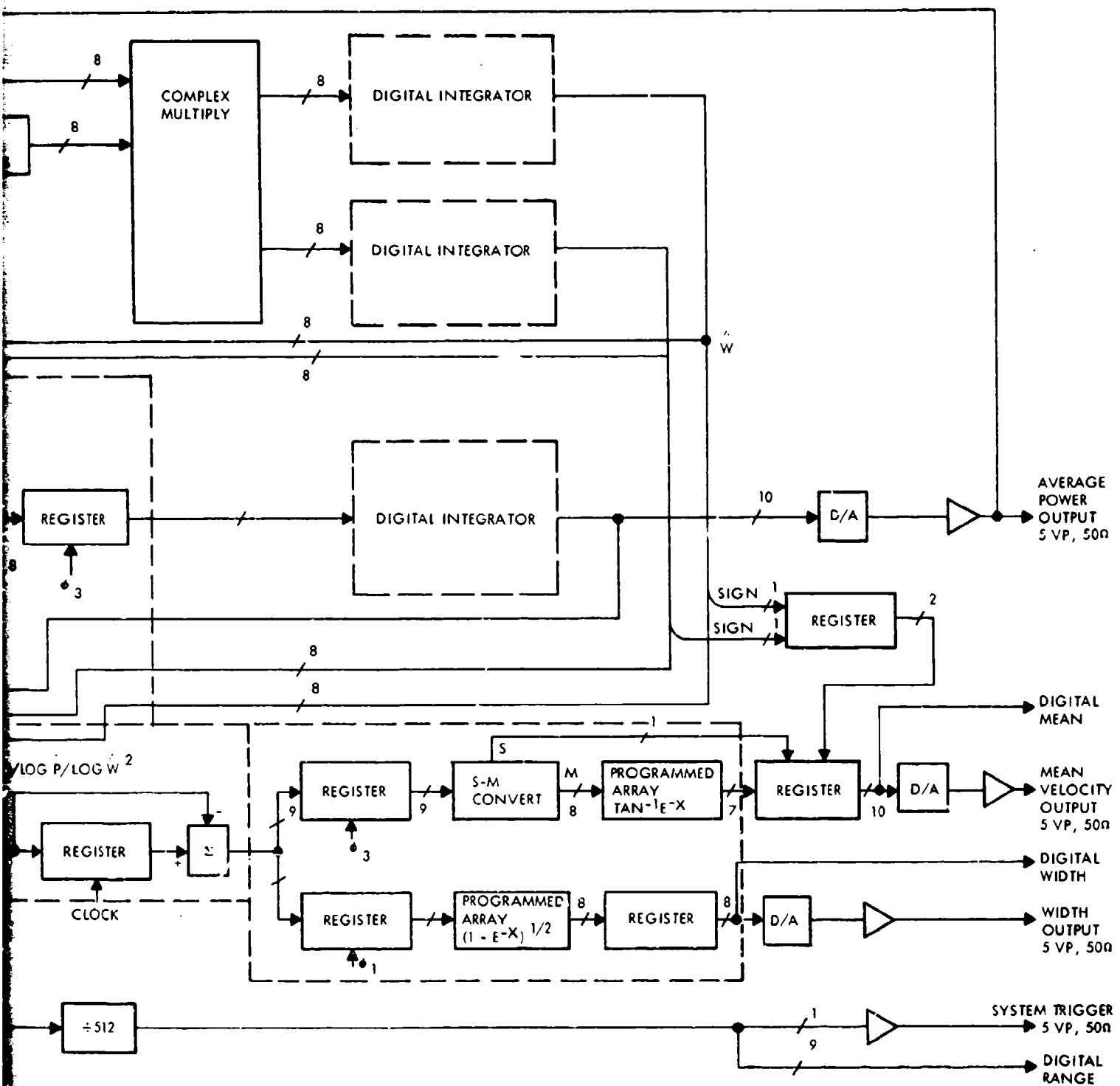


Figure 26. PPP Block Diagram

An IF amplifier-phase detector, Figure 27, was recently designed for the PORCUPINE radar which is acceptable for the PPP with slight modifications. The amplifier achieved approximately 60 dB AGC control range, with AGC applied to two out of a total of three identical gain stages. AGC response time was less than 200 ns. By adding AGC to the third gain stage, this amplifier is expected to achieve a 90 dB AGC control range without degradation of response time.

#### 4.3.2 Digitizer

The digitizer accepts in-phase and quadrature bipolar video and produces digitized estimates of these inputs. Eight bit quantization appears more than adequate to compute  $\hat{f}_0$  to the accuracy of the algorithm. A single A/D converter, such as the ILC Data Devices VADC-B, may be switched to quantize both input channels. This is preferable to the use of two simultaneous A/D converters because the single converter is less expensive and because problems of balancing the input channels are simplified by the use of a single A/D.

The suggested A/D converter can take an analog sample every 150 ns and is compatible with a range resolution of 500 ns. A 150 ns delay line must be used in one input channel to compensate for the A/D sampling delay. This A/D includes a sample and hold circuit, operates from standard +5V and  $\pm 15V$  power supplies and is contained on a single 8.8" x 4.5" circuit card.

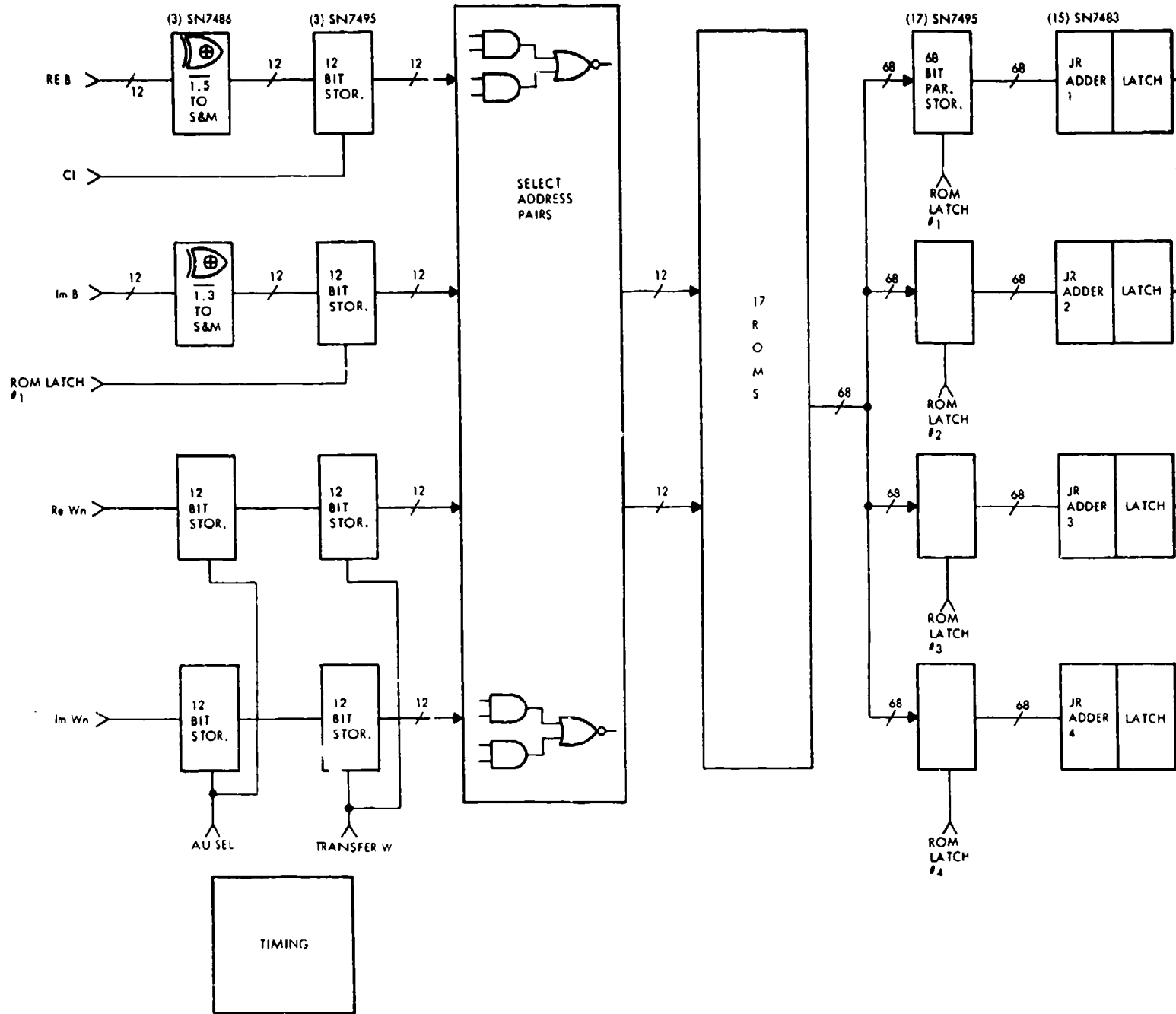
#### 4.3.3 Correlator

The correlator accepts complex video samples  $z_k$  from the digitizer and generates products of the form  $z_{k+1} z_k^*$  where the sample  $z_{k+1}$  is delayed by one range sweep time from the sample  $z_k$ . This delay is accomplished using MOS dynamic shift registers organized as 16 bits x 512 words. Recently available 1024 bit registers, such as the Intel 1404A, allow this delay to be fabricated quite compactly.

The complex multiplier which forms the  $z_{k+1} z_k^*$  products will be similar to the multiplier developed for a proprietary Raytheon FFT pulse compression system. This multiplier, shown in Figure 28, employs programmed arrays and adders to perform a 24 x 24 bit complex multiply and add every 0.5  $\mu$ s. Approximately 280 integrated circuits (DIP'S) are required, hence, the multiplier could be fabricated on four 72-DIP Augat panels. The PPP requires only a 16 x 16 bit complex multiplier; one circuit card could probably be saved by redesigning the FFT multiplier for the less demanding PPP requirement.







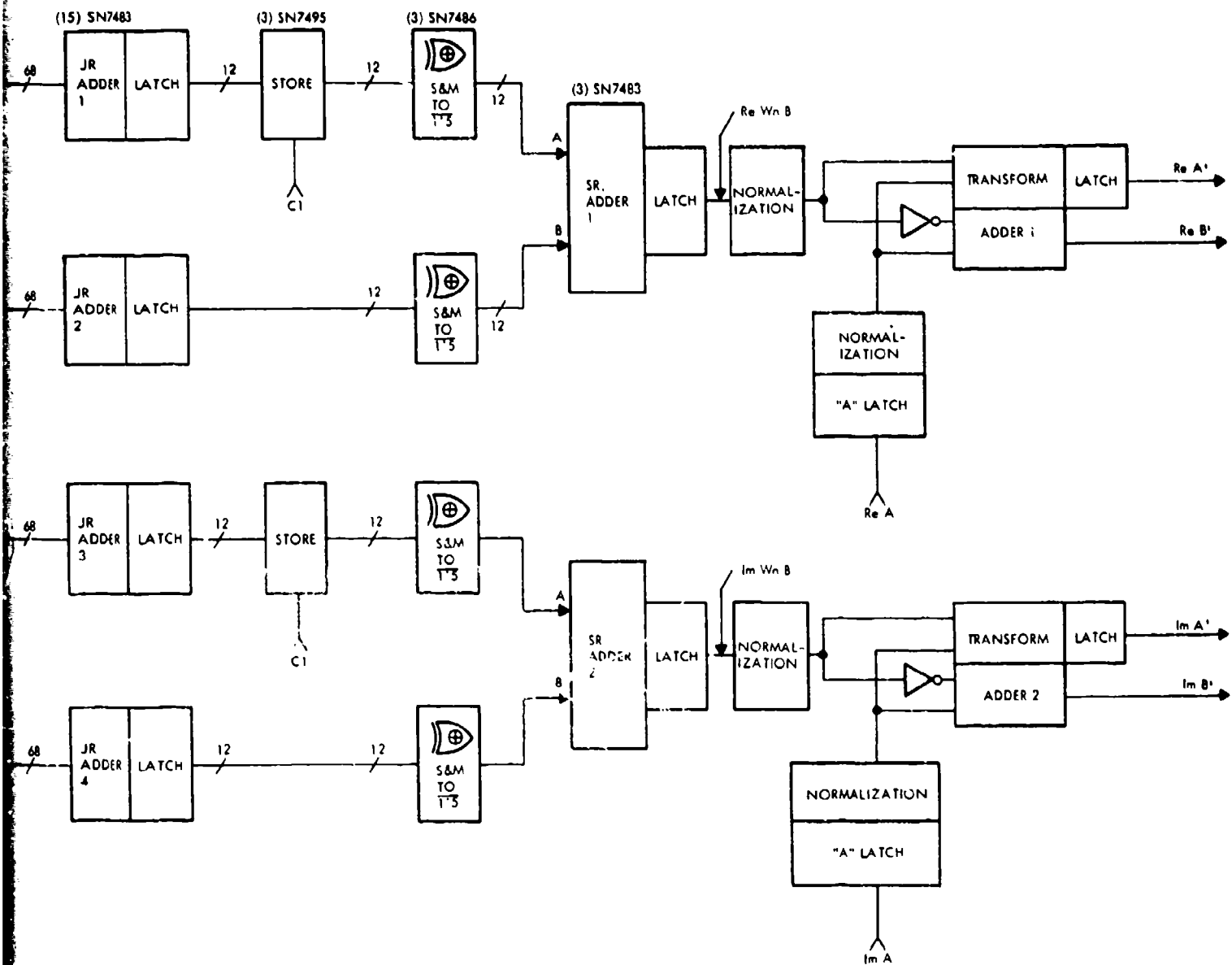


Figure 28. FFT Complex Multiplier

B

#### 4.3.4 Digital Integrators

A minimum of three digital integrators are required, two to compute the real and imaginary parts of  $\hat{u}$  and one to compute average power  $\hat{p}$ . These three integrators will be similar to an integrator recently designed for AFCRL, to minimize design costs, but the number of sweeps integrated will only be variable up to 1024 by factors of 2.

An integrated power measurement is required to operate the AGC. This output may be derived either from the power channel ( $\hat{p}$ ) of the PPP or through a separate integrator. The integrator which produces AGC output, whether separate or power channel, must be of the exponential rather than square moving window type. Theory shows that the gain and phase of the square window integrator,

$$|g_v(\omega)| = \frac{\sqrt{2}}{\omega T} \sqrt{1 - \cos \omega T} \quad (4-4)$$

$$\phi(\omega) = \text{Tan}^{-1} \frac{\cos \omega T - 1}{\sin \omega T} \quad (4-5)$$

makes it unsuitable for use in stable feedback loops with loop gain greater than 1. A design study should determine the performance differences in PPP's employing only three exponential window integrators, and PPP's employing three square window integrators to compute  $\hat{u}$  and  $\hat{p}$  and one exponential integrator for AGC.

#### 4.3.5 Function Generators

Three function generators are required for the PPP: a squared magnitude generator, a log generator and an output function generator. As shown in Figure 27, all function generators will consist of programmed arrays combined with registers, gating circuits and adders appropriate to the function computed.

Programmed arrays will contain the functions  $x^2$ ,  $\ln x$ ,  $\tan^{-1} e^{-x}$ , and  $(1 - e^{-x})^{1/2}$ . Each programmed array will consist of two integrated circuits such as the Monolithic Memories MM6300. The MM6300 is organized as an 8-bit in, 4-bit out array which may be programmed to contain any desired bit pattern; two such circuits form an 8-bit in, 8-bit out digital function generator. Approximately 50 ns after an 8-bit input word is supplied to the two programmed arrays, an 8-bit output word is available, allowing each pair of arrays to compute, and an output register to store, up to 4 outputs during an 0.5  $\mu$ s range cell.

These arrays may be ordered preprogrammed by the manufacturer or may be programmed by the user. Some vendors (e.g., Motorola) sell programmers for their arrays. Raytheon is currently constructing a programmer for the Monolithic Memories array in connection with a high speed pulse compression FFT development; this programmer is expected to be available for use in PPP fabrication.

#### 4.4 Performance

The detailed performance of the PPP will depend upon a number of design decisions, such as the AGC loop characteristics and the exact form of the function generators; operational considerations such as the signal characteristics and the number of pulses integrated; and the basic accuracy of the pulse pair algorithm. Analysis of these factors should be made in a design study but is beyond the scope of this hardware feasibility report.

By assuming a set of design goals for PPP hardware, subject to change in the design study, a few general comparisons may be made between the PPP and other related signal processing hardware. The design goals in Table 7 are therefore assumed for the purposes of comparison.

##### 4.4.1 Comparison with the CMF

The Porcupine Coherent Memory Filter is a spectrum analyzer, and does not produce estimates of spectral mean and width directly. Modification of the CMF to accommodate different pulse repetition rates and pulse widths is expensive and time consuming. By contrast, the PPP directly produces both spectral mean and width estimates in digital form in real time and operates over a variety of PRR's and pulse widths. Its quantitative estimates can also be recorded or remoted for further processing, plotting or display.

Recently, the CMF has been used to generate displays from which an observer can estimate mean frequency. The PPP can generate such displays with much finer time and frequency resolution by addition of a low cost voltage-to-delay converter. In addition, the PPP mean and standard deviation outputs can be directly displayed on a PPI scope to provide Plan Mean Indicator or Plan Width Indicator displays. These displays could be contoured if desired by using existing contour generator equipment (such as digital integrators).

The following compares the resolution capabilities of the CMF and PPP

	CMF	PPP	Unit
Range Resolution	1860	150	Meters (m)
Range Elements	192	1024	-
Velocity Resolution	$0.5 \lambda f_o / 50$	$0.5 \lambda f_o / 1024$	m/s
Dynamic Range	30	90	dB
Input Data Rate	1.75	32	M Bits/s
Size	1.0	0.3	19" rack x 6'

**Table 7. Proposed Design Goals for Pulse Pair Processor**

<u>DESIGN GOAL</u>	
Signal Input:	30 MHz IF, -80 dBm to +10 dBm Input Impedance 50 ohms
Reference Input:	30 MHz, 1 v p-p into 100 ohms
Trigger Input:	2 v p - 90 v p pulse 0.1 $\mu$ s - 100 $\mu$ s pulse width
Analog Outputs:	Mean frequency, standard deviation mean power and bipolar video Output Impedance - 50 ohms
Digital Outputs:	Mean frequency, standard deviation mean power and cell count buffered TTL level outputs 10, 8, and 10 bits respectively
Trigger Output:	Nominal 15 v p into 50 ohms - coincident with 1st range cell output
Range Cells Processed:	256, 512, 768 or 1024 nominal selectable by front panel switch
PRF:	300 pps - 5000 pps
Range Cell Width:	0.5 $\mu$ s, 1 $\mu$ s, or 2 $\mu$ s - selectable by front panel switch
Samples Processed:	16, 32, 64, 128, 256, 512, or 1024, selectable by front panel switch
Internal Quantization:	Digital signals shall be represented by a minimum of 8 bits at maximum input level
Dynamic Range:	Normal and quadrature bipolar video shall be represented internally by a minimum of 7 bits over an IF input range of 100 $\mu$ v rms - 1 v rms with 1024 samples processed
AGC:	The processor shall include a dynamic AGC system to provide independent gain control for each range cell processed.
Input Power:	115 v AC $\pm$ 10%, 60 Hz $\pm$ 2 Hz
Mechanical Configuration:	Mountable in a 19" rack cabinet
Ambient Temperature:	0 $^{\circ}$ C - 40 $^{\circ}$ C
Construction:	According to best commercial practice

#### 4.4.2 Comparison with Analog Spectrum Analyzers

Presently available analog spectrum analyzers such as the Federal Scientific "Ubiquitous" may, like the CMF, be used to generate a display from which an observer can estimate spectral means and widths indirectly. Unlike the CMF and PPP, however, such analyzers are not presently capable of processing the entire output of a weather radar in real time, and cannot generate any real-time displays. The following compares the resolution of the PPP and Ubiquitous analyzer.

	Ubiquitous	PPP	Unit
Range Resolution	1200 <sup>1</sup>	150	Meters (m)
Range Elements	10	1024	-
Velocity Resolution	$0.5 \lambda f_0 / 500$	$0.5 \lambda f_0 / 1024$	m/s
Dynamic Range	40	90	d/B
Input Data Rate	0.60 <sup>2</sup>	32	M Bits/s
Size	0.3	0.3	19" rack x 6'

- 1 Analyzer, operating without external sample and hold system
- 2 Maximum continuous

#### 4.4.3 Fast Fourier Transform Processing

FFT processing to compute spectral mean and width may be performed either by computer or by special purpose hardware. Computer processing requires that the weather radar signal be recorded and analyzed in non-real time, but subject to this restriction can provide essentially any desired frequency resolution. The PPP is compared below to a special purpose hardware FFT recently developed by Raytheon for pulse compression.

	FFT	PPP	Unit
Range Resolution	150	150	Meters (m)
Range Elements	2(1024)	1024	-
Velocity Resolution	$0.5 \lambda f_0 / 2048$	$0.5 \lambda f_0 / 1024$	m/s
Dynamic Range	60	90	dB
Input Data Rate	(32)	32	M Bits/s
Size	2(4)	0.3	19" rack x 6'

Numbers in ( ) indicate anticipated values for a 1024 gate machine.

#### 4.5 Conclusions

A hardware PPP capable of computing spectral mean and width for each of 1024  $1/2$ - $\mu$ s radar range gates appears completely feasible at this time. The processor can be fabricated primarily from available, designed components and is expected to occupy no more than 24" of 19" rack space. No other signal processing device now available can approach the dynamic range and data throughput capabilities of the PPP, except possibly the FFT, which would cost approximately 10 times more than a PPP of comparable resolution.

Table 7 gives a summary of the design goals for the proposed signal processor.

In the design phase of the PPP, detailed design tradeoffs of the following items must be accomplished.

1. The dynamic AGC loop
2. The digital function generation
3. The radar calibration system
4. The noise monitoring system

## 5.0 CONCLUSIONS AND RECOMMENDATIONS

The preceding sections of this report show analytically and verify by data from controlled simulation experiments that the pulse pair technique produces estimates of spectral mean and width that have predictable accuracy over a wide range of non-ideal operating conditions. Performance for unimodal spectra is insensitive to spectral shape and the degree of correlation between successive pulse pairs; the theory stands up under conditions of poor signal-to-noise ratio.

From a processor standpoint, it is shown that a flexible digital pulse pair processor capable of handling a large number of range cells simultaneously is feasible, and that it could be arranged to easily match a variety of radars and radar operating conditions, including PRFs, pulse widths and data rates. A theoretical basis for optimizing the waveform parameters of a radar for pulse pair processing is also presented.

A hardware implementation of a flexible digital pulse pair processor suitable for exploring the utility of the technique in real time processing of weather radar data is proposed. The design goals are defined, and its performance is compared with other contemporary signal processors.

The experimental work together with the simulation studies demonstrate that the pulse pair technique can yield good quality estimates of mean and variance using radar data at signal-to-noise ratios obtainable with existent Doppler weather radars. The hardware tradeoff studies as well as the comparative performance characteristics demonstrate that the pulse pair technique is not only feasible but efficient.

Based on these conclusions, the construction of a flexible experimental model of such a real-time pulse pair processor is recommended for the purpose of collecting a large data base on observable conditions. Experience gained while conducting research with the experimental model will provide the basis for defining the specifications for simpler models intended for operational use. A study should also be made to determine the best means to display, plot, and/or record the resulting data for further analysis, reduction and evaluation.

The fabrication phase for the experimental model should be preceded by a design evaluation phase, during which the final parameters for the equipment can be established from the results of tradeoff studies.

It is further recommended that some additional analysis be performed to provide theoretical guidelines for comparing pulse pair analysis to spectra data processors. In particular, although the theory of pulse pair estimation has now been established, no theoretical foundation exists at present for predicting the performance of width estimates derived from spectral analyzer data; such a theoretical foundation should be developed. Analyses are also required to properly relate and interface the pulse pair processor with particular radars, ancillary devices, and operational usages as a research tool.

## REFERENCES

1. Hofstetter, E. M., "Simple Estimates of Wake Velocity Parameters," Tech. Note 1970-11, 23 April 1970, M.I.T., Lincoln Laboratory, Lexington, Mass.
2. Rummler, W. D., "Introduction of a New Estimator for Velocity Spectral Parameters," Tech. Memo MM-68-4121-5, 3 April 1968, Bell Telephone Laboratories, Whippany, N.J.
3. Rummler, W. D., "Accuracy of Spectral Width Estimators Using Pulse Pair Waveforms," Tech. Memo MM-68-4121-14, 29 October 1968, Bell Telephone Laboratories, Whippany, N.J.
4. Rummler, W. D., "Two-Pulse Spectral Measurements," Tech. Memo MM-68-4121-15, 7 November 1968, Bell Telephone Laboratories, Whippany, N.J.
5. "Doppler Signal Processing and Instrumentation for Modified 'Porcupine' C-Band Pulse Doppler Radar," Final Report, May 1971, on Raytheon, Wayland, Mass. Contract No. F19628-68-0345 with AFCRL (pp 1-39 through 1-49).
6. Berger, T., "Analysis of Data from Pulse Pair Feasibility Experiment," Tech. Memo TB-108, September 9, 1970, Raytheon Co., Wayland, Mass.
7. Levin, M. J., "Generation of a Sampled Gaussian Time Series Having a Specified Correlation Function," IRE Trans. on Information Theory, Vol. IT-6, pp. 545-548, December 1960.

## APPENDIX A

### ANALYSIS OF ACCURACY OF SPECTRAL PARAMETER ESTIMATES BY PULSE PAIR ESTIMATION

H. L. Groginsky

#### ABSTRACT

This appendix gives a mathematical analysis of the performance of a pulse pair estimator of spectral mean and variance. It assumes that complex data (I & Q) is collected at a uniform rate from a distributed target whose underlying spectral density function is  $G(f)$  and that  $G(f)$  is observed only after it is mixed with white additive noise.

#### I. Introduction

If the signal spectrum is written as

$$G(f) = \frac{S}{w} R\left(\frac{f-f_0}{w}\right) \quad (1)$$

with  $R(f)$  real and positive for all  $f$ ,

$$R(-f) = R(f), \quad (2)$$

$$\int R(f) df = 1, \quad (3)$$

$$\int f R(f) df = 0, \quad (4)$$

$$\int f^2 R(f) df = 1, \quad (5)$$

$S$  = signal power,

and if the data  $r_k$  is given by

$$r_k = s_k + n_k \quad (6)$$

then the pulse pair estimators of  $f_0$  and  $W$  are given by

$$\hat{f}_0 = \frac{1}{2\pi T} \tan^{-1} \left( \frac{\text{Im} \{X\}}{\text{Re} \{X\}} \right) \quad (7)$$

and

$$\hat{w}^2 = \left( \frac{1}{2\pi T} \right)^2 \left[ 1 - \frac{|X|}{Y - \sigma_n} \right] \quad (8)$$

where

$$X = \frac{1}{M} \sum_{n=0}^{M-1} r_k r_{k+1}^* \quad (9)$$

$$Y = \frac{1}{M} \sum_{n=0}^{M-1} |r_k|^2 \quad (10)$$

$$\sigma_n = \langle n_k n_k^* \rangle = \langle |n_k|^2 \rangle \quad (11)$$

## 2. Spectral Mean Estimates

Let

$$g(\tau) = \int_{-\infty}^{\infty} G(f) e^{j2\pi f\tau} df \quad (12)$$

then

$$\langle s_k s_{k+j}^* \rangle = g(jT) \quad (13)$$

$$\langle s_k s_{k+j} \rangle = 0 \quad (14)$$

$$\langle n_k n_{k+j}^* \rangle = N \delta_{kj} \quad (15)$$

$$\langle n_k n_{k+j} \rangle = 0 \quad (16)$$

where

$$s_k = s(kT).$$

and  $\delta_{kj}$  is the Kronecker delta function.

Note that

$$\begin{aligned}
 g(T) &= \frac{S}{w} \int R\left(\frac{f-f_0}{w}\right) e^{j2\pi fT} df \\
 &= S e^{j2\pi f_0 T} \int R\left(\frac{f-f_0}{w}\right) e^{j2\pi \frac{(f-f_0)wT}{w}} df/w \\
 &= S e^{j2\pi f_0 T} \rho(wT)
 \end{aligned} \tag{17}$$

and that  $\rho(wT)$  is real.

Now

$$\begin{aligned}
 \langle X \rangle &= \frac{1}{M} \sum_{k=0}^{M-1} r_k r_{k+1}^* = g(T) \\
 &= S e^{j2\pi f_0 T} \rho(wT)
 \end{aligned} \tag{18}$$

Since  $S$  and  $\rho$  are real,

$$\arg \langle X \rangle = 2\pi f_0 T \tag{19}$$

which shows that the mean estimator is unbiased.

Now consider

$$\tan \hat{\theta} = \frac{\text{Im} \{X\}}{\text{Re} \{X\}} \tag{20}$$

$$\text{with } \hat{\theta} = 2\pi f_0 T \tag{21}$$

If  $\hat{\theta}$  is to be a useful estimator,  $\hat{\theta} \approx \theta_T$ , where  $\theta_T$  is the true mean phase change per pair. Writing

$$\hat{\theta} = \theta_T + \delta\hat{\theta}, \tag{22}$$

$$\text{Re} \{X\} = \text{Re} \{g(T)\} + \epsilon_1, \tag{23}$$

$$\text{Im} \{X\} = \text{Im} \{g(T)\} + \epsilon_2 \tag{24}$$

we have

$$\begin{aligned} \tan \theta_T &= \frac{\hat{\delta \theta}}{\cos^2 \theta_T} = \frac{\text{Im}\{g(T)\} + \epsilon_2}{\text{Re}\{g(T)\} + \epsilon_1} \\ &= \frac{\text{Im}\{g(T)\}}{\text{Re}\{g(T)\}} \left(1 + \frac{\epsilon_2}{\text{Im}\{g(T)\}}\right) \left(1 - \frac{\epsilon_1}{\text{Re}\{g(T)\}}\right) \end{aligned} \quad (25)$$

from which it follows that

$$\delta \hat{\theta} \approx \frac{\text{Re}\{g(T)\} \epsilon_2 - \text{Im}\{g(T)\} \epsilon_1}{|g(T)|^2} \quad (26)$$

$$\text{since } \cos \theta_T = \frac{\text{Re}\{g(T)\}}{|g(T)|} \quad (27)$$

Now by defining a complex error

$$\epsilon = \epsilon_1 + j\epsilon_2 \quad (28)$$

we may write

$$\begin{aligned} \delta \hat{\theta} &= \frac{(g(T) + g^*(T))(\epsilon - \epsilon^*) - (g(T) - g^*(T))(\epsilon + \epsilon^*)}{4j |g(T)|^2} \\ &= \frac{g^*(T) \epsilon - \epsilon^* g(T)}{2j |g(T)|^2} \\ &= \frac{\text{Im}(g^* \epsilon)}{|g|^2} \\ &= \text{Im} \left( \frac{\epsilon}{g(T)} \right) \end{aligned} \quad (29)$$

Now define a new complex estimator error

$$\delta \hat{\psi} = \operatorname{Re} \left( \frac{\varepsilon}{g(T)} \right) \quad (30)$$

then

$$\delta \hat{\psi} + j \delta \hat{\theta} = \frac{\varepsilon}{g(T)} \quad (31)$$

Thus

$$\langle (\delta \hat{\psi})^2 \rangle + \langle (\delta \hat{\theta})^2 \rangle = \left\langle \left| \frac{\varepsilon}{g(T)} \right|^2 \right\rangle \quad (32)$$

and

$$\langle (\delta \hat{\psi})^2 \rangle - \langle (\delta \hat{\theta})^2 \rangle = \operatorname{Re} \left\langle \frac{\varepsilon^2}{g^2(T)} \right\rangle \quad (33)$$

from which it follows that

$$\begin{aligned} \operatorname{Var} \delta \hat{\theta} &= \langle (\delta \hat{\theta})^2 \rangle = \frac{1}{2} \left[ \left\langle \left| \frac{\varepsilon}{g(T)} \right|^2 \right\rangle - \operatorname{Re} \left\langle \frac{\varepsilon^2}{g^2(T)} \right\rangle \right] \\ &= \frac{1}{2} \operatorname{Re} \left\{ \left\langle \left| \frac{\varepsilon}{g(T)} \right|^2 \right\rangle - \left\langle \frac{\varepsilon^2}{g^2(T)} \right\rangle \right\}. \end{aligned} \quad (34)$$

Now

$$X = g(T) + \varepsilon \quad (35)$$

Therefore

$$\left\langle \left| \frac{\varepsilon}{g(T)} \right|^2 \right\rangle = \frac{\operatorname{Var} |X|^2}{|g(T)|^2} \quad (36)$$

and

$$\left\langle \frac{\varepsilon^2}{g^2(T)} \right\rangle = \frac{\operatorname{Var} X^2}{g^2(T)}. \quad (27)$$

Note that  $\operatorname{Var} X^2$  is a complex quantity defined by

$$\begin{aligned} \operatorname{Var} X^2 &= \langle (X - g(T))^2 \rangle \\ &= \langle X^2 \rangle - g^2(T) \end{aligned} \quad (38)$$

and

$$\operatorname{Var} \delta \hat{\theta} = \frac{1}{2} \operatorname{Re} \left\{ \operatorname{Var} \frac{|X|^2}{|g(T)|^2} - \operatorname{Var} \frac{X^2}{g^2} \right\} \quad (38 \text{ bis})$$

Now we can evaluate the requisite expressions using the assumption of Gaussian statistics for the raw input data as follows:

$$\begin{aligned}
 |X| &= \frac{1}{M^2} \sum_{k=0}^{M-1} \sum_{l=0}^{M-1} \langle r_k r_{k+1}^* r_l r_{l+1}^* \rangle \\
 &= \frac{1}{M^2} \sum_{k=0}^{M-1} \sum_{l=0}^{M-1} \left[ \langle r_k r_{k+1}^* \rangle \langle r_l r_{l+1}^* \rangle \right. \\
 &\quad \left. + \langle r_k r_l^* \rangle \langle r_{k+1} r_{l+1} \rangle \right. \\
 &\quad \left. + \langle r_k r_{l+1} \rangle \langle r_{k+1} r_l^* \rangle \right] \tag{39}
 \end{aligned}$$

From (13)-(16) it follows that

$$\begin{aligned}
 \text{term 1} &= |g(T)|^2 \\
 \text{term 2} &= \left\{ \begin{array}{ll} |g((l-k)T)|^2 & l \neq k \\ |S+N|^2 & l = k \end{array} \right. \\
 \text{term 3} &= 0.
 \end{aligned}$$

Note  $S/N$  is the per sample signal to noise ratio. For notational convenience we will write

$$g_n = g(nT). \tag{41}$$

Then

$$\begin{aligned}
\langle |X|^2 \rangle &= |g_1|^2 + \frac{1}{M^2} \sum_{k=0}^{M-1} \sum_{\ell=0}^{M-1} |g_{\ell-k}|^2 \\
&+ \frac{1}{M^2} \sum_{k=0}^{M-1} \left[ (S+N)^2 - S^2 \right] \\
&= |g_1|^2 + \frac{1}{M} \left[ (S+N)^2 - S^2 \right] \\
&+ \frac{1}{M} \sum_{n=-(M-1)}^{M-1} |g_n|^2 f_M(n) \tag{42}
\end{aligned}$$

where

$$f_M(n) = 1 - \frac{1}{M} - \frac{|n|}{M} \tag{43}$$

Similarly

$$\begin{aligned}
\langle X^2 \rangle &= \frac{1}{M^2} \sum_{k=0}^{M-1} \sum_{\ell=0}^{M-1} \langle r_k r_{k+1}^* r_\ell r_{\ell+1}^* \rangle \\
&= \frac{1}{M^2} \sum_{k=1}^{M-1} \sum_{\ell=1}^{M-1} \left[ \langle r_k r_{k+1}^* \rangle \langle r_\ell r_{\ell+1}^* \rangle \right. \\
&\quad + \langle r_k r_\ell \rangle \langle r_{k+1}^* r_{\ell+1}^* \rangle \\
&\quad \left. + \langle r_k r_{\ell+1}^* \rangle \langle r_{k+1}^* r_\ell \rangle \right] \tag{44}
\end{aligned}$$

Then (13) - (16) yields

$$\begin{aligned} \text{term 1} &= g_1^2 \\ \text{term 2} &\equiv 0 \end{aligned}$$

$$\text{term 3} = \begin{cases} g_{l+1-k} g_{l-k-1}^* & l \neq k-1, k+1 \\ (S+N) g_{-2}^* & l = k-1 \\ g_2 (S+N) & l = k+1 \end{cases}$$

and substituting these in (44) yields

$$\begin{aligned} \langle X^2 \rangle &= g_1^2 + \frac{1}{M^2} \sum_{k=0}^{M-1} \sum_{l=0}^{M-1} g_{l+1-k} g_{l-k-1}^* \\ &+ \frac{N [g_2 + g_{-2}^*] (M-1)}{M^2} \\ &= g_1^2 + \frac{1}{M} \sum_{n=-(M-1)}^{M-1} g_{n+1} g_{n-1}^* f_M(n) \\ &+ \frac{N}{M} \left(1 - \frac{1}{M}\right) (g_2 + g_{-2}^*). \end{aligned} \quad (45)$$

Now substituting (44) and (45) in (38 bis) yields

$$\begin{aligned} \text{Var} \{ \hat{\theta} \} &= \frac{1}{2M} \text{Re} \left\{ \frac{(S+N)^2 - S^2}{|g_1|^2} - N \left(1 - \frac{1}{M}\right) \frac{(g_2 + g_{-2}^*)}{g_1} \right. \\ &+ \left. \sum_{n=-(M-1)}^{M-1} \left( \frac{|g_n|^2}{|g_1|^2} - \frac{g_{n+1} g_{n-1}^*}{g_1^2} \right) f_M(n) \right\} \end{aligned} \quad (46)$$

For large M and small wT (46) yields approximately

$$\begin{aligned} \text{Var} \{ \hat{\delta\theta} \} &= \frac{1}{2M} \left[ \frac{(1 + N/S)^2 - 1}{|\rho(wT)|^2} - \frac{N}{S} \frac{2\rho(2\pi)}{|\rho(wT)|^2} \right. \\ &\quad \left. + \frac{(2\pi wT)}{|\rho(wT)|^2} \sqrt{\pi} \right] \\ &= \frac{1}{2M} \left[ \frac{\frac{N}{S} \left[ \frac{N}{S} + 2(1 - \rho(2wT)) \right] + (2\pi wT) \sqrt{\pi}}{|\rho(wT)|^2} \right] \end{aligned} \quad (47)$$

Equation (47) is a general expression for predicting the variance of the pulse pair estimate of the mean Doppler frequency accounting for the correlations in the data itself. It is virtually independent of actual spectral shape.

### 3. Width Estimator

We have shown that the spectral width estimate is given by

$$\hat{w}^2 = \frac{2}{(2\pi T)^2} \left[ 1 - \frac{|X|}{Y - N} \right] = B^2 \quad (48)$$

If the estimate is useful, it must have small errors and hence

$$\begin{aligned} \bar{w}^2 + 2\bar{w} (\delta\hat{w}) &= B_T + \eta_B \\ &= B_T^2 + \left\{ - \frac{g_{1r} \epsilon_1 + g_{1Im} \epsilon_2^2}{|g_1| s} + \frac{|g_1| \eta}{s^2} \right\} \frac{2}{(2\pi T)^2} \end{aligned}$$

where

$$|X| \triangleq \sqrt{(g_{1r} + \epsilon_1)^2 + (g_{1Im} + \epsilon_2)^2} \quad (50)$$

$$\text{and } Y = S + N + \eta \quad (51)$$

Note that

$$g_1 r_{\epsilon_1} + g_1 \text{Im } \epsilon_2 = \text{Re}(g^* \epsilon) \quad (52)$$

so that

$$(2\pi T)^2 \overline{w} (\delta \hat{w}) = \frac{|g_1|}{S} \left[ \frac{\eta}{S} - \text{Re} \left\{ \frac{\epsilon}{g_1} \right\} \right] \quad (53)$$

It follows that

$$(2\pi T)^4 \left( \frac{\overline{w} S}{|g_1|} \right)^2 \text{Var } \hat{w} = \text{Var } (\delta \psi) + \text{Var} \left( \frac{\eta}{S} \right) - 2 \text{cov} \left\{ (\delta \psi) \left( \frac{\eta}{S} \right) \right\} \quad (54)$$

From (32) and (33) it follows that

$$\begin{aligned} \text{Var } (\delta \psi) &= \frac{1}{2} \text{Re} \left\{ \left\langle \left| \frac{\epsilon}{g_1} \right|^2 \right\rangle + \left\langle \frac{\epsilon^2}{g_1^2} \right\rangle \right\} \\ &= \frac{1}{2M} \left\{ \frac{(S+N)^2 - S^2}{|g_1|^2} + N \left(1 - \frac{1}{M}\right) \frac{(g_2 + g_{-2}^*)}{g_1^2} \right. \\ &\quad \left. + \sum_{n=-(M-1)}^{M-1} \left( \frac{|g_n|^2}{|g_1|^2} + \frac{g_{n+1} g_{n-1}^*}{g^2} \right) f_{M(n)} \right\} \quad (55) \end{aligned}$$

Following the methods used earlier we have

$$\left\langle \left( \frac{\eta}{S} \right)^2 \right\rangle = \frac{1}{S^2} \left[ \frac{1}{M^2} \sum_{k=0}^M \sum_{\ell=0}^M \langle |r_k|^2 |r_\ell|^2 \rangle - (S+N)^2 \right] \quad (56)$$

$$= \frac{1}{S^2} \left[ \frac{1}{M^2} \sum_k \sum_l |g_{l-k}|^2 + \frac{(S+N)^2 - S^2}{M} \right]$$

$$= \frac{1}{MS^2} \left[ \sum_{n=-M}^M |g_n|^2 f_{M+1}(n) + (S+N)^2 - S^2 \right]$$

Similarly

$$\text{Cov}(\delta\psi \bar{N}/S) = \frac{\text{Re}}{Sg_1} \langle (X-g_1)(Y-S-N) \rangle$$

$$= \frac{1}{Sg_1} \text{Re} \left\{ \frac{1}{M^2} \sum_k \sum_l \langle r_k r_{k+1}^* r_l r_l^* \rangle - g_1(S+N) \right\}$$

$$= \frac{1}{Sg_1 M} \left[ \sum_{Mn} g_n g_{n-1}^* f_M(n) + N(g_1 + g_{-1}^*) \right]$$

$$= \frac{1}{M} \left\{ \sum_n \frac{g_n g_{n-1}^*}{Sg_1} f_M(n) + \frac{N}{S} \frac{g_1 + g_{-1}^*}{g_1} \right\} \quad (57)$$

Now assembling all the pieces yields

$$(2\pi T)^4 \left( \frac{\bar{w}S}{|g_1|} \right) \text{Var}(\hat{w})$$

$$= \frac{1}{2M} \left\{ \left[ (1 + N/S)^2 - 1 \right] \left[ \frac{1}{\rho_1} + 2 \right] \right.$$

$$\left. + N \frac{g_2 + g_{-2}^*}{g_1} - \frac{4N}{S} \left( \frac{g_1 + g_{-1}^*}{g_1} \right) \right\}$$

$$+ \sum_{n=-(M-1)}^{M-1} \left[ |g_n|^2 \left( \frac{1}{|g_1|^2} + \frac{2}{S^2} \right) + \frac{g_{n+1} g_{n-1}^*}{g_1^2} - \frac{4 g_n g_{n-1}^*}{S g_1} \right] f_M^{(n)} \quad (58)$$

This is the requisite expression for the variance of the width parameter estimator.

#### 4. Example

To reduce the equations to useful form, it is of interest to evaluate them for a Gauss shaped spectrum. In this case

$$R(f) = \frac{1}{\sqrt{2\pi}} e^{-\frac{f^2}{2}} \quad (59)$$

so that

$$\rho(t) = e^{-\frac{(2\pi t)^2}{2}} \quad (60)$$

$$G(f) = \frac{S/w}{\sqrt{2\pi}} e^{-\frac{(f-f_0)^2}{2w^2}} \quad (61)$$

$$\begin{aligned} g_n &= S e^{j2\pi f_0 T} \rho(nwT) \\ &= S e^{j2\pi f_0 T} e^{-\frac{(2\pi nwT)^2}{2}} \end{aligned} \quad (62)$$

$$\frac{N(g_2 + g_{-2}^*)}{g_1^2} = 2 \frac{N}{S} \frac{|\rho_2|}{|\rho_1|^2} \quad (63)$$

$$\frac{g_{n+1} g_{n-1}^*}{g_1^2} = |\rho_n|^2, \quad (64)$$

$$\frac{g_1 + g_{-1}^*}{g_1} = 2, \quad (65)$$

$$\begin{aligned} \frac{g_n g_{n-1}^*}{S g_1} &= e^{-\frac{(2\pi T w)^2}{2} \left[ n^2 + (n-1)^2 - 1 \right]} \\ &= e^{- (2\pi T w)^2 n (n-1)} \\ &= e^{- (2\pi T w)^2 (m+1/2) (m-1/2)} \\ &= e^{\frac{1}{4} (2\pi T w)^2 - (2\pi m T w)^2} \end{aligned} \quad (66)$$

which leads to

$$\begin{aligned} 2M \text{ Var } \{\hat{\theta}\} &= \frac{1}{|\rho_1|^2} \left\{ (1 + N/S)^2 - 1 - 2N/S |\rho_2| \left(1 - \frac{1}{M}\right) \right. \\ &\quad \left. + \sum_{n=-(M-1)}^{M-1} |\rho_n|^2 (1 - |\rho_1|^2) f_M(n) \right\} \end{aligned} \quad (67)$$

$$\begin{aligned}
2M (2\pi T)^4 \left( \frac{w}{|f_1|} \right)^2 \text{Var } \hat{w} &= \frac{1}{|p_1|^2} \left\{ \left[ (1 + N/S)^2 - 1 \right] \left[ 1 + 2 |p_1|^2 \right] \right. \\
&\quad \left. + 2 \frac{N}{S} |p_2| - \frac{8N}{S} |p_1|^2 \right. \\
&\quad \left. + \sum_{n=-(M-1)}^{M-1} |p_n|^2 \left[ 1 + 3 |p_1|^2 - 4 |p_1|^2 e^{\frac{1}{4} (2\pi T w)^2} \right] \right\} \quad (68)
\end{aligned}$$

These expressions may be simplified as follows (for large M and  $2\pi T w \ll 1$ )

$$\begin{aligned}
(1 + N/S)^2 - 1 - 2 N/S |p_2| \left( 1 - \frac{1}{M} \right) &= N/S (2 + N/S) - 2 N/S |p_2| \\
&= N/S [(N/S + 2 (1 - |p_2|))] \quad (69)
\end{aligned}$$

$$\begin{aligned}
&\sum |p_n|^2 (1 - |p_1|^2) f_M(n) \\
&\approx \sum_{-\infty}^{\infty} |p_n|^2 (1 - |p_1|^2) \\
&\approx (2\pi w T)^2 \sum_{-\infty}^{\infty} e^{-(2\pi n w T)^2} \\
&\approx 2\pi w T \int_{-\infty}^{\infty} e^{-t^2} dt \\
&= 2\pi w T \sqrt{\pi} \quad (70)
\end{aligned}$$

Similarly

$$\begin{aligned}
 & \left[ (1 + N/S)^2 - 1 \right] \left[ 1 + 2|\rho_1|^2 \right] + \frac{2N}{S} |\rho_2| - \frac{8N}{S} |\rho_1|^2 \\
 &= N/S (N/S + 2) (1 + 2|\rho_1|^2) + \frac{2N}{S} |\rho_2| - \frac{8N}{S} |\rho_1|^2 \\
 &= N/S \left[ N/S (1 + 2|\rho_1|^2) + 2 + 2|\rho_2| - 4|\rho_1|^2 \right] \\
 &= N/S \left[ N/S (1 + 2|\rho_1|^2) + 2(1 - |\rho_1|^2)^2 \right], \tag{71}
 \end{aligned}$$

$$\begin{aligned}
 & \sum |\rho_n|^2 \left[ 1 + 3|\rho_1|^2 - 4|\rho_1|^2 e^{\frac{1}{4}(2\pi wT)^2} \right] f_M(n) \\
 &= \sum |\rho_n|^2 \left[ 1 + 3e^{(2\pi wT)^2} - 4e^{-\frac{3}{4}(2\pi wT)^2} \right] \\
 &\approx \frac{3}{8} (2\pi wT)^4 \sum |\rho_n|^2 \\
 &\approx \frac{3}{8} (2\pi wT)^3 \sqrt{\pi}. \tag{72}
 \end{aligned}$$

As a result it is possible to reduce the variance expressions to

$$\begin{aligned}
 2 M \text{Var} \{ \hat{\theta} \} &= e^{(2\pi wT)^2} \left[ \frac{N}{S} \left( \frac{N}{S} + 2 \left( 1 - e^{-2(2\pi wT)^2} \right) \right) \right. \\
 &\quad \left. + 2\pi wT \sqrt{\pi} \right] \tag{73}
 \end{aligned}$$

$$2M (2\pi\omega T)^2 \text{Var} (2\pi\hat{\omega}T) = \frac{N}{S} \left[ \frac{N}{S} \left( 1 + 2 e^{-(2\pi\omega T)^2} \right) + 2 \left( 1 - e^{-(2\pi\omega T)^2} \right)^2 \right] \\ + \frac{3}{8} (2\pi\omega T)^3 \sqrt{\pi} \quad (74)$$

Figures 1 and 2 are essentially plots of (73) and (74) and enable the prediction of system performance for various choices of parameters.

Standard Deviation of  
 pulse pair count frequency estimate  
 as a function of true spectral width  
 with frequency as a parameter

K $\Sigma$  SEMI-LOGARITHMIC 46 5493  
 3 CYCLES X 70 DIVISIONS MAR 19 64  
 KEUFFEL & ESSER CO

$\sigma$  (2 $\pi$ fT)

BM

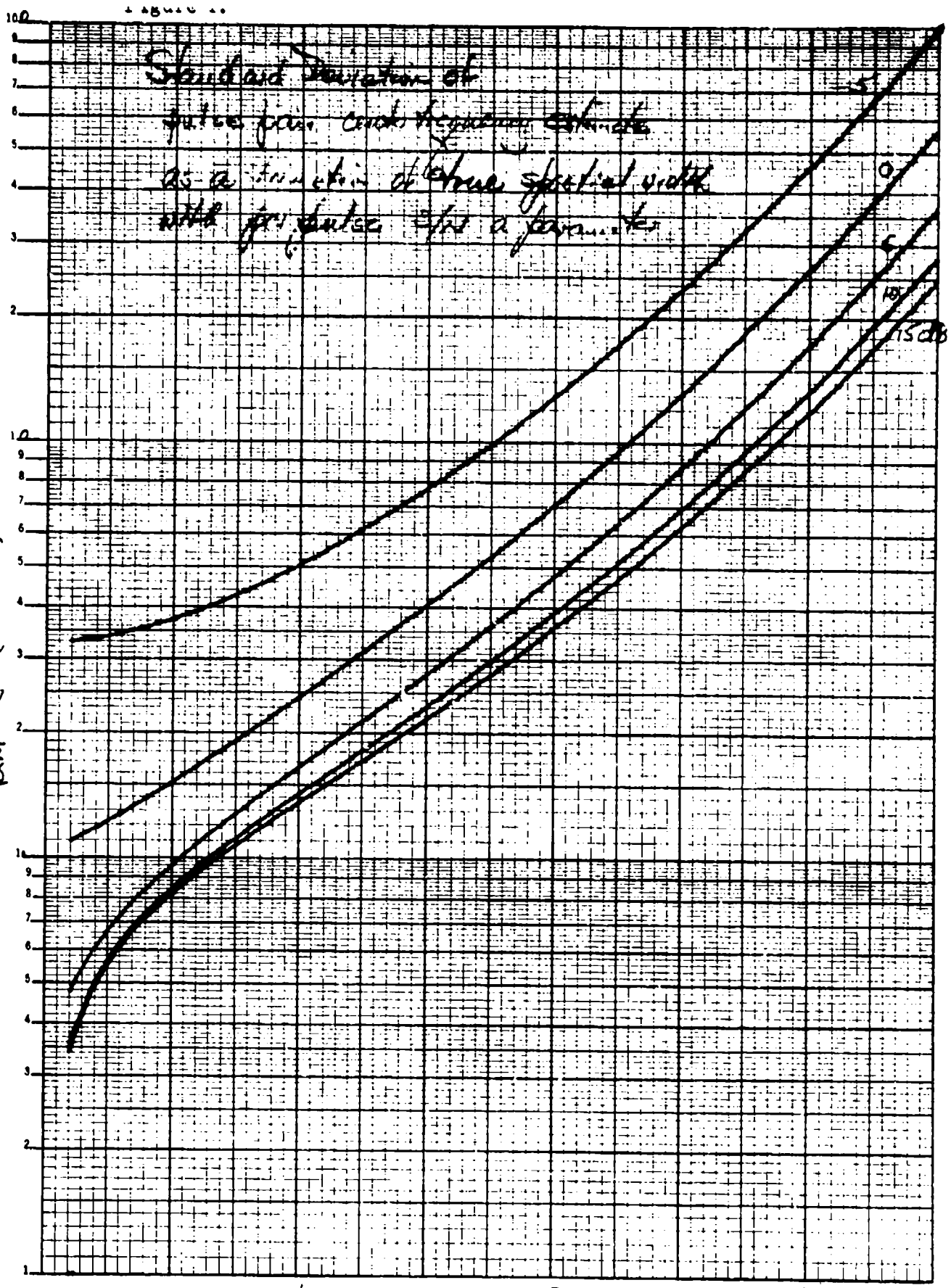
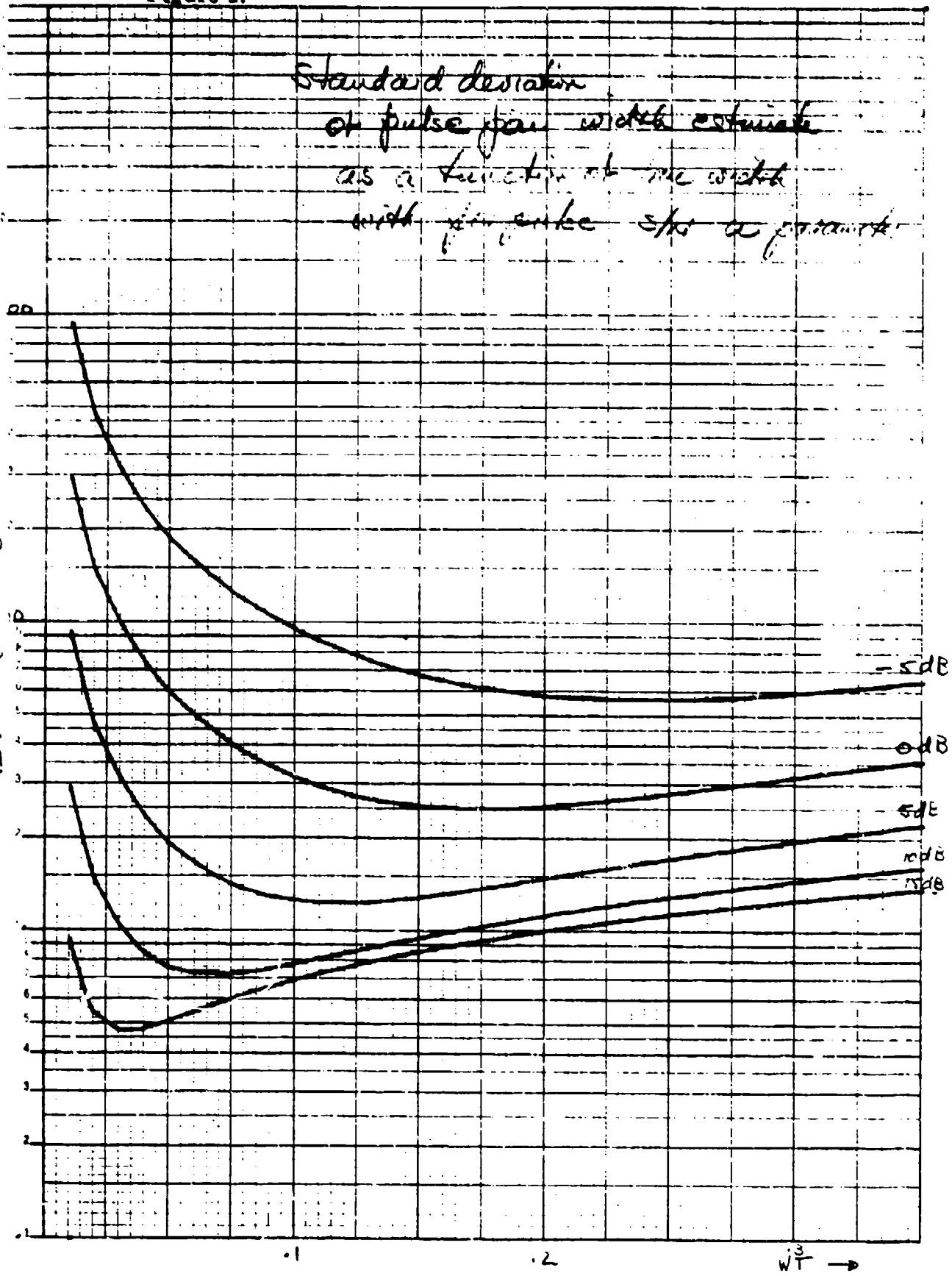


Figure 2.

Standard deviation  
of pulse pair width estimate  
as a function of pulse width  
with  $\tau$  pulse rate a parameter

K&E BENILOGARITMIK 46 6010  
 REF. 1001 000000  
 12M G PART 3



## APPENDIX B

### MATHEMATICAL DERIVATIONS RELATING TO THE GENERATION OF SIMULATED DOPPLER RETURN

a. Second Moment:

$$m_2 = \frac{\left(\frac{1}{2\pi j}\right)^3 \int_{-j\infty}^{+j\infty} H(s) H(-s) (-s^2) ds}{\frac{1}{2\pi j} \int_{-j\infty}^{+j\infty} H(s) H(-s) ds} = w^2$$

$$\begin{aligned} \frac{1}{2\pi j} \int_{-j\infty}^{+j\infty} H(s) H(-s) ds &= \frac{1}{2\pi j} \int_{-j\infty}^{+j\infty} \frac{a^4}{(s+a)^2 (-s+a)^2} ds \\ &= a^4 \frac{d}{ds} \left[ \frac{1}{(-s+a)^2} \right] \Big|_{s=-a} \\ &= \frac{1}{4} a, \text{ where } a = 2\pi w \end{aligned}$$

Similarly,

$$\frac{1}{2\pi j} \int_{-j\infty}^{+j\infty} H(s) H(-s) (-s^2) ds = \frac{1}{4} a^3$$

therefore,

$$m_2 = w^2$$

b. Half Power Points ( $\omega_3$ ):

$$|H(j\omega)| = \frac{a^2}{\omega^2 + a^2} = \frac{1}{\sqrt{2}}$$

$$\therefore \omega_3 = a [\sqrt{2} - 1]^{1/2}$$

c. Recursion Relation:

$$\frac{Y(Z)}{X(Z)} = H(Z) = \frac{Z^{-1} a^2 T e^{-aT}}{(1 - 2e^{-aT} Z^{-1} + e^{-2aT} Z^{-2})}$$

$$Y(Z) = a^2 T e^{-aT} X(Z) Z^{-1} + 2e^{-aT} Y(Z) Z^{-1} - e^{-2aT} Y(Z) Z^{-2}$$

which yields

$$y_n = a^2 T e^{-aT} x_{n-1} + 2e^{-aT} y_{n-1} - e^{-2aT} y_{n-2}$$

d. Signal to Noise:

$$= \text{Signal Power} = \frac{2}{2\pi j} \oint_1 H(Z) H(1/Z) \frac{dZ}{Z}$$

The factor 2 is due to the power from both the real and imaginary channels. The contour of integration is the unit circle. The Z-transform is used because a digital signal is the desired output from the simulator; therefore, signal power should be found in terms of the Z-transform. To continue,

$$S = \frac{2}{2\pi j} \oint_1 \frac{a^4 T^2 Z dZ}{(Z - e^{-aT})^2 (Z - e^{aT})^2}$$

Since there is only one (second order) pole inside the unit circle at  $Z = e^{-aT}$ , the value of S is given by:

$$= \frac{2 \cdot 2\pi j}{2\pi j} \frac{d}{dZ} \left[ \frac{a^4 T^2 Z}{(Z - e^{-aT})^2} \right] \Big|_{Z=e^{-aT}}$$

Resulting in

$$= 2a^4 T^2 \frac{(3e^{-aT} + e^{aT})}{(e^{-aT} - e^{-aT})^3}$$

Noise power, N, is given by:

$$N = 2 \sigma_N^2$$

The factor 2 results from noise power in the real and imaginary channels.

Therefore the S/N ratio is given by:

$$S/N = \frac{a^4 T^2 (3e^{-aT} + e^{aT})}{\sigma_N^2 (e^{-aT} - e^{-aT})^3}$$

APPENDIX C  
FORTRAN MAIN PROGRAMS

C-1	DOPGEN
C-2	PPSTAT
C-3	SPEC

**APPENDIX C-1**  
**DOPGEN Program Coding**

C COMMENT--SYSTEM SUPPLIED SUBROUTINES REQUIRED--DOPOLT,ENDPLT  
COMMENT--USER SUPPLIED SUBROUTINES REQUIRED--GARN,FORT

REAL MAGWK  
COMPLEX WK  
COMPLEX Z,W,B

C DIMENSION: RN(24),Z(1524),X(1024),Y(1024),YR(3),YI(3),LAB(3),  
1 S(513)

C EQUIVALENCE (Z(1),Y(1)) , (Z(513 ),X(1))

C DATA LAB / ICH P.L.KELLY, IOH 7025 , IOH MISC /

C NAMELIST /N1/ A,FHZ,FMU,SIG,XR,N,AT,EAT,C1,C2,C3,WNOT,WT  
NAMELIST /N2/ FM2,C5,C6,SIGDB,PRF

C PI=3.141592653  
T=1.0/3300.0  
PRF=3300.0  
XR=82593476.  
FMU=0.0

C SIG=1.0  
N=1024  
NM=10  
NBLKS=0  
IPRINT=1  
REWIND 9

C 10 READ(5,1000)AVGDOP,SIGDOP,STON,IBLK1,IBLK2,IFFT  
WRITE(6,1000)AVGDOP,SIGDOP,STON,IBLK1,IBLK2,IFFT  
IF(1BLK1.EQ.0)GO TO 500

C SET UP CONSTANTS

C FHZ=AVGDOP  
A=2.\*PI\*SIGDOP  
CB=STON  
FM2=A\*\*2/(4.0\*PI\*\*2)  
FNPK=3.0\*PRF\*PI/A+1.0  
NN=FVPK  
IF (NN.GT.500) GO TO 610

```

C6=0.0
SIGUB=0.0
AT=A*T
EAT=1.0/EXP(AT)
C1=A*AT*EAT
C2=2.0*EAT
C3=1.0/EXP(2.0*AT)
C4=EXP(AT)

NOISE=0
IF (DB.GT.100.0) GO TO 5
NOISE=1
C5=10.0*(DB*0.1)
C6=A**4*T**2*(3.0*EAT+C4)/((C4-EAT)**3)
SIGDB=SQRT(C6/C5)
5 WNDY=2.0*PI*FHZ
INITIALIZE FILTER
DO 20 J=1,2
YR(J)=0.0
20 YI(J)=0.0
IF (XR.EQ.0.0) GO TO 30
YY=RANF(XR)
XR=0.0
RMARG=0.0
30 CONTINUE

DO 700 ICT=1BLK1,1BLK2

IF(1CT.NE.1BLK1)IFFT=0
NBLKS=NBLKS+1
GENERATE N COMPLEX NUMBERS

DO 100 I=1,N10
CALL GNRN (RN,X1,X2,SIG,FMU)
YR(3)=X1*C1+YR(2)*C2-YR(1)*C3
YI(3)=X2*C1+YI(2)*C2-YI(1)*C3

```

```

Z(I)=CMPLX(YR(3),YI(3))
C
C UPDATE SEQUENCE
C
DO 50 J=1,2
YR(J)=YR(J+1)
50 YI(J)=YI(J+1)
C
100 CONTINUE
C
DO 105 I=1,N
105 Z(I)=Z(I+NN)
C
C GENERATE WEIGHTED COMPLEX INPUT SEQUENCE
C
WT=WN0T*I
C
DO 110 I=1,N
FI=I-1
ARG=WT*FI
W=CMPLX(COS(ARG),SIN(ARG))
110 Z(I)=Z(I)*W
C
C IF (NOISE.EQ.0) GO TO 200
C
DO 115 I=1,N
CALL GNRN (RN,X1,X2,SIGDB,0.0)
B=CMPLX(X1,X2)
115 Z(I)=Z(I)+B
C
200 WRITE (9) ICT,A,PRF,FM2,FHZ,FMU,SIG,XR,DB,N,MM,IFFT,
1 (Z(J),J=1,N)
C
700 CONTINUE
GO TO 10
C
500 END FILE 9
REWIND 9
WRITE (6,2000)
WRITE(6,4000)NBLKS
C
510 READ (9) ICT,A,PRF,FM2,FHZ,FMU,SIG,XR,DB,N,MM,IFFT,
1 (Z(J),J=1,N)
IF (EOF(9)) 600,520

```

```
C 520 WRITE(6,2030)ICT,A,PRF,FM2,FHZ,FMU,SIG,XR,DB,N,MM,IFFT
C
C IF (IFFT.EQ.0) GO TO 510
C
C INTERMEDIATE OUTPUT
C
C M=N/4
C KK=0
C 120 CONTINUE
C IF (IPRINT.EQ.1)GO TO 135
C WRITE(6,2000)
C DO 130 I=1,M
C I1=I+M
C I2=I1+M
C I3=I2+M
C 130 WRITE (6,2010 )I,Z(I),I1,Z(I1),I2,Z(I2),I3,Z(I3)
C 135 CONTINUE
C
C IF (KK.GT.0) GO TO 140
C
C IFS=-1
C
C CALL FORT (Z,MM,S,IFS,IFERR)
C
C KK=1
C GO TO 120
C
C COMPUTE AND OUTPUT THE MAGNITUDE OF THE FFT OUTPUT
C
C 140 DO 150 I=1,N
C 150 Y(I)=SQRT((REAL(Z(I)))**2+(AIMAG(Z(I)))**2)
C
C KK=0
C 155 CONTINUE
C IF (IPRINT.EQ.1)GO TO 165
C WRITE(6,2000)
C DO 160 I=1,M
C I1=I+M
C I2=I1+M
C I3=I2+M
C 160 WRITE (6,2020) I,Y(I),I1,Y(I1),I2,Y(I2),I3,Y(I3)
C 165 CONTINUE
C IF (KK.EQ.1) GO TO 180
C KK=1
```

DOPGEN.5

```
C      YMAX=Y(I)
      DO 152 I=2,N
      IF (YMAX.LT.Y(I)) YMAX=Y(I)
152  CONTINUE
      DO 153 I=1,N
153  Y(I)=Y(I)/YMAX
C
      DO 170 I=1,N
      X(I)=I-1
170  Y(I)=20.0*ALOG10(Y(I))
      GO TO 155
C
      PLOT RESULTS
C
      IF 0 CONTINUE
      CALL DQFLOT (LAB,X,Y,N,IH ,1,12H20 LOG (MAG),12,0,0)
      I PLOT=1
C
      GO TO 510
C
      600 IF (I PLOT.EQ.1)CALL ENDPLT
      REWIND 9
      CALL EXIT
      610 WRITE (6,2040)
      CALL EXIT
C
      1000 FORMAT(3F10.0,3I10)
      2000 FORMAT (1H1/)
      2010 FORMAT (1X,4(15,2E13.5))
      2020 FORMAT (1X,4(15,E13.5,13X))
      2030 FORMAT(/1X,15,8E12.4,2X,3I5)
      2040 FORMAT (10X,13HV1 100 LARGE)
      3000 FORMAT (/ /4(1X,6E15.6)/ /10X,3E20.8)
      4000 FORMAT(1X,15,23H DATA BLOCKS GENERATED)
      END
C
      17
      17
```

**APPENDIX C-2**  
**PPSTAT Program Coding**

PROGRAM PPSTAT(INPUT,OUTPUT,TAPE9=3000,TAPES=INPUT,TAPE6=OUTPUT)

COMMENT--SYSTEM SUPPLIED SUBROUTINES REQUIRED--NONE  
COMMENT--USER SUPPLIED SURROUTINES REQUIRED--NONE

REAL MEANE1,MEANE2  
REAL MEANE3  
COMPLEX Z,W,WH,SWH

DIMENSION Z(1024),D(8),NS(40)  
DIMENSION E1(30,7),E2(30,7)  
DIMENSION VARE4(7),VARE5(7),SIGE4(7),SIGE5(7)

5 REWIND 9

10 CONTINUE  
READ(5,1100)NMAX,NSETS,NINC,IBLK1,ISUM,ISN,IRW,FNOISE  
WRITE(6,1100)NMAX,NSETS,NINC,IBLK1,ISUM,ISN,IRW,FNOISE  
IF (NINC.EQ.0) GO TO 300  
IBLK2=IBLK1+NSETS-1  
JJ=0  
DO 11 I=IBLK1,IBLK2  
JJ=JJ+1

11 NS(JJ)=I  
WRITE(6,1000)(NS(I),I=1,NSETS)

NALKS=NSETS  
NM=NMAX-1

DO 200 I=1,NSETS  
NN=NS(I)  
NRS=NINC

15 READ(9) ICT,(D(J),J=1,8),N,MM,IFFT,(Z(J),J=1,1024)  
IF (EOF(9)) 5,20  
20 WRITE(6,1000)ICT

IF (NN.NE.1) GO TO 15

SNDB=D(8)  
XXX1=SNDB/10.0  
SN=10.\*\*XXX1  
SIGDOP=SQRT(D(3))  
WRITE(6,1500)(N,N,D(8),D(4),SIGDOP

```

C WRITE(6,1550)Z(1),Z(2)
C WRITE(6,1560)Z(1023),Z(1024)
C WRITE(6,2000)

C SMH=CMPLX(0.0,0.0)
C SK=REAL(Z(1))*2+AIMAG(Z(1))*2

C KK=0
C DD 30 J=1,NM

C M=CONJG(Z(J))*Z(J+1)
C SMH=SMH+W
C SK=SK+REAL(Z(J+1))*2+AIMAG(Z(J+1))*2

C IF (J.EQ.NM) GO TO 25
C IF (J.EQ.NRS-1)GO TO 25
C GO TO 30

C 25 CONTINUE
C SNK=1.
C IF (ISN.EQ.1)SNK=SN/(1.+SN)
C IF (ISN.LE.1)FNOISE=0.
C FJ=J
C WH=SMH/FJ
C SKK=(SK/(FJ+1.))*SNK-FNOISE
C PI=3.141592653
C FMU=1650.*ATAN(AIMAG(WH)/REAL(WH))/PI
C AW=SQRT(REAL(WH))*2+AIMAG(WH)*2
C UK=(1.0-AW/SKK)/(2.0*PI**2)
C IF(UK.LT.0.)UK=0.
C J)=3300.**2*UK
C VAR=SQRT(SQ)

C JJ=J+1

C WRITE(6,2010)JJ,WH,FMU,SKK,UK,SQ,VAR

C KK=KK+1
C E1(I,KK)=FMU
C E2(I,KK)=SQ

C NRS=2*NRS
C

```

30 CONTINUE

C

200 CONTINUE

C

IF (ISUM.EQ.0)GO TO 5

C

WRITE(6,3000)

DO 270 I=1,KK

SE1=0.0

SE2=0.0

SE3=0.0

SE1SQ=0.0

SE2SQ=0.0

SE3SQ=0.0

SE4SQ=0.0

SE5SQ=0.0

VARE1=0.0

VARE2=0.0

VARE3=0.0

DO 250 J=1,NBLKS

SE1=SE1+E1(J,I)

SE2=SE2+E2(J,I)

SE3=SE3+SQRT(E2(J,I))

250 CONTINUE

C-11

MEANE1=SE1/NBLKS

MEANE2=SE2/NBLKS

MEANE3=SE3/NBLKS

IF(NBLKS.EQ.1)GO TO 260

DO 255 J=1,NBLKS

SE1SQ=SE1SQ+(E1(J,I)-MEANE1)\*\*2

SE3SQ=SE3SQ+(SQRT(E2(J,I))-MEANE3)\*\*2

SE4SQ=SE4SQ+(E2(J,I)-SIGDOP)\*\*2

SE5SQ=SE5SQ+(SQRT(E2(J,I))-SIGDOP)\*\*2

255 SE2SQ=SE2SQ+(E2(J,I)-MEANE2)\*\*2

VARE1=SE1SQ/(NBLKS-1)

VARE2=SE2SQ/(NBLKS-1)

VARE3=SE3SQ/(NBLKS-1)

VARE4(1)=SE4SQ/NBLKS

VARE5(1)=SE5SQ/NBLKS

SIGE1=SQRT(VARE1)

SIGE2=SQRT(VARE2)

SIGE3=SQRT(VARE3)

SIGE4(1)=SQRT(VARE4(1))

SIGE5(1)=SQRT(VARE5(1))

```

260 WRITE(6,4000)MEANE1,VARE1,SIGE1,MEANE2,YAREZ,SIGE2,
      1 MEANE3,VARE3,SIGE3
270 CONTINUE
DO 275 I=1,KK
275 WRITE(6,5000)VARE4(I),SIGE4(I),VARE5(I),SIGE5(I)
      C
      IF(IRW.EQ.1)REWIND 9
      GO TO 10
      C
      300 REWIND 9
      C
      1000 FORMAT(10I5)
      1100 FORMAT(7I5,E15.5)
      1500 FORMAT(1H1,5H9LOCK,15,10X,3HN =,15,13X,5HS/N =,F5.0,
      1 11X,14HMEAN DOPPLER =,F5.0,11X,13HSIG DOPPLER =,F5.0)
      1550 FORMAT(/1X,9HZ( 1 ) =,11X,2E15.5,10X,9HZ( 2 ) =,11X,2E15.5)
      1560 FORMAT(/1X,9HZ(1023) =,11X,2E15.5,10X,9HZ(1024) =,11X,2E15.5)
      2000 FORMAT(/8X,12HWK HAT(REAL),3X,
      1 12HWK HAT(IMAG),6X,7HMUKHAT ,10X,2HMK,13X,2HUK,
      2 11X,7HSIGK*2,9X,4HSIGK)
      2010 FGRMAT(1X,15,7E15.6)
      3000 FORMAT(1H-,6X,9HMEAN MEAN,7X,8HVAR MEAN,7X,8HSIG MEAN,
      1 7X,8HMEAN VAR,8X,7HVAR VAR,8X,7HSIG VAR,
      2 7X,8HMEAN SIG,8X,7HVAR SIG,8X,7HSIG SIG)
      4000 FORMAT(1H ,9E15.5)
      5000 FORMAT(/1X,60X,2E15.5,15X,2E15.5)
      END

```

APPENDIX C  
SPEC Program Coding

\*\*\*\*\*  
\*\*\*\*\*

PROGRAM SPEC TRACE CDC 6600 FTN V3.0-2270+ OPT=0 03/2

PROGRAM SPEC(INPUT,OUTPUT,TAPE5=INPUT,TAPE6=OUTPUT,TAPE8,TAPE9)

COMMENT--SYSTEM SUPPLIED SUBROUTINES REQUIRED--DQPLT,ENDPLT  
COMMENT--USER SUPPLIED SUBROUTINES REQUIRED--COCC,BEST,FORT

C THE FOLLOWING CONTROL CARDS ARE NEEDED WHEN PLOTS ARE DESIRED  
C FTN(A)  
C ATTACH,PEN,PENPLOTS,MR=1.  
C SETCORE.  
C LOAD,PEV.  
C REQUEST,TAPE33.  
C REQUEST,TAPE8,MT.(RPK09/NORING).  
C REQUEST,TAPE8,MI.(RPK08/NORING)  
C LGO.  
C UNLOAD,TAPE33.  
C UNLOAD,TAPE9.  
C UNLOAD,TAPE9.

REAL MEAN  
COMPLEX Z  
DIMENSION Z(1024),A(1024),X(1024),Y(1536)  
DIMENSION S(513),LAB(3)

DATA LAB /104 P.L.KELLY,104 7025 ,104 MIS /  
IFS=-1  
M=10  
N=1024  
KPLT=0  
IPLT=0  
JAVG=0  
IRM=0

REWIND 8  
REWIND 3

CALL COCC(A)

10 READ(5,1000)IBLK,NUNIT,LIMIT1,LIMIT2,IRM,IPLT,IBIAS  
WRITE(6,1000)IBLK,NUNIT,LIMIT1,LIMIT2,IRM,IPLT,IBIAS  
IF(1IBLK.EQ.0)GO TO 11  
IF(LIMIT1.EQ.0)GO TO 12  
GO TO 11  
12 LIMIT1=1  
LIMIT2=1024  
13 CONTINUE

IF(IRM.EQ.1)REWIND NUNIT

15 READ(NUNIT)Z(1),Z(2),Z(3),Z(4),Z(5),Z(6),Z(7),Z(8),Z(9),Z(10),Z(11),Z(12),Z(13),(Z(I),I=1,1024)  
WRITE(5,1000)Z(1),Z(2),Z(3),Z(4),Z(5),Z(6),Z(7),Z(8),Z(9),Z(10),Z(11),Z(12),Z(13)  
IF(IRM.EQ.1)WRITE(6,1000)Z(1),Z(2),Z(3),Z(4),Z(5),Z(6),Z(7),Z(8),Z(9),Z(10),Z(11),Z(12),Z(13)  
DO 20 I=1,1024  
20 Z(I)=Z(I)/N

```
CALL FORT(Z,4,S,IFS,IFERR)
DO 30 I=1,1024
30 Y(I)=REAL(Z(I))**2+AIMAG(Z(I))**2

YMAX=Y(1)
DO 40 I=1,1024
40 IF(YMAX.LT.Y(I))YMAX=Y(I)

IF(IPLOT.EQ.0)GO TO 75
DO 50 I=1,1024
50 Y(I)=Y(I)/YMAX

FFF=-1.0
DO 60 I=1,1024
FFF=FFF+1.0
X(I)=FFF
60 Y(I)=10.*ALOG10(Y(I))

CALL DDPLOT(LAB,X,Y,N,14,1,12H20 LOG (MAG),12,0,0)
KFLOT=1

DO 70 J=1,1024
70 Y(J)=10.*(Y(J)/10.)*YMAX
75 CONTINUE

IF(IAVG.EQ.0)GO TO 200
AVG=0.
DO 76 I=1,1024
76 AVG=AVG+Y(I)
AVG=AVG/100.

DO 77 I=1,1024
77 Y(I)=Y(I)-AVG
200 IF(IBIAS.EQ.J)GO TO 230
ISHFT=512-IBIAS
DO 210 I=1,1024
J1=1024+ISHFT+1-I
K1=1024+1-I
210 Y(J1)=Y(K1)
DO 220 I=1,ISHFT
J2=ISHFT+1-I
K2=1024+ISHFT+1-I
220 Y(J2)=Y(K2)
230 CONTINUE
WRITE (6,2000)

THR=0.

DO 100 I=1,20
THR=THR+2.

YMINV=YMAX/(10.0**(THR*0.1))
```

PROGRAM SPEC TRACE CDC 6600 FTN V3.0-P270+ OPT=0 03/2

S1=0.

S2=0.

FM=LIMIT1-1

DO 80 J=LIMIT1,LIMIT2

FM=FM+1.

IF(Y(J).LE.YMINV)GO TO 80

YSQ=Y(J)

S1=S1+YSQ

S2=S2+FM\*YSQ

80 CONTINUE

UKP=S2/S1

MEAN=(3300./1024.)\*UKP

S3=0.

FM=LIMIT1-1

DO 90 J=LIMIT1,LIMIT2

FM=FM+1.

IF(Y(J).LE.YMINV)GO TO 90

YSQ=Y(J)

S3=S3+YSQ\*(FM-UKP)\*\*2

90 CONTINUE

VKP=S3/S1

SKP=SQRT(VKP)

SIG=(3300./1024.)\*SKP

WRITE(6,3000)IHR,UKP,MEAN,SKP,SIG

100 CONTINUE

GO TO 10

110 CONTINUE

IF(KPLOT.EQ.1)CALL ENOPLT

REWIND 8

REWIND 9

CALL EXIT

1000 FORMAT(7I10)

2000 FORMAT(14I)

3000 FORMAT(1X,F3.0,4E15.5)

END

APPENDIX D  
FORTRAN SUBROUTINES

D-1 FORT  
D-2 PAIR  
D-3 UNPK  
D-4 CDCC  
D-5 BESI  
D-6 STAR  
D-7 GNRN

APPENDIX D-1

FORT

```

C C UNIVAC 1108 VERSION OF THE FAST FOURIER TRANSFORM SUBROUTINE
C C FORT, ONE-DIMENSIONAL FINITE COMPLEX FOURIER TRANSFORM.
C C SUBROUTINE FORT, M,S,IFS,IFERR)
C C
C C FOURIER TRANSFORM SUBROUTINE, PROGRAMMED IN SYSTEM/360,
C C BASIC PROGRAMMING SUPPORT, FORTRAN IV. FORM C28-6504
C C THIS DECK SET UP FOR IBSYS ON IBM 7094.
C C
C C DOES EITHER FOURIER SYNTHESIS, I.E., COMPUTES COMPLEX FOURIER SERIES
C C GIVEN A VECTOR OF N COMPLEX FOURIER AMPLITUDES, OR, GIVEN A VECTOR
C C OF COMPLEX DATA X DOES FOURIER ANALYSIS, COMPUTING AMPLITUDES.
C C A IS A COMPLEX VECTOR OF LENGTH N=2**M COMPLEX NOS. OR 2*N REAL
C C NUMBERS. A IS TO BE SET BY USER.
C C M IS AN INTEGER 0..13, SET BY USER.
C C S IS A VECTOR S(J)= SIN(2*PI*I*J/NP), J=1,2,.....,NP/4-1,
C C COMPUTED BY PROGRAM.
C C IFS IS A PARAMETER TO BE SET BY USER AS FOLLOWS-
C C IFS=0 TO SET NP=2**M AND SET UP SINE TABLE.
C C IFS=1 TO SET NP=2**M, SET UP SIN TABLE, AND DO FOURIER
C C SYNTHESIS, REPLACING THE VECTOR A BY
C C
C C X(J)= SUM OVER K=0,N-1 OF A(K)*EXP(2*PI*I/N)**(J*K),
C C J=0,N-1, WHERE I=SQRT(-1)
C C
C C THE X S ARE STORED WITH RE X(J) IN CELL 2*J+1
C C AND IM X(J) IN CELL 2*J+2 FOR J=0,1,2,....,N-1.
C C THE A S ARE STORED IN THE SAME MANNER.
C C
C C IFS=-1 TO SET N=NP=2**M, SET UP SIN TABLE, AND DO FOURIER
C C ANALYSIS, TAKING THE INPUT VECTOR A AS X AND
C C REPLACING IT BY THE A SATISFYING THE ABOVE FOURIER SERIES.
C C IFS=+2 TO DO FOURIER SYNTHESIS ONLY, WITH A PRE-COMPUTED S.
C C IFS=-2 TO DO FOURIER ANALYSIS ONLY, WITH A PRE-COMPUTED S.
C C IFERR IS SET BY PROGRAM TO-
C C =0 IF NO ERROR DETECTED.
C C =1 IF M IS OUT OF RANGE., OR, WHEN IFS=+2,-2, THE
C C PRE-COMPUTED S TABLE IS NOT LARGE ENOUGH.
C C =-1 WHEN IFS =+1,-1, MEANS ONE IS RECOMPUTING S TABLE
C C UNNECESSARILY.
C C
C C NOTE- AS STATED ABOVE, THE MAXIMUM VALUE OF M FOR THIS PROGRAM
C C ON THE IBM 7094 IS 13. FOR 360 MACHINES HAVING GREATER STORAGE
C C CAPACITY, ONE MAY INCREASE THIS LIMIT BY REPLACING 13 IN

```

FORT 002  
 FORT 003  
 FORT 004  
 FORT 005  
 FORT 006  
 FORT 007  
 FORT 008  
 FORT 009  
 FORT 010  
 FORT 011  
 FORT 012  
 FORT 013  
 FORT 014  
 FORT 015  
 FORT 016  
 FORT 017  
 FORT 018  
 FORT 019  
 FORT 020  
 FORT 021  
 FORT 022  
 FORT 023  
 FORT 024  
 FORT 025  
 FORT 026  
 FORT 027  
 FORT 028  
 FORT 029  
 FORT 030  
 FORT 031  
 FORT 032  
 FORT 033  
 FORT 034  
 FORT 035  
 FORT 036  
 FORT 037  
 FORT 038  
 FORT 039  
 FORT 040  
 FORT 041  
 FORT 042  
 FORT 043  
 FORT 044

```

C      STATEMENT 3 BELOW BY LOG2 N, WHERE N IS THE MAX. NO. OF
C      COMPLEX NUMBERS ONE CAN STORE IN HIGH-SPEED CORE. ONE MUST
C      ALSO ADD MORE DO STATEMENTS TO THE BINARY SORT ROUTINE
C      FOLLOWING STATEMENT 24 AND CHANGE THE EQUIVALENCE STATEMENTS
C      FOR THE K S.
C
      DIMENSION A(1), S(1), K(14)
      EQUIVALENCE (K(13),K1),(K(12),K2),(K(11),K3),(K(10),K4)
      EQUIVALENCE (K( 9),K5),(K( 8),K6),(K(7),K7),(K( 6),K8)
      EQUIVALENCE (K( 5),K9 ),(K( 4),K10),(K( 3),K11),(K( 2),K12)
      EQUIVALENCE (K( 1),K13),( K(1),N2)
      IF(M)2,2,3
3  IF(M-13) 5,5,2
2  IFERR=1
1  RETURN
5  IFERR=0
   N=2**M
   IF( IABS(IFS) - 1 ) 200,200,10
   WE ARE USING TRANSFORM ONLY. SEE IF PRE-COMPUTED
   S TABLE IS SUFFICIENTLY LARGE
10 IF( N-NP )20,20,12
12 IFERR=1
   GO TO 200
C      SCRAMBLE A, BY SANDE S METHOD
20 K(1)=2*N
22 K(L)=K(L-1)/2
   DO 24 L=M,12
24 K(L+1)=2
C      NOTE EQUIVALENCE OF KL AND K(14-L)
C      BINARY SORT-
   IJ=2
   KOPT=K1
   DO 30 J1=2,KOPT,2
   DO 30 J2=J1,K2,K1
   DO 30 J3=J2,K3,K2
   DO 30 J4=J3,K4,K3
   DO 30 J5=J4,K5,K4
   DO 30 J6=J5,K6,K5
   DO 30 J7=J6,K7,K6
   DO 30 J8=J7,K8,K7
   DO 30 J9=J8,K9,K8
   DO 30 J10=J9,K10,K9
   DO 30 J11=J10,K11,K10

```

FORT 045  
FORT 046  
FORT 047  
FORT 048  
FORT 049  
FORT 050  
FORT 051  
FORT 052  
FORT 053  
FORT 054  
FORT 055  
FORT 056  
FORT 057  
FORT 058  
FORT 059  
FORT 060  
FORT 061  
FORT 062  
FORT 063  
FORT 064  
FORT 065  
FORT 066  
FORT 067  
FORT 068  
FORT 069  
FORT 070  
FORT 071  
FORT 072  
FORT 073  
FORT 074  
FORT 075  
FORT 076  
  
FORT 078  
FORT 079  
FORT 080  
FORT 081  
FORT 082  
FORT 083  
FORT 084  
FORT 085  
FORT 086  
FORT 087

FORT 086  
 FORT 089  
 FORT 090  
 FORT 091  
 FORT 092  
 FORT 093  
 FORT 094  
 FORT 095  
 FORT 096  
 FORT 097  
 FORT 098  
 FORT 099  
 FORT 100  
 FORT 101  
 FORT 102  
 FORT 103  
 FORT 104  
 FORT 105  
 FORT 106  
 FORT 107  
 FORT 108  
 FORT 109  
 FORT 110  
 FORT 111  
 FORT 112  
 FORT 113  
 FORT 114  
 FORT 115  
 FORT 116  
 FORT 117  
 FORT 118  
 FORT 119  
 FORT 120  
 FORT 121

FORT 123  
 FORT 124  
 FORT 125  
 FORT 126  
 FORT 127  
 FORT 128  
 FORT 129  
 FORT 130

```

DO 30 J12=J11,K12,K11
DO 30 J1=J12,K13,K12
IF(IJ-J1)28,30,30
28 T=A(IJ-1)
A(IJ-1)=A(J1-1)
A(J1-1)=T
T=A(IJ)
A(IJ)=A(J1)
A(J1)=T
30 IJ=IJ+2
IF(IFS)32,2,36
C DOING FOURIER ANALYSIS,SO DIV. BY N AND CONJUGATE.
32 FN = N
DO 34 I=1,N
A(2*I-1) = A(2*I-1)/FN
34 A(2*I)=-A(2*I)/FN
SPECIAL CASE- L=1
36 DO 40 I=1,N,2
T = A(2*I-1)
A(2*I-1) = T + A(2*I+1)
A(2*I+1)=T-A(2*I+1)
T=A(2*I)
A(2*I) = T + A(2*I+2)
40 A(2*I+2)= T - A(2*I+2)
IF(M-1) 2,1 ,50
SET FOR L=2
50 LEXP1=2
LEXP1=2**(L-1)
LEXP=8
LEXP=2**(L+1)
NPL = 2**MT
NPL = NP* 2**-L
60 DO 130 L=2,M
SPECIAL CASE- J=0
N2OPT=N2
DO 80 I=2,N2OPT,LEXP
I1=I + LEXP1
I2=I1+ LEXP1
I3 =I2+LEXP1
T=A(I1-1)
A(I1-1) = T +A(I2-1)
A(I2-1) = T-A(I2-1)
T =A(I1)
A(I) = T+A(I2)
    
```

# FORT-4

FORT 131  
 FORT 132  
 FORT 133  
 FORT 134  
 FORT 135  
 FORT 136  
 FORT 137  
 FORT 138  
 FORT 139  
 FORT 140  
 FORT 141  
 FORT 142  
 FORT 143  
 FORT 144  
 FORT 145  
 FORT 146  
 FORT 147  
 FORT 148  
 FORT 149  
 FORT 150  
 FORT 151  
 FORT 152  
 FORT 153  
 FORT 154  
 FORT 155  
 FORT 156  
 FORT 157  
 FORT 158  
 FORT 159  
 FORT 160  
 FORT 161  
 FORT 162  
 FORT 163  
 FORT 164  
 FORT 165  
 FORT 166  
 FORT 167  
 FORT 168  
 FORT 169  
 FORT 170  
 FORT 171  
 FORT 172  
 FORT 173  
 FORT 174

```

A(I2) = T-A(I2)
T = -A(I3)
TI = A(I3-1)
A(I3-1) = A(I1-1) - T
A(I3) = A(I1) - TI
A(I1-1) = A(I1-1) + T
80 A(I1) = A(I1) + TI
90 KLAST=N2-LEXP
JJ=NPL
DO 110 J=4,LEXPI,2
NPJJ=NT-JJ
UR=S(NPJJ)
UI=S(JJ)
ILAST=J+KLAST
DO 100 I=J,ILAST,LEXP
I1=I+LEXP1
I2=I1+LEXP1
I3=I2+LEXP1
T=A(I2-1)*UR-A(I2)*UI
TI=A(I2-1)*UI+A(I2)*UR
A(I2-1)=A(I1)-T
A(I2) =A(I1) - TI
A(I1-1) =A(I1-1)+T
A(I1) =A(I1)+TI
T=-A(I3-1)*UI-A(I3)*UR
TI=A(I3-1)*UR-A(I3)*UI
A(I3-1)=A(I1-1)-T
A(I3) =A(I1) -TI
A(I1-1)=A(I1-1)+T
100 A(I1) =A(I1) +TI
C
110 JJ=JJ+NPL
C
120 LEXP1=2*LEXP1
LEXP = 2*LEXP
130 NPL=NPL/2
C
140 IF(IFS)145,2,1
C
150 DO 150 I=1,N
160 A(2*I) =-A(2*I)
GO TO 1
RETURN
  
```

DOING FOURIER ANALYSIS. REPLACE A BY CONJUGATE.

```

C      MAKE TABLE OF S(J)=SIN(2*PI*J/NP), J=1,2,...,NT-1,NT=NP/4
      NP=N
      MP=M
      NT=N/4
      MT=M-2
      IF(MT) 260,260,205
      THETA=.7853981634
      THETA=PI/2**(L+1)      FOR L=1
      210  JSTEP = NT
      JSTEP = 2*( MT-L+1 ) FOR L=1
      JDIF = NT/2
      JDIF = 2*(MT-L) FOR L=1
      S(JDIF) = SIN(THETA)
      IF (MT-2)260,220,220
      220  DO 250 L=2,MT
      THETA = THETA/2.
      JSTEP2 = JSTEP
      JSTEP = JDIF
      JDIF = JDIF/2
      S(JDIF)=SIN(THETA)
      JCI=NT-JDIF
      S(JCI)=COS(THETA)
      JLAST=NT-JSTEP2
      IF(JLAST-JSTEP)250,230,230
      230  DO 240 J=JSTEP,JLAST,JSTEP
      JC=NT-J
      JD=J+JDIF
      240  S(JD)=S(J)*S(JCI)+S(JDIF)*S(JC)
      250  CONTINUE
      260  IF(IFS)20,1,20
      END

```

FORT 175  
 FORT 176  
 FORT 177  
 FORT 178  
 FORT 179  
 FORT 180  
 FORT 181  
 FORT 182  
 FORT 183  
 FORT 184  
 FORT 185  
 FORT 186  
 FORT 187  
 FORT 188  
 FORT 189  
 FORT 190  
 FORT 191  
 FORT 192  
 FORT 193  
 FORT 194  
 FORT 195  
 FORT 196  
 FORT 197  
 FORT 198  
 FORT 199  
 FORT 200  
 FORT 201  
 FORT 202  
 FORT 203  
 FORT 204  
 FORT 205

APPENDIX D-2

PAIR

PAIR-1

SUBROUTINE PAIR(Z,N,PRF,NOISE,MEAN,SIG,POWER)

REAL NOISE

REAL MEAN,MUKHAT

COMPLEX Z,MKHAT

DIMENSION Z(N)

PI=3.141592653

MKHAT=CMPLX(0.,0.)

SK=REAL(Z(1))\*\*2+AIMAG(Z(1))\*\*2

M=N-1

DO 10 I=1,M

MKHAT=MKHAT+CONJG(Z(I))\*Z(I+1)

SK=SK+REAL(Z(I+1))\*\*2+AIMAG(Z(I+1))\*\*2

MKHAT=MKHAT/(N-1)

MUKHAT=(PRF/2.)\*ATAN2(AIMAG(MKHAT),REAL(MKHAT))/PI

MEAN=MUKHAT

SK=SK/N

POWER=SK

SK=SK-NOISE

UK=(1.-SQRT(REAL(MKHAT)\*\*2+AIMAG(MKHAT)\*\*2)/SK)/(2.\*PI\*\*2)

VAR=(PRF)\*\*2\*UK

SIG=SQRT(VAR)

RETURN

END

APPENDIX D-3

UNPK

UNPK.:

```

SUBROUTINE UNPK(X,Y)
INTEGER X,Y
DIMENSION X(200),Y(521)
X EQUALS PACKED INPUT ARRAY
Y EQUALS UNPACKED OUTPUT ARRAY
I EQUALS INDEX OF X WORD BEING UNPACKED
J EQUALS INDEX OF Y WORD BEING OBTAINED FROM X
K EQUALS POSITION IN X OF BYTE BEING EXTRACTED
I=1
J=0
K=0
10 J=J+1
K=K+1
IF(J.EQ.522)GO TO 20
Y(J)=MBYTE(X(I),K)
IF(K.LT.5)GO TO 10
K=0
I=I+1
GO TO 10
C ACCOUNT FOR NEGATIVE NUMBERS
20 DO 30 N=1,521
30 IF(Y(N).GT.2047)Y(N)=2048-Y(N)
RETURN
END
D.11
```

APPENDIX D-4

CDCC

SUBROUTINE CDCC(A)  
60 DB DOLPH CHEBYSHEV WEIGHTING COEFFICIENTS

C

```

DIMENSION A(1024)
N=1024
R=1000.0
V=ALOG(R+SQRT(R*R-1.0))
CALL RESI(V,BV,IER)
FN=N-1
C=2.0/FN
M=0
DO 40 J=1,N
M=M+1
FJ=J-1
Z=FFJ*C-1.0
IF(J.NE.1.AND.J.NE.N)GO TO 20
A(M)=FN/(2.0*V*BV)
GO TO 30
20 T=SQRT(1.0-Z*Z)
VTT=V*T
CALL RESI(VTT,BVT,IER)
A(M)=BVT/(T*BV)
30 CONTINUE
40 CONTINUE
RETURN
END
```

APPENDIX D-5

BESI

BESI-1

```
C      SUBROUTINE BESI(X,BI,IER)
      MODIFIED BESSEL FUNCTION OF THE FIRST KIND, FIRST ORDER
      IER=0
      BI=0.0
      IF(X.NE.0.0)GO TO 10
      GO TO 100
10     IF(X.GT.0.0)GO TO 20
      IER=1
      GO TO 100
20     TOL=1.E-6
      IF(X.GT.12.0)IER=2
      XX=X/2.0
      TERM=XX
      BI=XX
      XX=XX*XX
      DO 30 K=1,500
      IF(ABS(TERM).LT.ABS(BI*TOL))GO TO 100
      FK=K*(K+1)
      TERM=TERM*XX/FK
      BI=BI+TERM
      IER=3
30     RETURN
100    END
```

APPENDIX D-6

STAR

STAR -1

```
SUBROUTINE STAR(N)
DIMENSION IFORM(81)
IF(N.LE.0)RETURN
IF(N.GT.80)RETURN
DO 1 I=1,81
1 IFORM(I)=1H
1 IFORM(I)=9H(1H+,51X,
M=N+1
DO 2 I=2,M
2 IFORM(I)=4H1H+
IFORM(M)=4H1H*
PRINT IFORM
RETURN
END
```

APPENDIX D-7

GNRN

GNRN-1

```
C : SUBROUTINE GNRN (RN, X1, X2, SIG, FMU)
C : DIMENSION RN(24)
C : GENERATE UNIFORM RANDOM NUMBERS
C : DO 30 J=1,24
C : 30 RN(J)=RANF(RNARG)

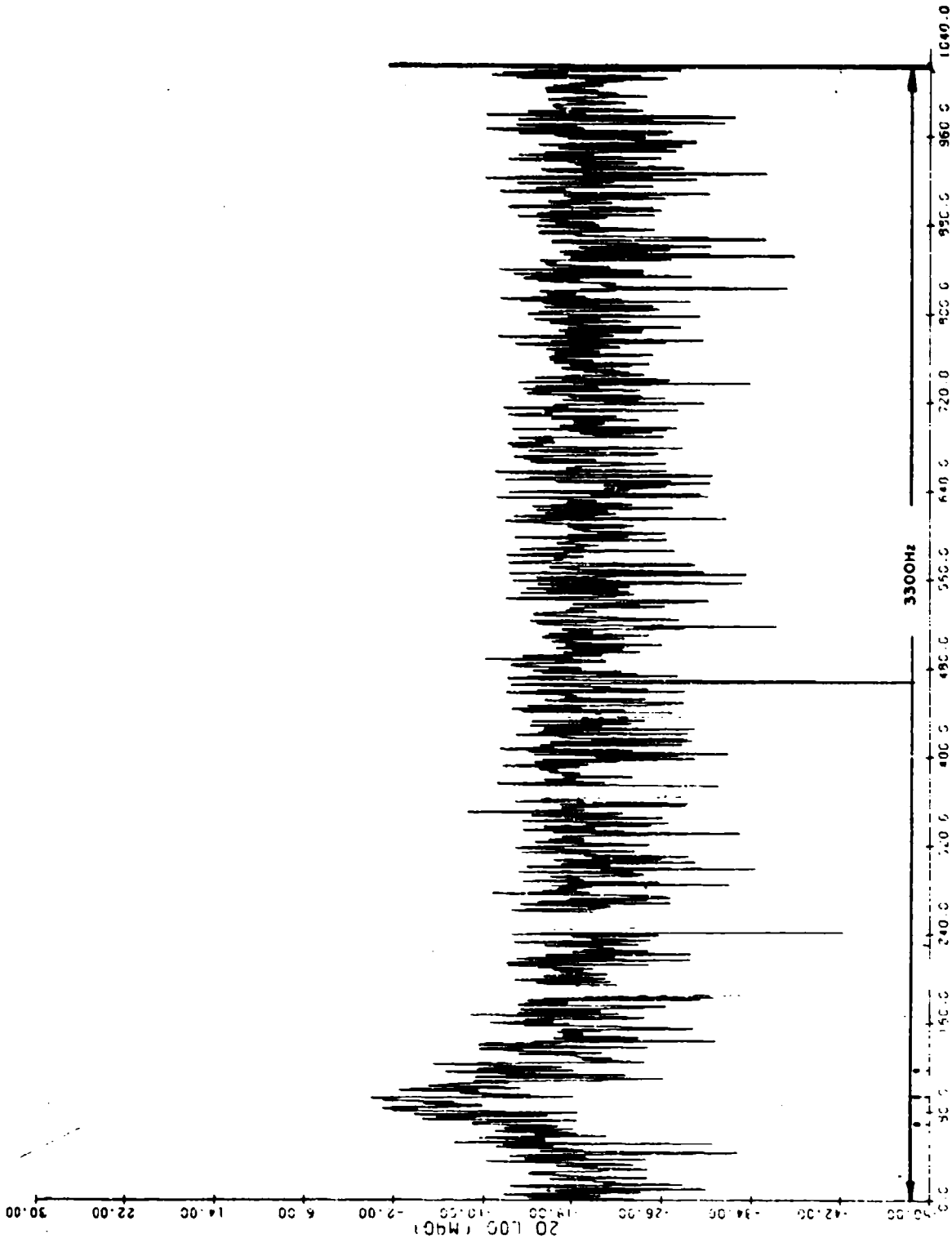
C : GENERATE 2 NORMAL RANDOM NUMBERS
C :
C : X1=RN(1)
C : X2=RN(13)
C : DO 40 J=2,12
C : X1=X1+RN(J)
C : X2=X2+RN(J+12)
C : X1=(X1-6.0)*SIG+FMU
C : X2=(X2-6.0)*SIG+FMU
C : RETURN
C : END
```

## APPENDIX E

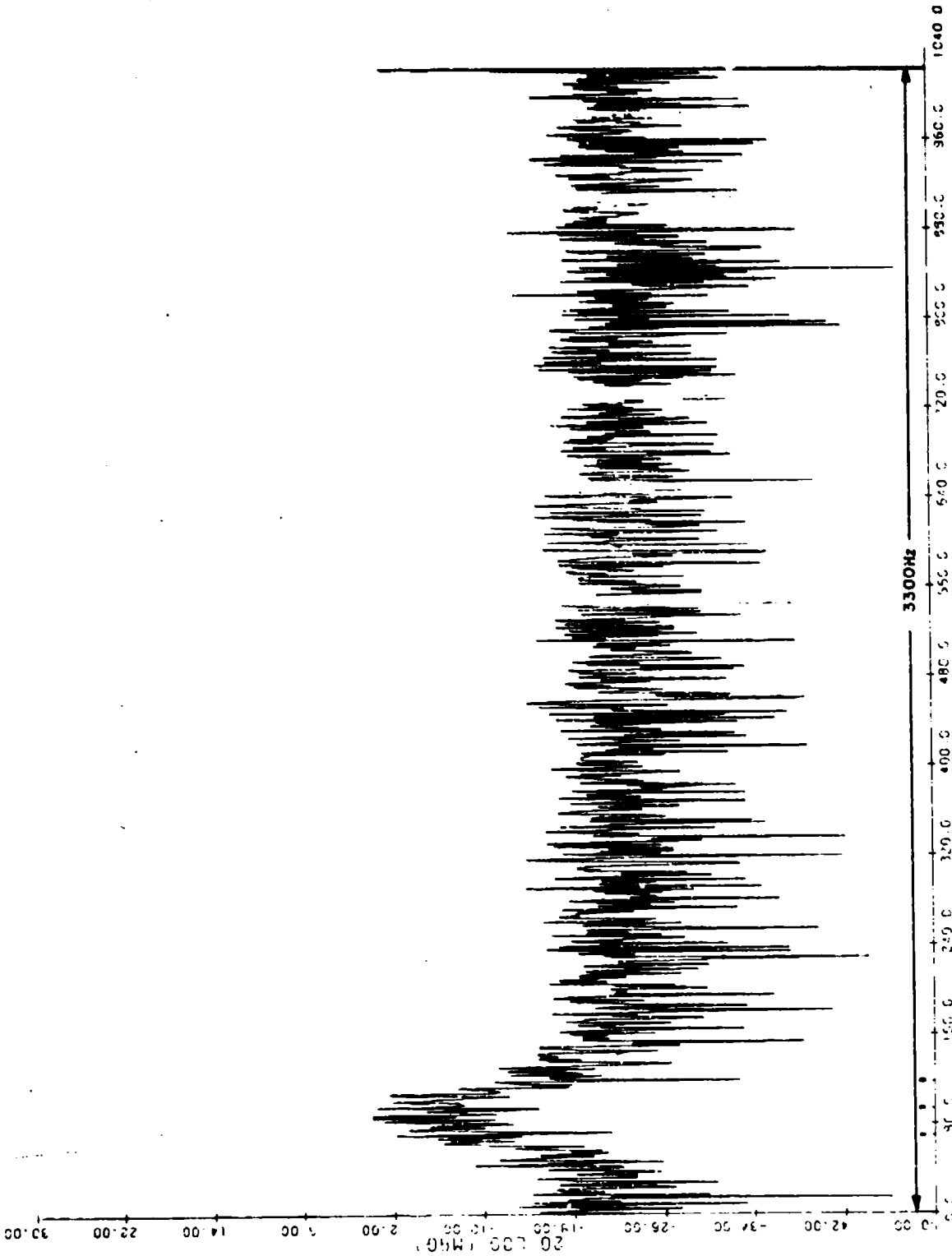
### SPECTRAL ANALYSIS PLOTS OF TYPICAL SEQUENCES OF SIMULATED DOPPLER RADAR TARGET RETURN

The radar PRF is 3300 PPS in all cases. Mean, width, and single pulse S/N parameters are as listed below:

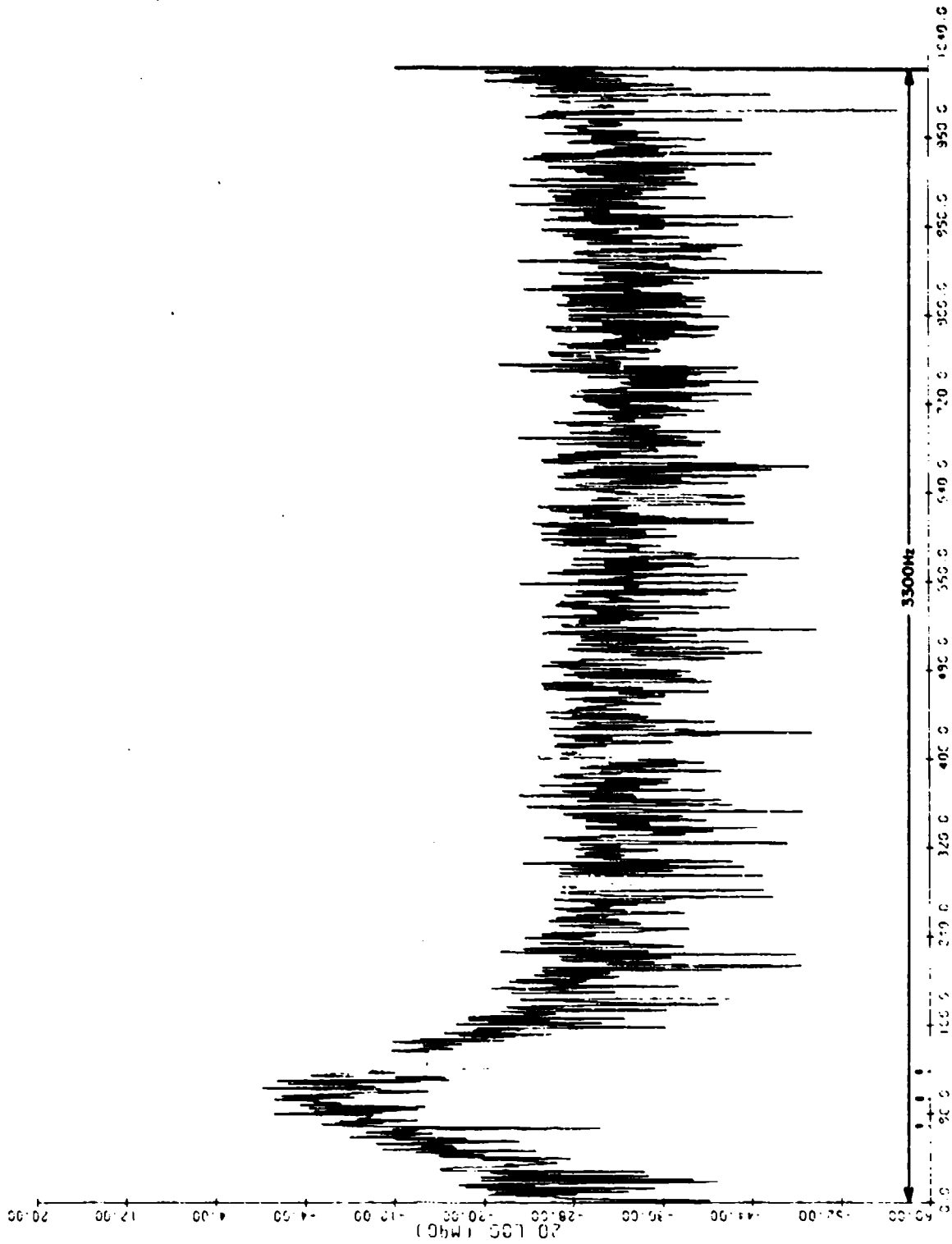
<u>Case</u>	<u>Mean (<math>\mu</math>) Hz</u>	<u>Width (<math>\sigma</math>) Hz</u>	<u>Single-Pulse S/N dB</u>
1	300	78	0
2	300	78	5
3	300	78	15
4	300	78	∞
5	600	156	0
6	600	156	5
7	600	156	15
8	600	156	∞
9	900	234	0
10	900	234	5
11	900	234	15
12	900	234	∞

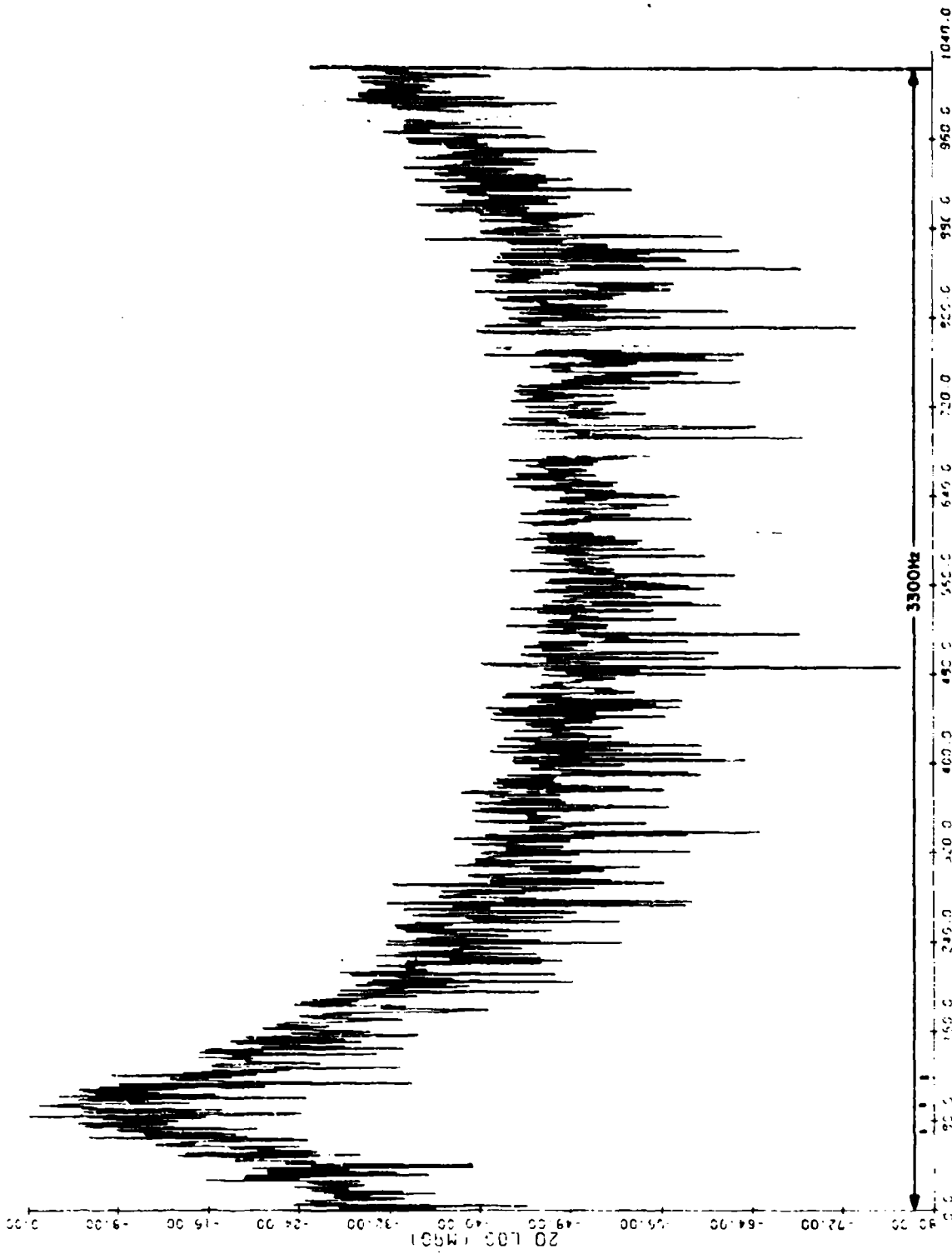


CASE 1:  $\mu = 300 \text{ Hz}$ ,  $\sigma = 78 \text{ Hz}$ ,  $S/N = 0 \text{ dB}$

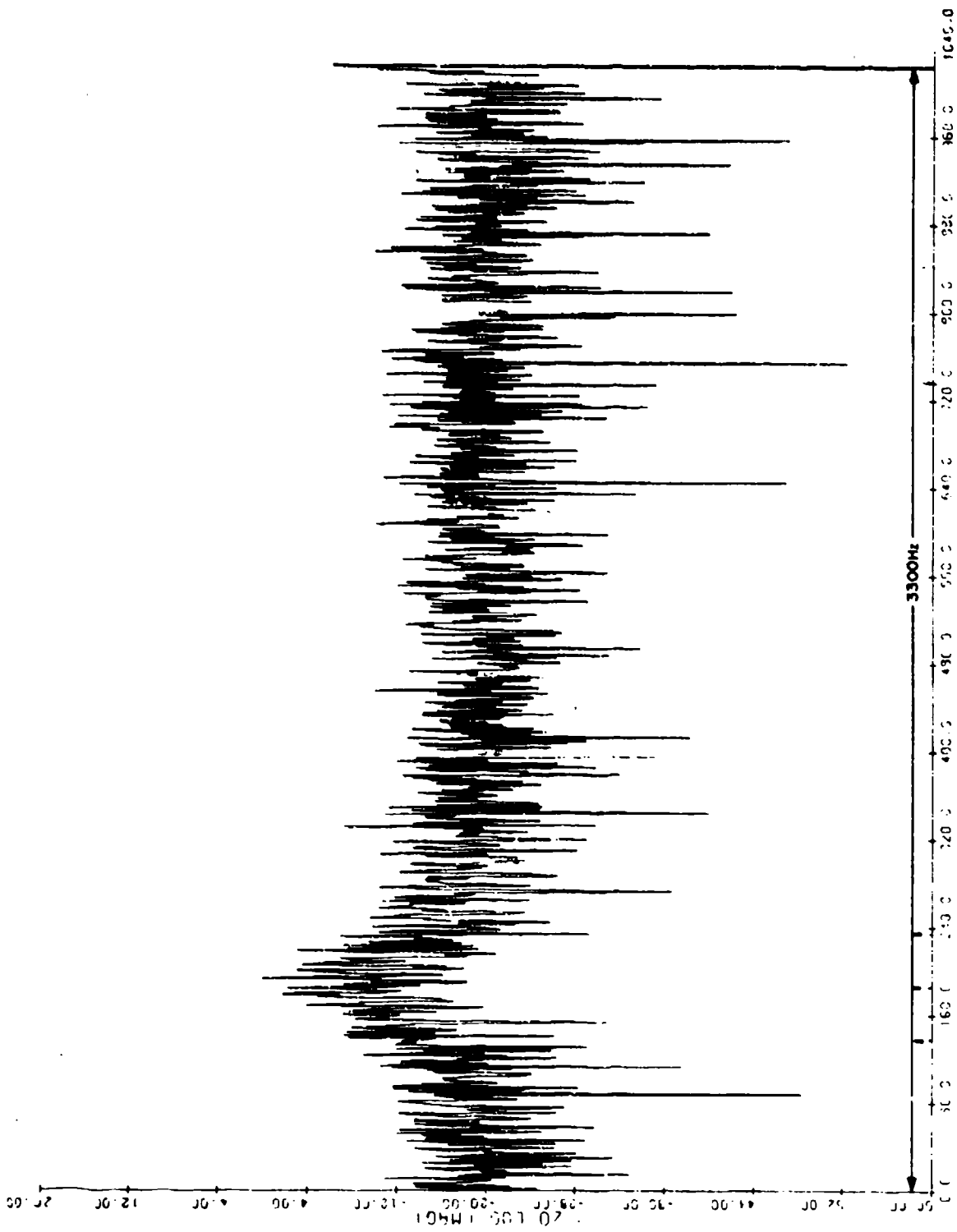


CASE 2:  $\mu = 300 \text{ Hz}$ ,  $\sigma = 78 \text{ Hz}$ ,  $S/N = 5 \text{ dB}$

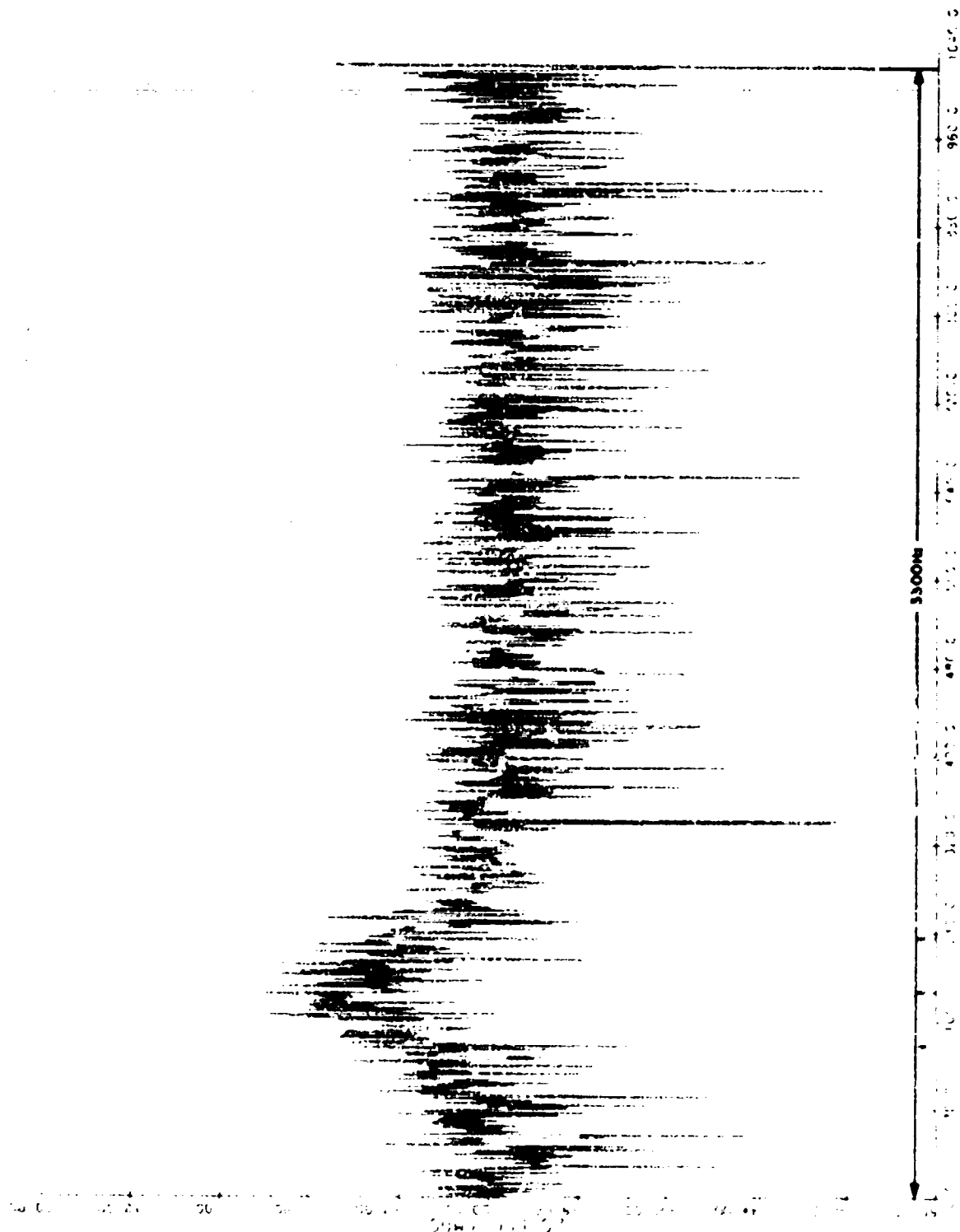




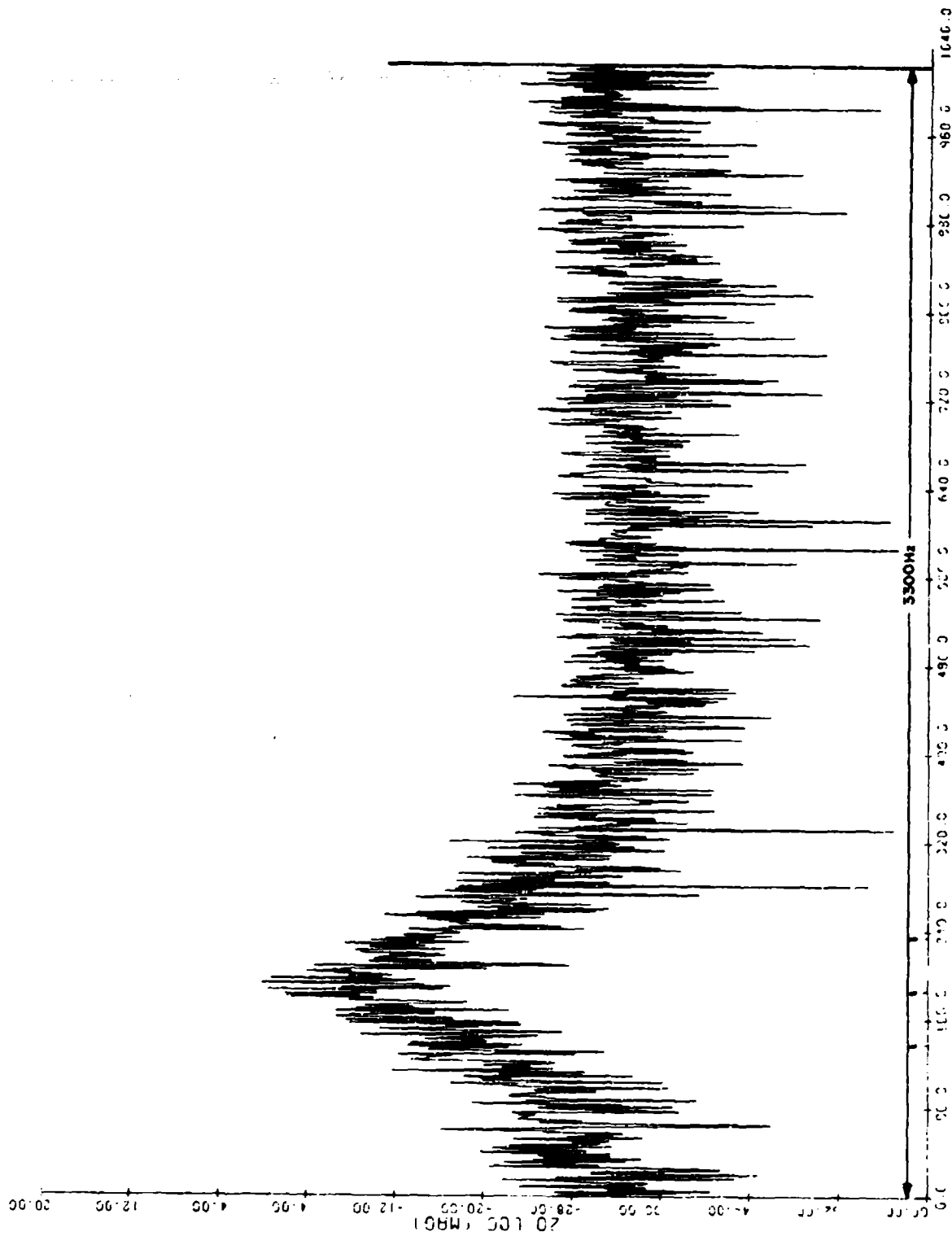
CASE 4:  $\mu = 300 \text{ Hz}$ ,  $\sigma = 78 \text{ Hz}$ ,  $S/N = \infty$



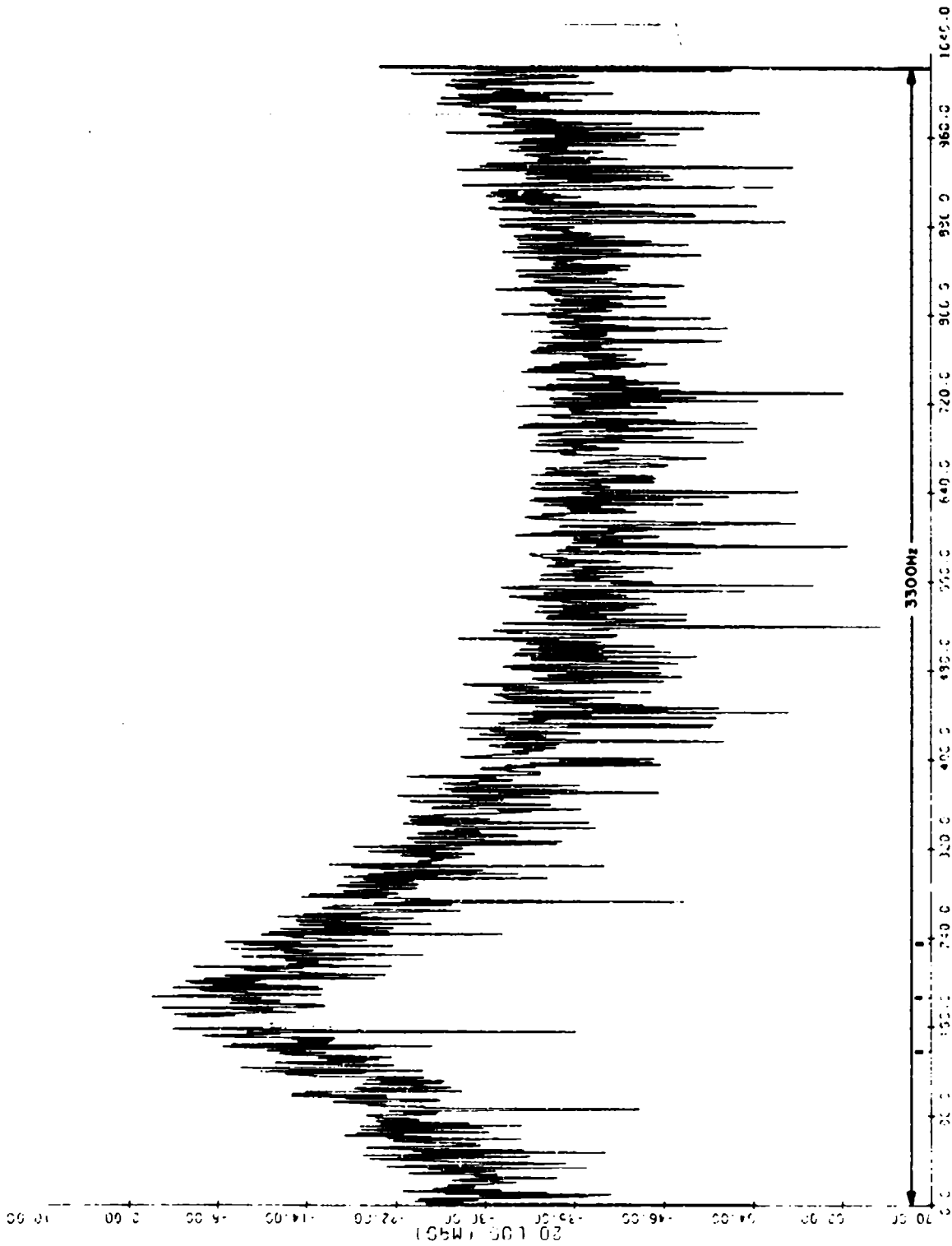
CASE 5:  $\mu = 600$  Hz,  $\sigma = 156$  Hz,  $S/N = 0$  dB



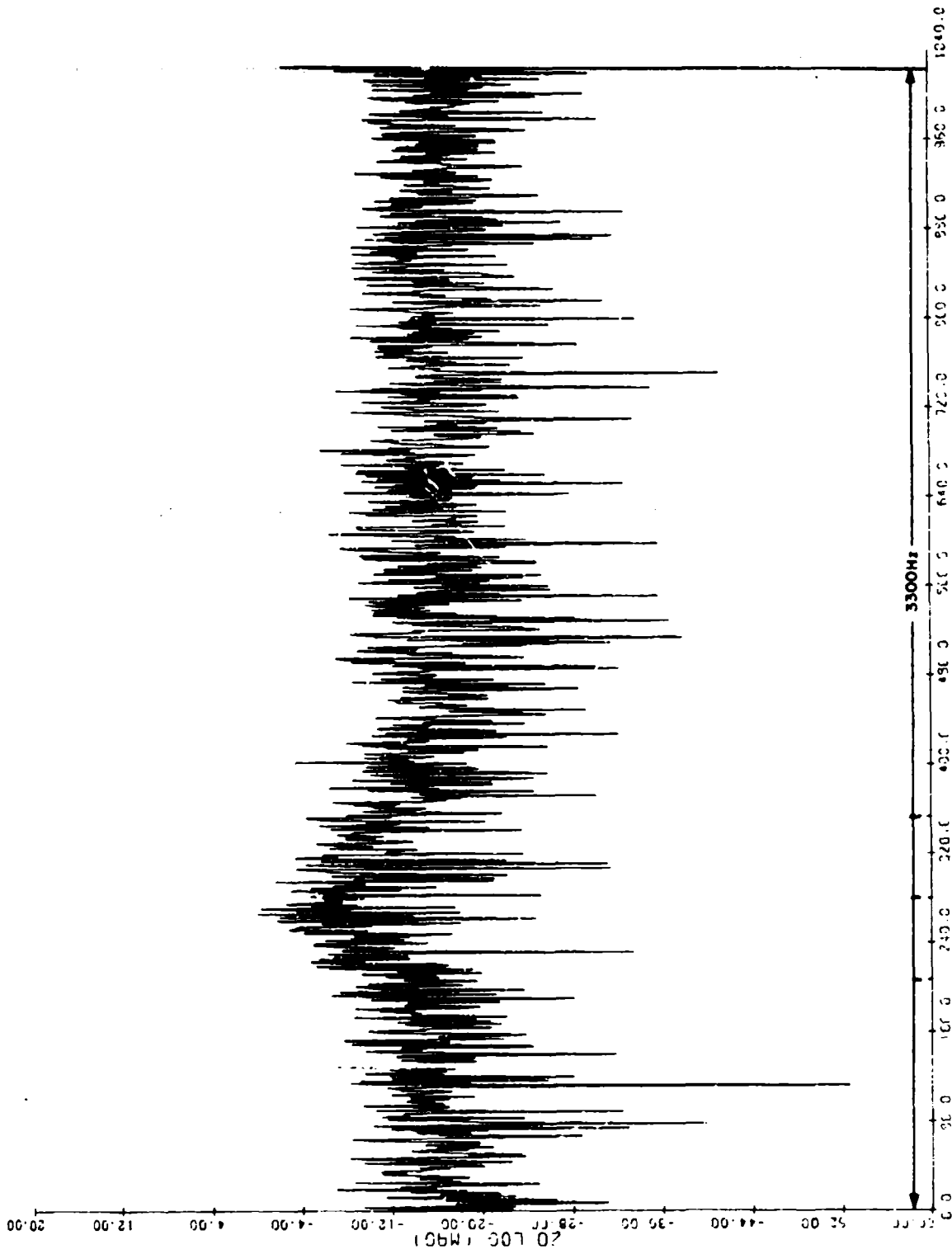
CASE 6:  $\mu = 600$  Hz,  $\sigma = 156$  Hz,  $S/N = 5$  dB



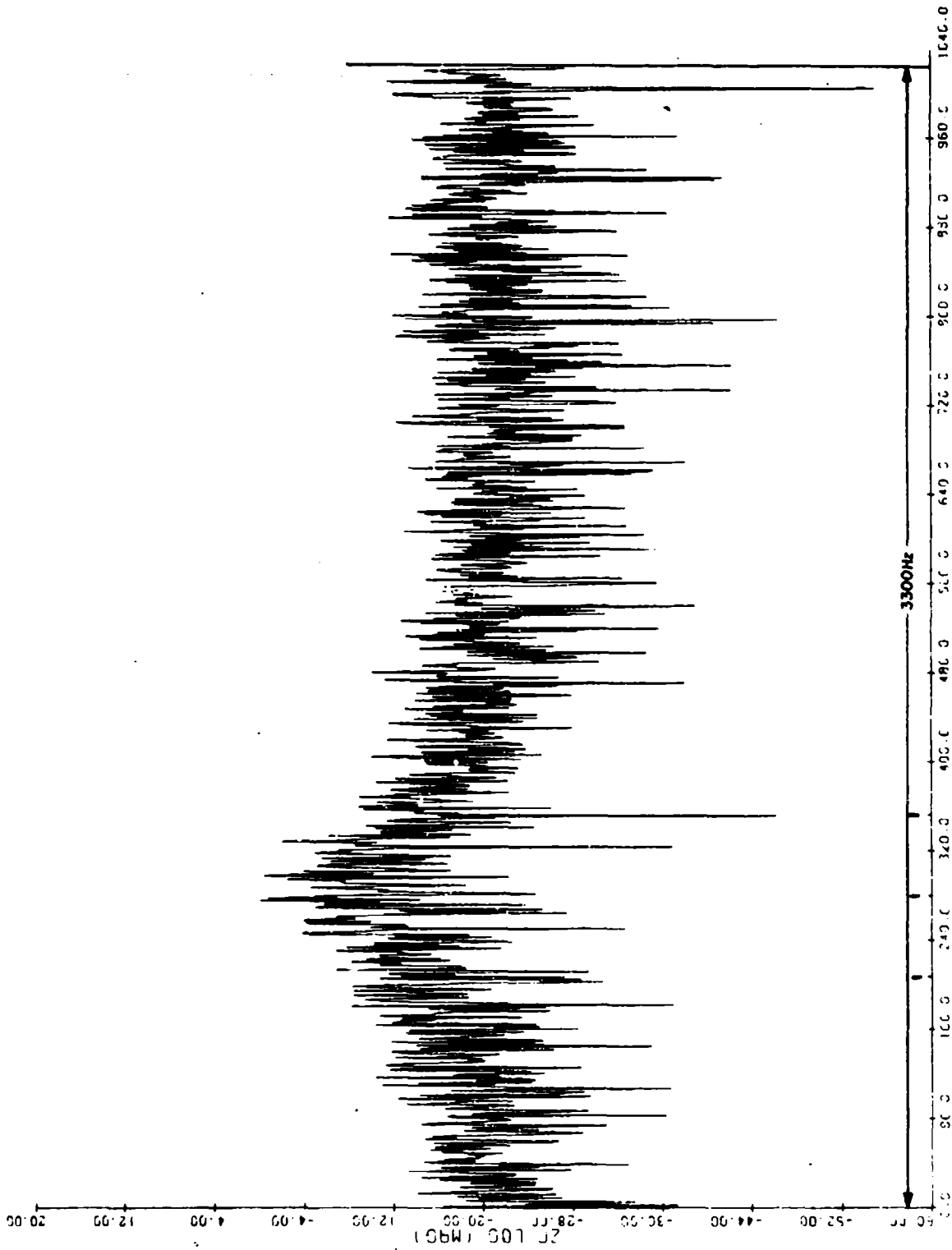
CASE 7:  $\mu = 600$  Hz,  $\sigma = 156$  Hz,  $S/N = 15$  dB



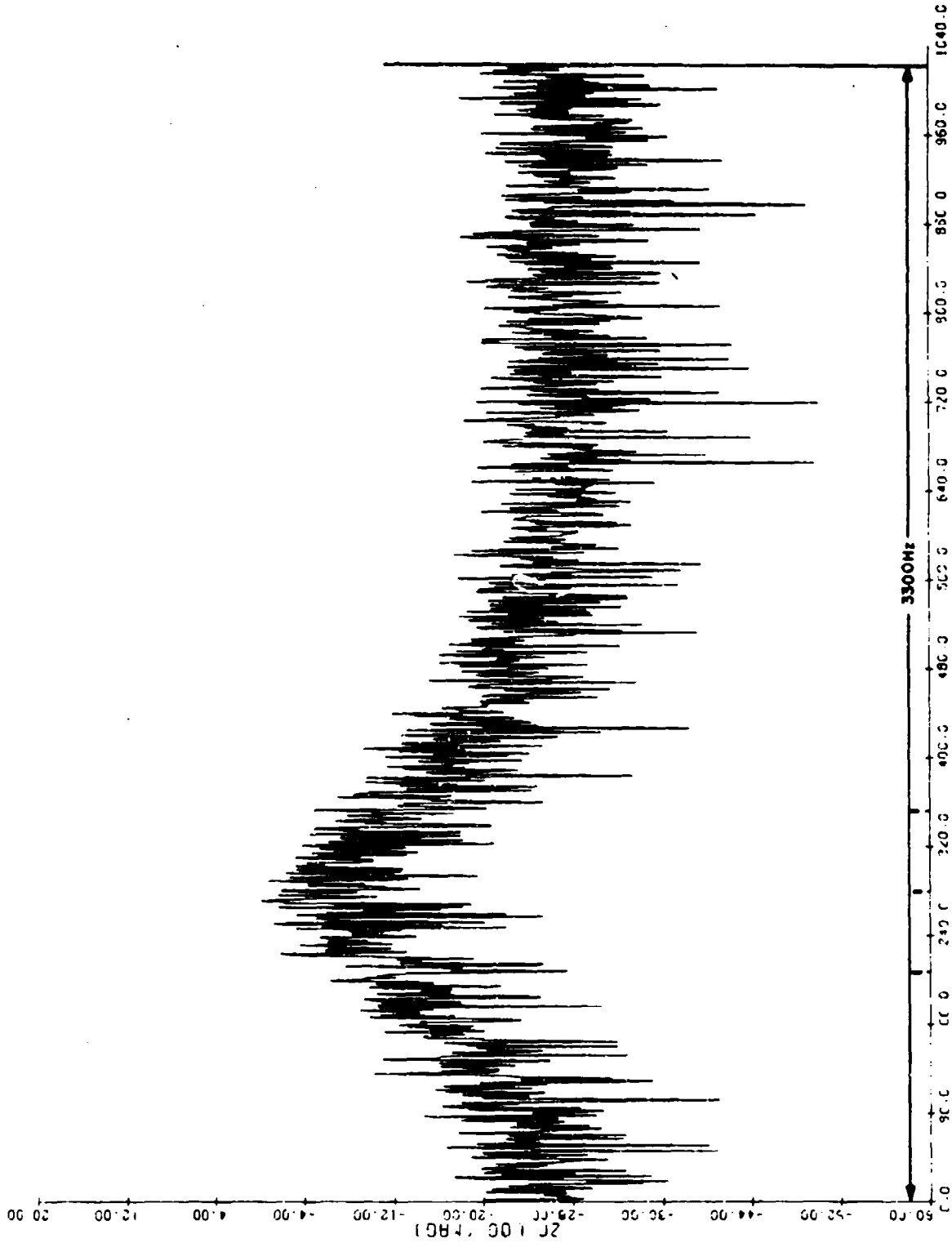
CASE 8:  $\mu = 600 \text{ Hz}$ ,  $\sigma = 156 \text{ Hz}$ ,  $S/N = \infty$



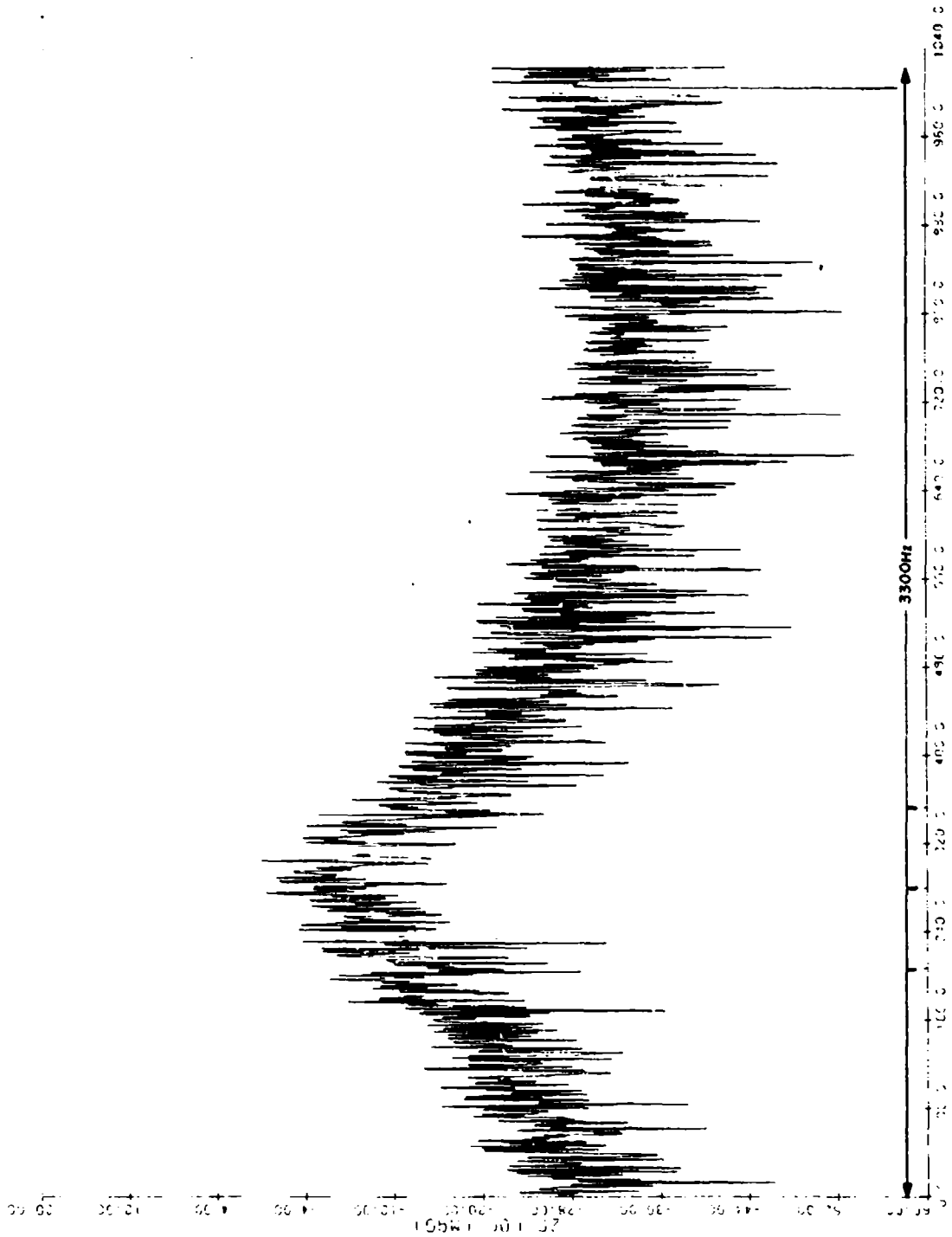
CASE 9:  $\mu = 900 \text{ Hz}$ ,  $\sigma = 234 \text{ Hz}$ ,  $S/N = 0 \text{ dB}$



CASE 10:  $\mu = 900 \text{ Hz}$ ,  $\sigma = 234 \text{ Hz}$ ,  $S/N = 5 \text{ dB}$



CASE 11:  $\mu = 900$  Hz,  $\sigma = 234$  Hz,  $S/N = 15$  dB



CASE 12:  $\mu = 900 \text{ Hz}$ ,  $\sigma = 234 \text{ Hz}$ ,  $S/N = \infty$